REPORT TO THE TWENTY-THIRD LEGISLATURE
STATE OF HAWAII
2006

PURSUANT TO SCR 135, S.D.1 2005, REQUIRING THE DEPARTMENT OF HEALTH TO SHARE ITS FINDINGS AND A REPORT ON THE PLAN WITH THE BIG ISLAND COMMUNITY ON THE VOG EMISSION MONITORING SYSTEM

Prepared by:
State of Hawaii
Department of Health
Clean Air Branch
December 2005

TABLE OF CONTENTS

List of Figures

List of Tables

Appendices

Summaries of vog and meteorological studies

INTRODUCTION

This report is submitted pursuant to Senate Concurrent Resolution No. 135, S.D.1, which was adopted by the Senate and the House of Representatives of the Twenty-Third Legislature of the State of Hawaii, Regular Session of 2005. The resolution calls for the Department of Health (DOH) to report its vog monitoring system.

The Kilauea Volcano on the Island of Hawai´i has been erupting almost continuously since 1983 and typically emits thousands of tons of sulfur dioxide (SO_2) per day. SO_2 is an inhalable irritant that can produce respiratory distress, especially at elevated levels and in those with a pre-existing respiratory condition. The SO_2 gas oxidizes in the atmosphere and over time is converted into its particulate form of sulfuric acid mists and sulfate particles. This aerosol made up of liquid and solid particles produces a visible haze which the locals refer to as "vog".

Where vog affects populated areas depends on the wind direction and speed. During prevailing northeasterly trade winds, SO_2 blows towards the southwest affecting the Ka´u area and continues moving in the South Kona area having converted to its particulate form. During Kona or southerly wind conditions, SO_2 blows towards the northeast affecting South and North Hilo and if the winds are persistent, the vog may also impact other islands up the chain.

Volcanic emission is recognized as an important public health issue. The Department of Health, Clean Air Branch (CAB) has been actively involved in monitoring the level of sulfur dioxide and particulates in the ambient air. The CAB operates two ambient air monitoring stations on the Island of Hawai´i located in Kona and Hilo. The main purpose for the two stations is to monitor the impact that the volcanic emissions may have in areas where the majority of the population live and work. An additional SO_2 monitor was set up at one of our geothermal stations in Puna.

In addition to monitoring, the CAB maintains a vog index for the Kona area which is affected by vog during the prevailing trade wind conditions. Hilo and Puna districts, although closer to the volcano, are usually affected during the less frequent southerly wind conditions. The vog index provides information from one specific location in Kona and is accessible through a hot line. CAB is exploring further enhancements to the vog index.

The Department of Health (DOH) is concerned with the impact that vog may have on public health and has for many years conducted various health studies on the Island of Hawaii to gain further information on the nature and effects of the volcanic emissions. Currently, a health study is being conducted by the University of Hawaii with Dr. Elizabeth Tam as the principal investigator.

Other past studies have conducted short-term SO_2 monitoring at various locations such as Mountain View, Waimea, Kohala, North Kona, South Kona and Ka´u.

The National Park Service (NPS) currently has two SO_2 monitoring stations in Hawaii Volcanoes National Park. The NPS has developed their own air advisory and website to alert visitors and park employees of the SO_2 levels from the two monitoring stations (Figure 1). Since this highly active volcano emits approximately 2000 tons of SO_2 per day, it is not surprising that SO_2 levels within the park can be quite high at times depending on the localized meteorological conditions.

The CAB has reviewed and analyzed Hilo and Kona vog data, Big Island wind and air flow studies, other health and monitoring studies, information from the Hawai´i Volcanoes National Park SO_2 alert website, and has consulted with Dr. Elizabeth Tam and the scientific advisory committee. This report, prepared by the CAB, addresses the current efforts and a future plan for vog monitoring. As with any program, funds and manpower resources are limited and are always a consideration. However, the CAB has explored the feasibility of additional SO_2 monitoring and has selected two potential locations. Determining the best representative location is difficult and is subject to change. In addition, the sulfur dioxide impact on a particular location is variable and highly dependent on the meteorological conditions. CAB is considering the dissemination of the monitored results to the public through an accessible website and/or telephone hotline.

Figure 1

Current Sulfur Dioxide Conditions (SO_2) at Hawaii Volcanoes National Park

Kilauea Visitor Center	Good As of 10/20/2005 12:30 PM HST	
Jaggar Museum	Good As of 10/20/2005 1:30 PM HST	

Unhealthy
Unhealthy for Sensitive People
Moderate
Good

SO2 gas plume crosses road near Halemaumau and low on Chain of Craters Road. Sensitive individuals should limit exposure in these areas.

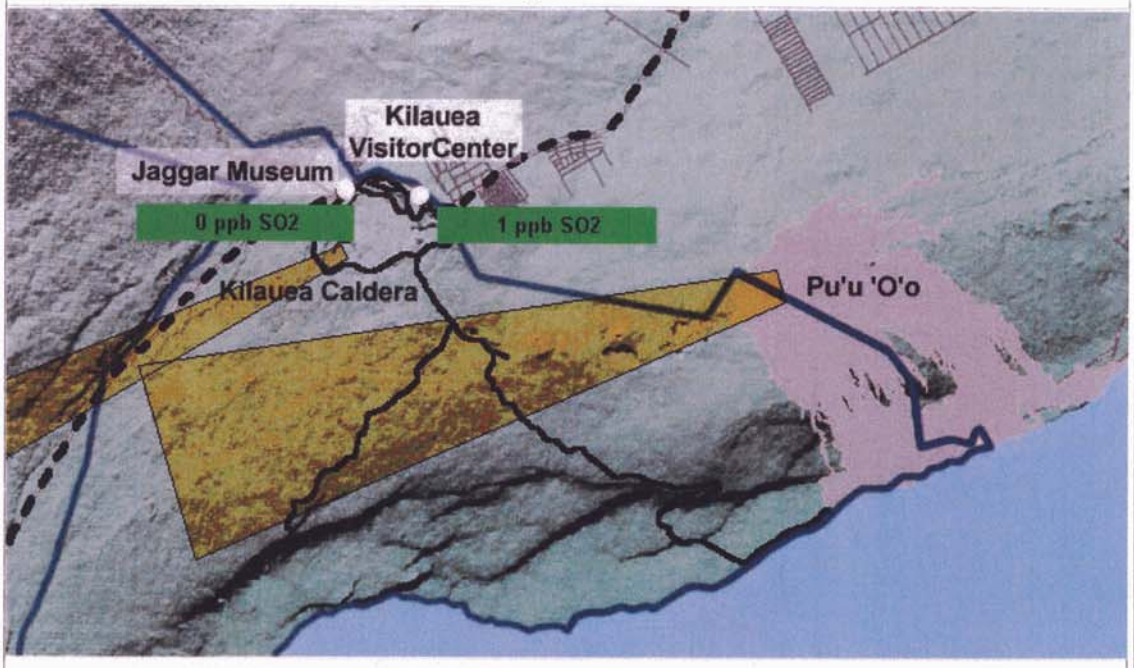

Current Data

	Jaggar Museum	Kilauea Visitor Center
Wind Speed and Direction	N W E S; 20 15 10 5 0	N W E S
	64 degrees, 2.2 m/s	68 degrees, 3.5 m/s
SO_2 Concentration	0 ppb	1 ppb

24-hour Timeline Charts
12-hour Timeline Charts
6-hour Timeline Charts

EXISTING VOG MONITORING STATIONS

The U.S. Environmental Protection Agency (EPA) has established primary and secondary National Ambient Air Quality Standards (NAAQS) for sulfur dioxide (SO_2). *Primary standards* are limits set to protect public health, including the health of sensitive populations such as asthmatics, children, and the elderly. *Secondary standards* are established to protect public welfare, including protection against decreased visibility, damage to animals, crops, vegetation, and buildings.

Table 1 The NAAQS for SO_2

	Averaging Period	**Standard (ppb)**
Primary (health)	24 hours	140
Primary (health)	Annual	30
Secondary (welfare)	3 hours	500

The CAB currently has three stations on the Island of Hawaii monitoring for SO_2. These stations are located in Hilo, Kona, and Puna. The Hilo station began operation in 1995, the Kona station started in 1997 (Figure 2), and the Puna station just recently began monitoring for SO_2 in February 2005. The NAAQS for SO_2 have never been exceeded at any of these monitoring stations.

Additionally, from May 1997 to August 2000, SO_2 monitoring was conducted in Honoka'a to determine vog levels on the north side of the Island of Hawaii. The data collected confirmed that SO_2 levels were low in the Honoka'a area.

Included in this report is a summary of Honoka'a SO_2 data collected between 1999 and 2000, and SO_2 and wind direction data collected from July 2004 to June 2005 at the Hilo, Kona and Puna stations (Figures 3, 4, 5 and 6, respectively).

In Hilo, the effects of the southerly wind conditions can be seen in the elevated levels of SO_2 but are still below the NAAQS. Tradewind patterns prevail approximately 90% of the time during the summer but only about 60% during the winter months when the winds often shift out of the south due to seasonal cold fronts [1]. In Kona and Puna, SO_2 and even the vog particulates remain relatively low regardless of the wind direction.

[1] Per verbal communication with Dr. Yi-Leng Chen, Professor of Meteorology, University of Hawaii

Figure 2

Department of Health Clean Air Branch
Air Monitoring Stations in Hilo and Kona

Hilo monitoring station located at 1099 Waianuenue Ave.

Kona monitoring station located on the grounds of Konawaena High School

Figure 3 **SO_2 for Honoka'a from July 1999 to June 2000**
(Wind direction data not available)

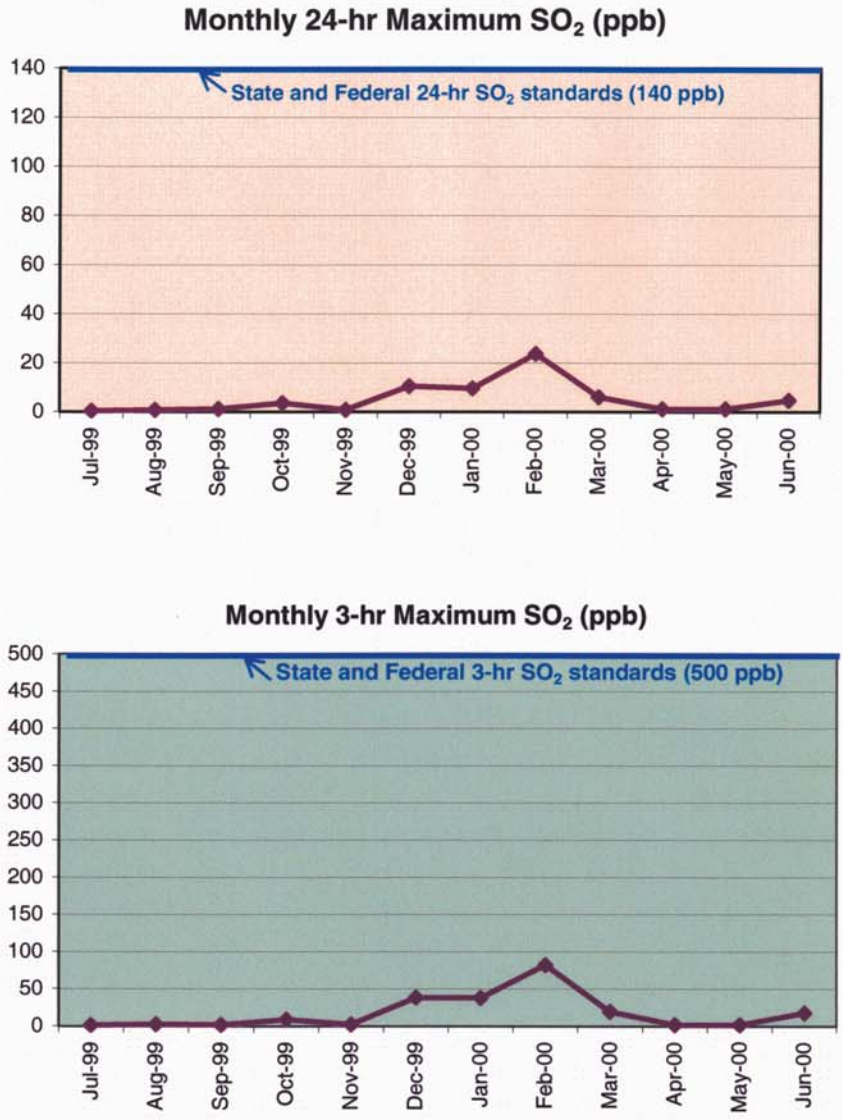

Figure 4 **SO_2 and Wind Direction for Hilo from July 2004 to June 2005**

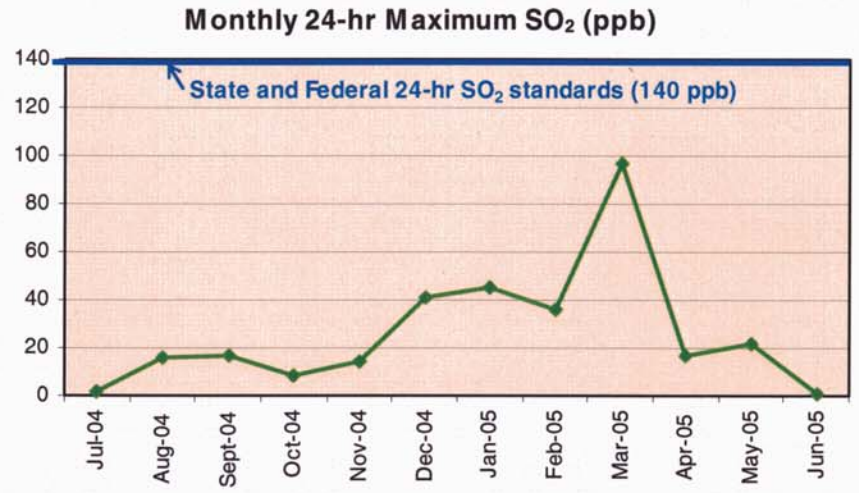

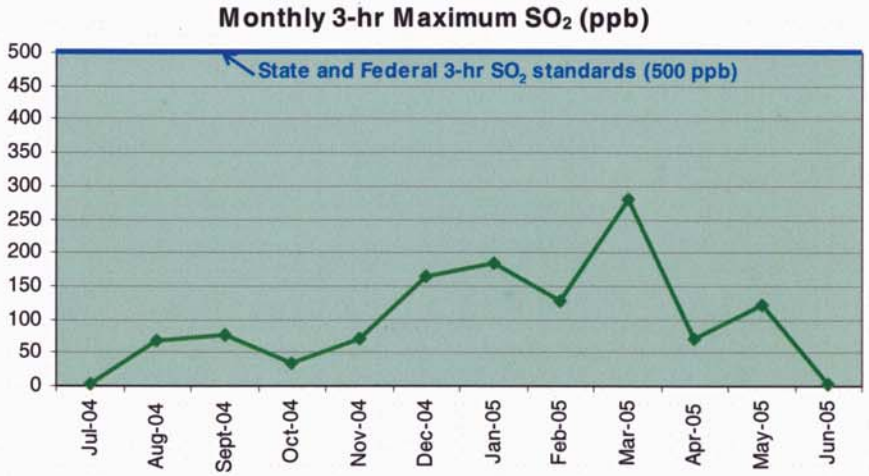

Direction	Frequency of Wind Direction (% of Month)											
	Jul	Aug	Sept	Oct	Nov	Dec	Jan	Feb	Mar	Apr	May	Jun
1° to 90°	26	22	28	18	12	12	16	20	19	29	36	29
91° to 180°	13	14	9	14	18	16	18	11	17	8	8	5
181° to 270°	49	50	48	51	60	56	56	47	48	43	39	41
271° to 360°	13	13	15	17	10	16	10	21	16	20	17	25

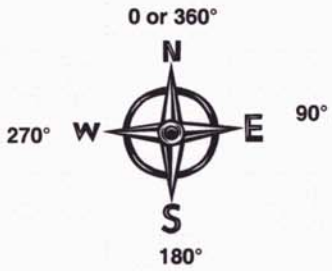

Figure 5 **SO_2 and Wind Direction for Kona from July 2004 to June 2005**

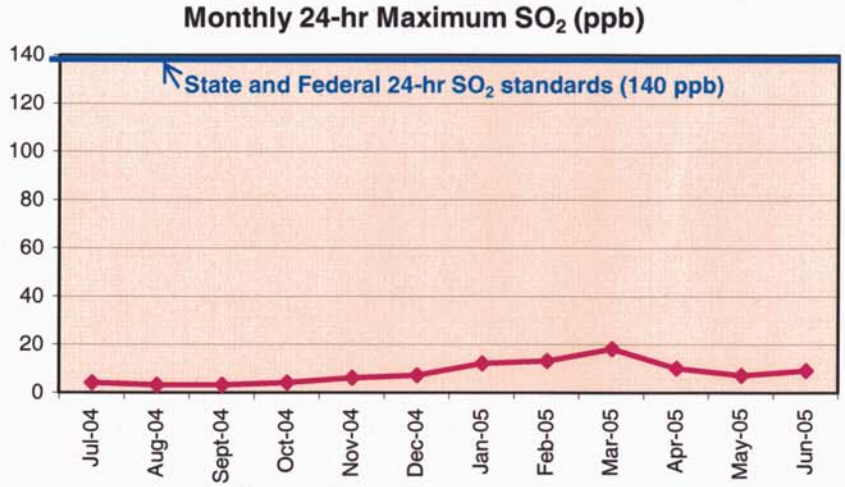

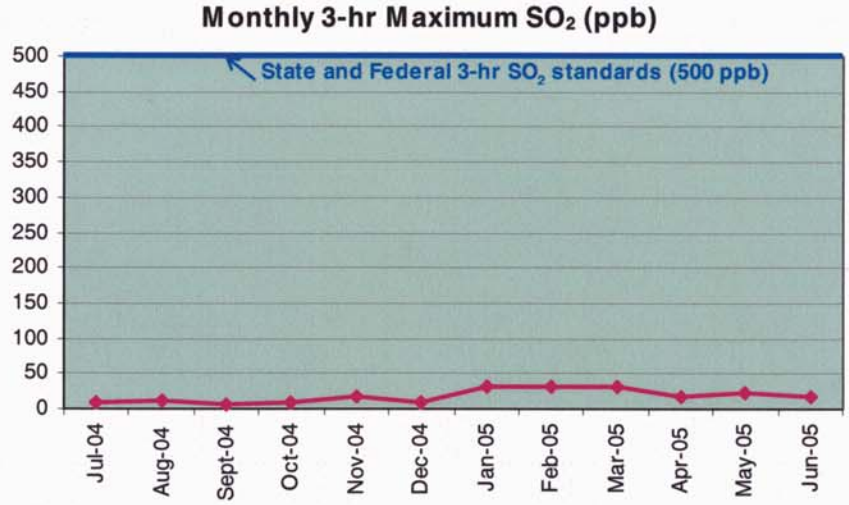

Direction	Frequency of Wind Direction (% of Month)											
	Jul	Aug	Sept	Oct	Nov	Dec	Jan	Feb	Mar	Apr	May	Jun
1° to 90°	39	42	28	47	51	54	46	49	45	42	38	38
91° to 180°	19	17	9	13	11	10	18	15	15	15	20	21
181° to 270°	19	28	48	30	22	20	24	28	32	32	34	30
271° to 360°	23	13	15	11	15	16	12	8	7	11	8	11

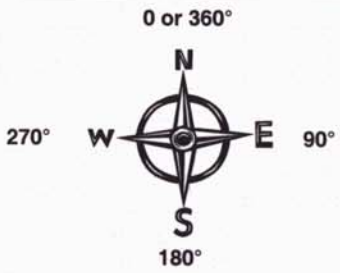

Figure 6 SO_2 and Wind Direction for Puna from February to June 2005

Monthly 24-hr Maximum SO_2 (ppb)

(Station began monitoring for SO_2 end of February 2005)

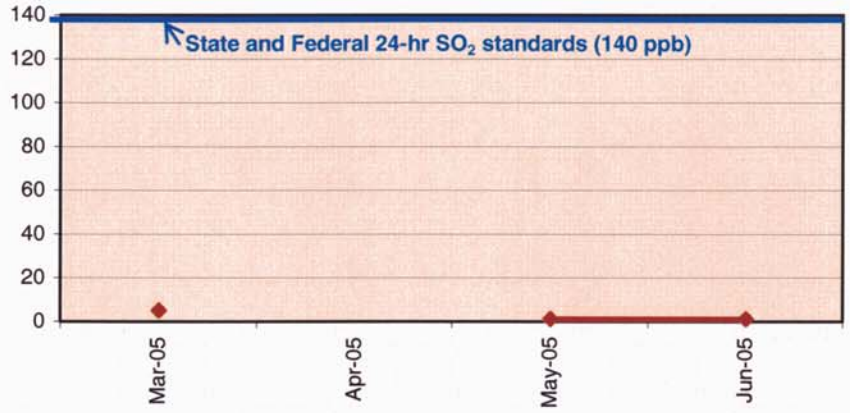

Monthly 3-hr Maximum SO_2 (ppb)

(Station began monitoring for SO_2 end of February 2005)

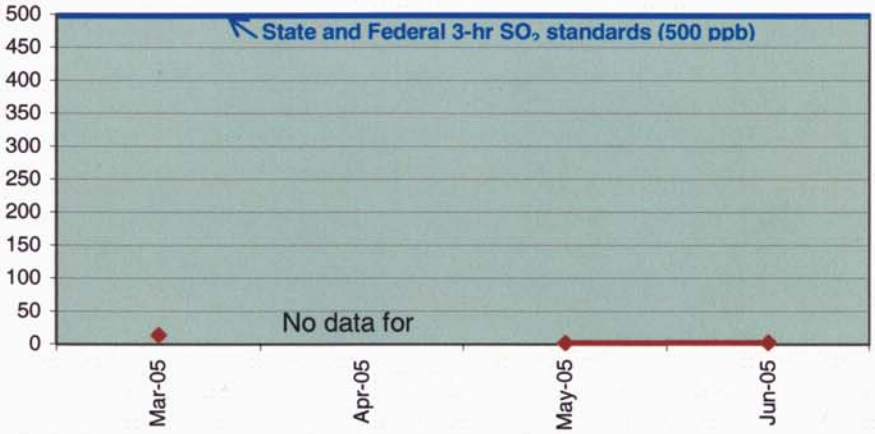

Direction	Frequency of Wind Direction (% of Month)											
	Jul	Aug	Sept	Oct	Nov	Dec	Jan	Feb	Mar	Apr	May	Jun
1° to 90°								30	21		26	38
91° to 180°								20	23		22	16
181° to 270°								13	30		16	13
271° to 360°								37	27		37	33

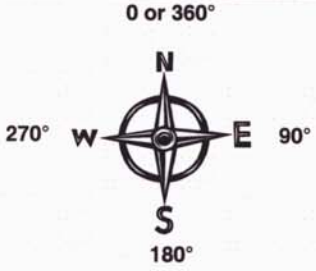

PROPOSED LOCATIONS FOR ADDITIONAL STATIONS

The CAB is proposing to establish two additional stations on the southeast side of the Island of Hawaii, one upwind and one downwind of the Pu'u O'o vent (Figure 7). The locations were chosen in part based on population (Figure 8), sulfur dioxide and wind flow studies, physical space that is sufficient, secure, and available to place the monitoring trailers, and areas that do not currently have monitoring for sulfur dioxide. Consultations with Dr. Tam's scientific advisory group and reviews of various monitoring data and studies were conducted to determine the best locations for these stations.

The National Park Service has two sulfur dioxide monitoring stations located in the Hawaii Volcanoes National Park, and the CAB operates three stations, one each in Hilo, Kona and Puna (Figure 7). With the two proposed stations in Mountain View and Pahala, there will be a total of seven stations monitoring for sulfur dioxide on the Island of Hawaii.

The two proposed sites were selected by CAB staff based on EPA siting guidance set forth in Title 40 of the Code of Federal Regulations (40CFR), Part 58. The continuous sulfur dioxide monitor will be a federal equivalent method as described in 40CFR53 and quality assurance criteria will be followed as promulgated in 40CFR58. Additionally, each station will be equipped with meteorological instruments to measure the wind speed and wind direction.

Prior to establishing the two new stations, passive sulfur dioxide monitoring will be performed to assess the SO_2 levels in seven locations: Hilo, Kea'au, Mountain View, Puna, Volcano Village, Pahala, and Kona. In passive sampling, stationary filters are set up and exposed to the ambient air for two weeks at a time, preferably during tradewind and "Kona" wind conditions. The data collected from this passive sampling exercise will be analyzed and considered in siting the proposed the air monitoring stations.

Figure 7. Current and Potential Vog Monitoring Stations

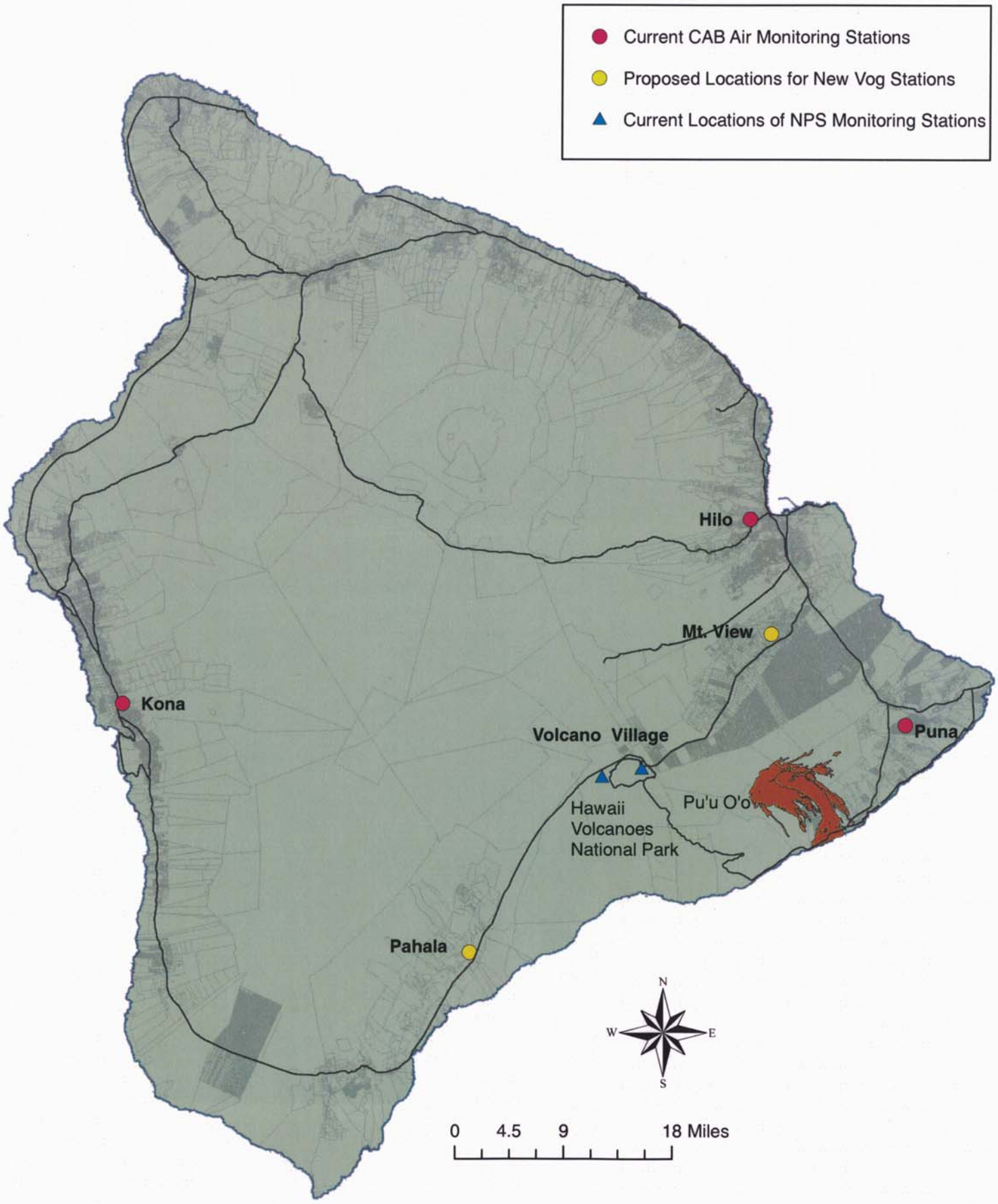

Figure 8. 2000 Census Designated Places

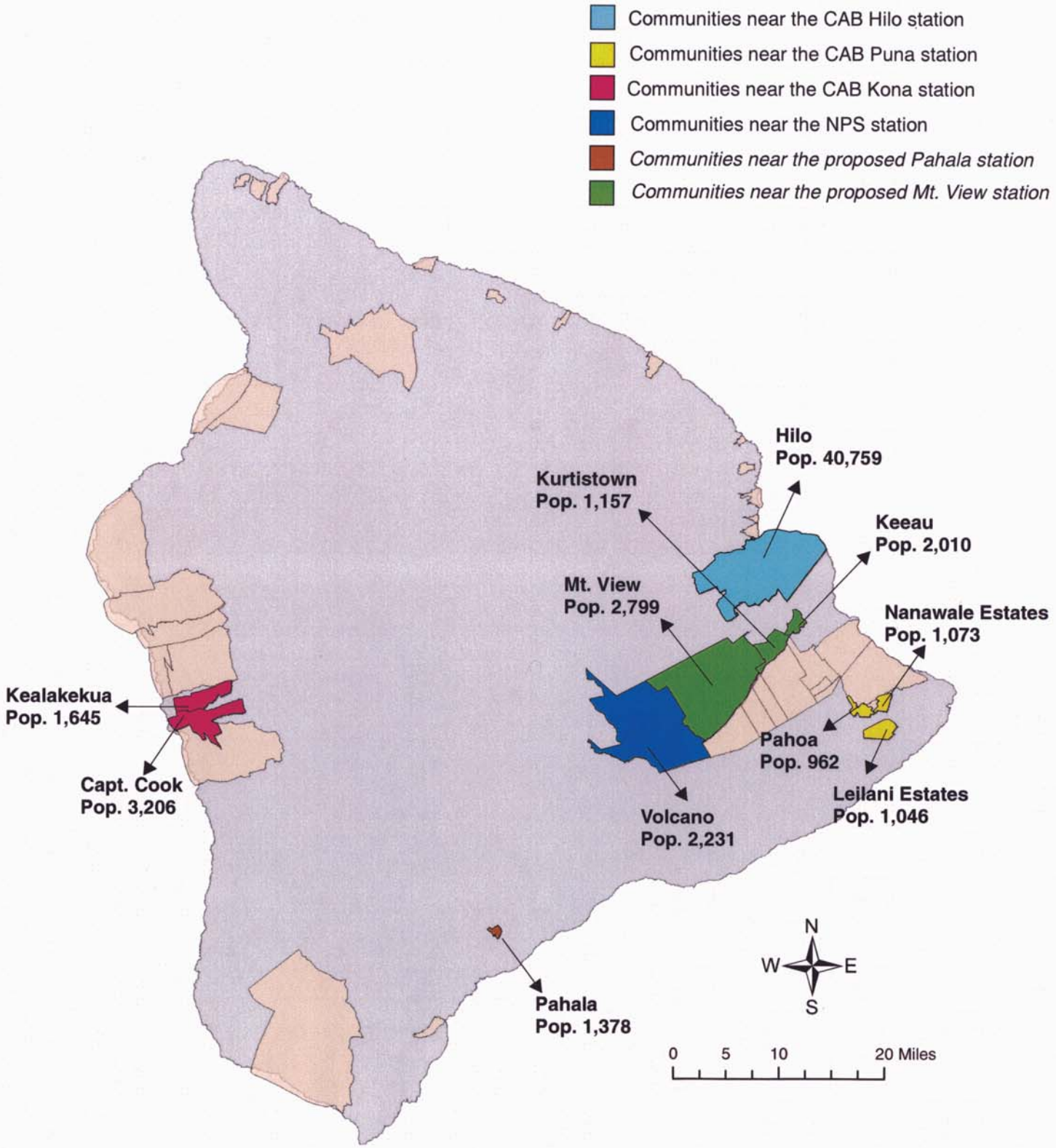

2000 Census Designated Places map and data from the
Office of Planning, Dept. of Business, Economic Development and Tourism, State of Hawaii

MONITORING STATION COSTS

The cost associated with an air monitoring station consists of equipment, recurring operational, and manpower. Table 2 supplies a cost estimate for monitoring equipment which totals approximately $80,000 per station. For two proposed stations, the cost estimate would be approximately $160,000. There are also initial infrastructure costs which include electrical and telephone hook ups, ground preparation, and construction contracts, which have not been included. The recurring monthly costs include telephone, electricity, rent, travel cost for technicians to conduct regular quality assurance audits and station maintenance such as general grounds keeping, roof repairs, painting, etc. Manpower needs include one technician to service the proposed two stations as well as two existing vog stations on the Island of Hawaii.

The CAB has used funds from a previous federal grant to establish the first monitoring station at $80,000. The CAB was proposing to establish a second monitoring station with the FY 2006 federal grant funds, but due to a recently-announced funding shortfall and the inclusion of an additional critical project, the second station will have to be postponed unless general funds are provided. Since the CAB was only recently notified of the cuts in the federal funds, it was too late for the program to submit a general fund request for the establishment of a second monitoring station in the FY 2007 Administrative Budget. Once the two additional monitoring stations are operational, the island of Hawaii will have a total of seven monitoring stations necessitating a position count and general funds for a full-time technician. If the 2006 Legislature is unable to provide the state general funds for the second monitoring station and for the technician, then a formal request will be submitted to the following 2007 Legislature in the FY 2008 Administrative Budget.

SCHEDULING

The goal for deployment of these two additional stations is possibly by January 2007 if the additional funding can be obtained for the second station. Purchasing of the equipments will be rather quick; however, obtaining a lease, in our experience, may take approximately one year. This process has been lengthy because the legal document must first be negotiated with the Lessor, upon agreement be reviewed and approved by the Department of Land and Natural Resources (DLNR), the Board of Land and Natural Resources, and the Attorney Generals Office.

Developing and initiating an advisory system can be done concurrently but is also dependent on the completion of the first monitoring station and on how quickly contract services can be procured.

TABLE 2

COST ESTIMATE
FOR SULFUR DIOXIDE MONITORING STATION

EQUIPMENT COST	GENERAL FUND COST
Monitoring Station Equipment (Shelter, sulfur dioxide analyzer, gas calibrator, zero air supply, meteorological system, computer system, data logger hardware, strip chart recorder)	$80,000
State Vehicle (to service monitoring station)	$25,000
TOTAL	**$105,000**

ANNUAL OPERATING COST	GENERAL FUND COST
Operating Cost (Utilities, rent, station maintenance, software support, gas standards)	$3,000
Manpower (Air Quality Electronic Technician, including fringe and indirect costs)	$60,000
Vehicle Operational Cost	$7,000
TOTAL	**$70,000**

ADVISORY SYSTEM

The EPA has established a national air quality standard for SO_2 to protect public health as discussed earlier in this report. The EPA also has in place an Air Quality Index (AQI) (Figure 9) which is used to report daily air quality. The Index is used to inform the public on the status of the monitored air and the associated health effects of interest to individuals. The AQI focuses on health effects that may be experienced within a few hours or days after being exposed to the measured levels. The CAB is proposing to use this index system in issuing a public advisory.

The AQI is calculated daily by converting monitored results to AQI values using standard formulas developed by EPA. An AQI value of a 100 generally corresponds to the national air quality standard for the air pollutant, in this case the health-based standard for SO_2. When AQI values are above 100, air quality is considered to be unhealthy for the sensitive groups of people and as the AQI values increase further, then for the healthy persons. The AQI is divided into the six categories and explained in Figure 5.

The near real-time SO_2 values and the AQI value will be reported to the public using the internet and possibly a telephone hotline. The media such as newspaper, television or radio will also have access to the daily information through the internet and telephone hotline. The web site will probably contain general information about vog and SO_2, the near real-time values, AQI values and steps the public can take to protect their health. Individuals can then decide what measures they would take to protect themselves.

Before final advisory levels and a public notification system is established, CAB will seek input from Dr. Tam's scientific advisory group and other health agencies, including DOH's Hazard Evaluation and Emergency Response Office.

Figure 9 Air Quality Index (AQI): Sulfur Dioxide (SO_2)

24–hr SO_2 ppb Range:	Equals this AQI Value	Levels of Health Concern		Sensitive Groups	Health Effects Statements	Cautionary Statements
0 - 34	0 to 50	GOOD	Air quality is considered satisfactory and air pollution poses little or no risk	People with asthma are the group most at risk.	None	None
35 - 144	51 to 100*	MODERATE	Air quality is acceptable; however, for some pollutants there may be a moderate health concern for a very small number of people.	People with asthma are the group most at risk.	None	None
145 - 224	101 to 150	UNHEALTHY FOR SENSITIVE GROUPS	Members of sensitive groups may experience health effects. This means they are likely to be affected at lower levels than the general public. The general public is not likely to be affected when the AQI is in this range.	People with asthma are the group most at risk.	Increasing likelihood of respiratory symptoms, such as chest tightness and breathing discomfort, in people with asthma.	People with asthma should consider limiting outdoor exertion.
225 - 304	151 to 200	UNHEALTHY	Everyone may begin to experience health effects. Members of sensitive groups may experience more serious health effects.	People with asthma are the group most at risk.	Increased respiratory symptoms, such as chest tightness and wheezing in people with asthma; possible aggravation of heart or lung disease.	Children, asthmatics, and people with heart or lung disease should limit outdoor exertion.
305 - 604	201 to 300	VERY UNHEALTHY	At this range a health alert is triggered, meaning everyone may experience more serious health effects.	People with asthma are the group most at risk.	Significant increase in respiratory symptoms, such as wheezing and shortness of breath, in people with asthma; aggravation of heart or lung disease.	Children, asthmatics, and people with heart or lung disease should avoid outdoor exertion; everyone else should limit outdoor exertion.
≥605	301 to 500	HAZARDOUS	At this range health warnings of emergency conditions are triggered. The entire population is more likely to be affected.	People with asthma are the group most at risk.	Severe respiratory symptoms, such as wheezing and shortness of breath, in people with asthma; increased aggravation of heart or lung disease; possible respiratory effects in general population.	Children, asthmatics, and people with heart or lung disease should remain indoors; everyone else should avoid outdoor exertion.

*An AQI of 100 for sulfur dioxide corresponds to an SO_2 level of 0.14 parts per million (averaged over 24 hours).

Source: 40 CFR Part 58, Appendix G; EPA Air Quality Index, A Guide to Air Quality and Your Health, EPA-454/K-03-002; AIRNOW AQI Calculator, www.airnow.gov/index (accessed October 2005).

CONCLUSION (SUMMARY)

The CAB currently has three vog monitoring stations measuring SO_2 located in Hilo, Puna, and Kona. Two additional stations are proposed to be located in Mountain View and Pahala for a total of five air monitoring stations operated by CAB to measure volcanic emissions. Consultations with Dr. Tam's scientific advisory group and reviews of various monitoring data and studies were conducted to determine the best locations for these stations. The stations will be equipped with continuous SO_2 monitors and meteorological equipment. Quality assurance of the data will be performed according to EPA guidelines.

The CAB is also proposing that the near real-time data be made accessible to the public through a website and telephone hotline. The health advisory levels will be established using EPA's AQI system.

A public meeting will be scheduled to share and discuss the vog monitoring proposal with the communities on the Island of Hawaii. The input and comments obtained from the public meeting will be considered before implementing the plan.

APPENDIX

SUMMARIES OF VOG AND METEOROLOGICAL STUDIES

SO_2 AND FINE AEROSOL DISPERSION FROM THE KILAUEA PLUME, KA'U DISTRICT, HAWAI'I, USA (Appendix 1)

Bernadette Mae Longo
Anita Grunder
Raymond Chuan
Annette Rossignol

Sulfur dioxide (SO_2) is present at lower elevations and there is an increase in aerosol with altitude due to oxidation of the SO_2. SO_2 and fine aerosol concentrations were elevated in the Ka'u district relative to background district of Hawi. The study used a quartz crystal microbalance cascade impactor (QCM) to sample the aerosol samples. The SO_2 was measured with SO_2-specific passive diffusion tubes, made by Harwell Scientifics.

The "Clean Air" Layer at Sea Level along the Kona Coast (Appendix 2)

Steven Ryan

Along the leeward Kona coastline of the Big Island from sea level to about 100 meters above sea level there are very few or no volcanic particles. The 24-hour particle concentrations (condensation nuclei/submicron particles) were between 400-1000 particles per cubic centimeter over 24 hours, similar to the concentration found along the windward coast. At elevations above 100 meters, a vog layer forms during the day with a maximum peak extending to about 900 meters above sea level with condensation nuclei concentrations averaging 4000 to 10,000 particles per cc. Above the 900 meter elevation, concentration decreases with height. Between midnight and 4 a.m., the average concentration is usually less than 1500 particles per cc at all elevations.

Submicron particles in the atmosphere were measured at seven sites on the island of Hawai'i since early 2002 by the VOGNET program. VOGNET was a collaboration between the National Oceanic and Atmospheric Administration and several public and private high schools. Particles were measured using an instrument designed by the author. Particles were detected by causing a water droplet to form around each particle inside of a chamber. A laser diode light beam was projected through the chamber onto a detector. The instrument recorded the fraction of light which was scattered by the water droplet fog, and used a calibration table to calculate the particle concentration from this ratio.

The Distribution of Volcanic Aerosols in Hawaii from VOGNET (Appendix 3)

Steven Ryan

The VOGNET was organized in September 1996 as a partnership between Mauna Loa Observatory (NOAA) and teachers from several Big Island public and private high schools. NOAA provided surplus equipment and trained the volunteer high school teachers. Daytime measurements were made at Ka'u High School, Konawaena High School, Hawai'i Preparatory Academy, Waiakea High School, and Pahoa High School. Aerosol optical depth was calculated from observations using NOAA J-Series handheld sunphotometers. Condensation nuclei were measured with Gardner Counters. It was found that the average optical depth was greatest at the leeward sites of Ka'u and Konawaena, and decreased clockwise around the island, with a minimum at the windward Waikea High School sampling site . Average condensation nuclei concentrations were greatest at Ka'u and significantly less at Konawaena and the other sites. The automated condensation nuclei sampled at Ka'u High School, Konawaena High School, Hawaii Preparatory Academy, and Kaumana residential neighborhood from 1998-1999. All sites had minimum particle concentrations between midnight and 5 a.m. The particle concentrations began rising at 6 a.m. at all four locations. At all sites except Ka'u, maximum concentration occurred just before noon. At Ka'u there was a maximum at 8 a.m. The study also mentioned that westerly or southerly winds could bring high concentrations of volcanic aerosols to the eastern coast of the island.

Airflow Over the Island of Hawaii (Appendix 4)

Yi-Leng Chen

The island of Hawaii's geography affects the wind pattern. Along the windward coast of the Island of Hawaii, the airflow moves around the mountains and are also channeled between the Kohala Mountains and Mauna Kea and the saddle between Mauna Kea and Mauna Loa. On the leeward side of the island, the trade winds are completely blocked by Mauna Kea and Mauna Loa. The island also experiences a diurnal heating cycle with a strong down-slope wind component at night and an upslope component during the day. The "wake vortices" consists of two counter-rotating eddies that occur west of the west coast of Hawai'i. "Aerosol concentration in the southerly eddy is elevated due to the entrainment of Kilauea plume."

Diurnal Variation of Surface Airflow and Rainfall Frequencies on the Island of Hawai'i (Appendix 5)

Yi-Leng Chen and Andrew J. Nash

The island of Hawai'i's geography affects the wind pattern, similar to "Airflow Over the Island of Hawai'i." Surface airflow over the island of Hawai'i was studied using Portable Automated Mesonet (PAM) stations. The windward coast experiences winds from a northerly direction. The northern and southern tips of the island exhibit an easterly wind pattern because the trade winds are forced around Mauna Kea and Mauna Loa. On the leeward sides of Mauna Kea and Mauna Loa the trade winds are absent with calm winds. Except in the high wind regions, most of the island shows an upslope-onshore wind component during the day switching to a down-slope offshore wind component at night.

References

Chen, Yi- Ling, Airflow Over the Island of Hawaii

Chen, Yi-Ling, Nash, Andrew, Diurnal Variation of Surface Airflow and Rainfall Frequencies on the Island of Hawaii, American Meteorological Society, Volume 122, page 34-55.

EPA (U.S. Environmental Protection Agency), AIRNOW AQI Calculator, www.airnow.gov/index, (accessed October 2005).

EPA (U.S. Environmental Protection Agency), Air Quality Index, A Guide to Air Quality and Your Health, EPA-454/K-03-002

Longo, Bernadette Mae, Grunder, Anita, Chuan, Raymond, Rossignol, Annette, SO2 and Fine Aerosol Dispersion From The Kilauea Plume, Kau District, Hawaii, USA, A Dissertation submitted to Oregon State University by Bernadette Mae Longo.

Ryan, Steven, The "Clean Air" Layer at Sea Level along the Kona Coast, http://vognet.hpa.edu, (accessed October 2005).

Ryan, Steven, The Distribution of Volcanic Aerosols in Hawaii from VOGNET, http://www.mlo.noaa.gov/Projects/Vognet/vognet.htm, (accessed October 2005).

Title 40, Code of Federal Regulations, Part 58, Appendix G.

Appendix 1

The Senate
The Twenty-Third Legislature
of the
State of Hawaii

STATE CAPITOL
HONOLULU, HAWAII 96813

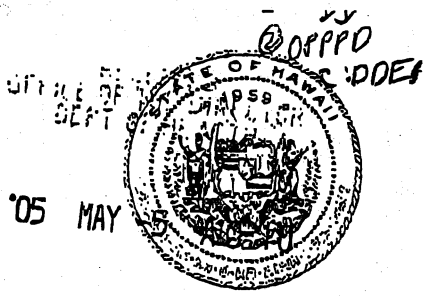

May 3, 2005

Dr. Chiyome L. Fukino
Director
Department of Health
P.O. Box 3378
Honolulu, HI 96801

Dear Dr. Fukino:

I transmit herewith a copy of Senate Concurrent Resolution No. 135, S.D.1, which was adopted by the Senate and the House of Representatives of the Twenty-Third Legislature of the State of Hawaii, Regular Session of 2005.

Sincerely,

Paul T. Kawaguchi
Chief Clerk
Hawaii State Senate

THE SENATE
TWENTY-THIRD LEGISLATURE, 2005
STATE OF HAWAII

S.C.R. NO. 135 S.D. 1

SENATE CONCURRENT RESOLUTION

REQUESTING THE DEPARTMENT OF HEALTH TO SHARE ITS FINDINGS AND THE STATUS OF ITS ACTIVITIES REGARDING THE CREATION OF A COMPREHENSIVE VOG EMISSIONS MONITORING SYSTEM FOR THE ISLAND OF HAWAII.

WHEREAS, Kilauea on the island of Hawaii is one of the most active volcanoes in the world; and

WHEREAS, during eruptions, not only does the volcano produce molten lava, but it also releases gases containing water vapor, sulfur dioxide, and carbon dioxide; and

WHEREAS, once airborne, the gases, particularly the sulfur dioxide, react with other chemicals in the air to form both liquid and solid particulate volcanic smog called "vog"; and

WHEREAS, vog is often irritating to the eyes, nose, throat, and lungs, and it has been shown to increase the occurrences of adolescent allergies, asthma, and respiratory disease on the island of Hawaii; and

WHEREAS, unfortunately, the wind carries the vog into populated areas, and the direction of the wind determines which part of the island is affected; and

WHEREAS, when the prevailing northeasterly tradewinds are blowing, vog tends to collect on the Kona side of the island before blowing to sea, and when southerly (Kona) winds are blowing, vog affects the Hilo side of the island and may also impact other islands farther up the chain; and

WHEREAS, the Department of Health is concerned with the impact that volcanic emissions may have on public health and has been actively involved in monitoring the levels of sulfur dioxide gas and particulate in the ambient air at two monitoring stations, one in Kona and the other at Hilo Hospital; and

S.C.R. NO. 135 S.D. 1

WHEREAS, the monitoring stations were placed in these locations because the majority of the population lives and works there; and

WHEREAS, however, the vog monitoring in these areas does not help the residents living and working in surrounding communities, especially near the volcano, which is the source of the emissions; and

WHEREAS, further, there is no notification system in place to alert residents during periods of really high levels of vog emissions; and

WHEREAS, the Department of Health Clean Air Branch is actively engaged in developing an SO2 monitoring plan and a vog advisory for applicable areas on the island of Hawaii; and

WHEREAS, the Department of Health Clean Air Branch is reviewing the monitoring aspects of several studies presently being conducted, such as the "UH NIH Hawaii Island Lung Assessment Study" by Dr Elizabeth Tam, M.D., that has been monitoring and collecting data of particulate matter since 2002 for the locations of Hilo, Kau, Keaau, Kohala, North Kona, and South Kona; and

WHEREAS, Dr. Tam has convened a scientific advisory committee comprised of representatives from Harvard School of Public Health, University of Southern California, United States Geological Survey, University of Hawaii School of Ocean and Earth Sciences, University of Hawaii John A. Burns School of Medicine, the Hawaii District Health Office, and others, to assist and provide advice on the many aspects of this important health issue; and

WHEREAS, after the information and data have been reviewed and analyzed, the Department of Health Clean Air Branch expects to develop a monitoring plan and prepare a report addressing the approach including the number of stations, locations, quality assurance measures, advisory system, scheduling, material costs, and manpower requirements; and

WHEREAS, a report on the plan and the status of current activities is expected by the end of 2005; now, therefore,

S.C.R. NO. 135 S.D. 1

BE IT RESOLVED by the Senate of the Twenty-third Legislature of the State of Hawaii, Regular Session of 2005, the House of Representatives concurring, that the Department of Health is requested to share its findings and a report on the plan with the Big Island community and the Legislature; and

BE IT FURTHER RESOLVED that the report should include the status of the Department of Health's current efforts and any future plans to:

(1) Quantify the number of monitoring stations adequate for the entire island of Hawaii;

(2) Identify the locations for each monitoring station on the island of Hawaii;

(3) Determine the type, location, and frequency of testing, if any, that should be performed;

(4) Determine the system for monitoring at each station; and

(5) Develop a uniform emissions scale to alert residents of vog emissions levels; and

BE IT FURTHER RESOLVED that the Department of Health is requested to report its findings and the status of its activities, together with any recommendations for legislation, to the Legislature no later than twenty days before the convening of the Regular Session of 2006; and

BE IT FURTHER RESOLVED that certified copies of this Concurrent Resolution be transmitted to the Director of Health.

I hereby certify that the foregoing is a true and correct copy of Senate Concurrent Resolution No. 135 SD1, which was duly adopted by the Senate of the State of Hawaii on April 7, 2005, with the concurrence of the House of Representatives Dated: May 3, 2005

Assistant Clerk of the Senate

The Kilauea Volcano Adult Health Study, Hawai`i, U.S.A.
A Dissertation submitted to Oregon State University by Bernadette Mae Longo

Chapter II Manuscript

SO_2 AND FINE AEROSOL DISPERSION FROM THE KILAUEA PLUME, KAU DISTRICT, HAWAI`I, USA

Bernadette Mae Longo

Anita Grunder

Raymond Chuan

Annette Rossignol

GEOLOGY

The Geological Society of America
3300 Penrose Place, P.O. Box 9140
Boulder, Colorado 80301-9140, USA

Accepted November 2004
Publication March 2005

Abstract

Proximal ground-level assessment of sulfur dioxide gas and fine aerosol in the volcanic gas plume downwind from Kilauea volcano indicates high levels of both species. SO_2 and fine aerosol data were collected in the Kau district, from 37 to 74 km downwind from the eruption, and at a nonexposed control site in Hawi, Hawai`i. Typical trade winds and effusive eruption occurred during sampling in August–September 2003. Ambient SO_2 concentrations, measured with diffusion tubes, ranged from 6 to 34 ppbv and correlated negatively with altitude. In contrast, fine aerosol (≤0.3 μm size) concentrations, measured with a cascade impactor, ranged from 0.61 to 11.82 $\mu g/m^3$ and correlated positively with altitude. We attribute decrease of SO_2 with altitude to rapid oxidation as diurnal wind patterns blow the plume from oceanic terrain landward to more abundant oxidation sources. Aerosol increase with altitude likely reflects emission of H_2SO_4 from Kilauea, supplemented by oxidation of SO_2 in atmospheric hydrosols. Kau residents are exposed to volcanogenic pollutants at concentrations that warrant concern for adverse health effects.

Introduction

Effusive eruption at Kilauea volcano, Hawai`i, has persisted since 1986, releasing an average of 1600 tons of sulfur dioxide (SO_2) per day into the troposphere (Sutton & Elias, 2002). Unlike Plinian eruptions that send particles and gases into the stratosphere, effusive Hawaiian eruptions release gases into the lower troposphere where humans reside. An estimated 500 million humans live near active volcanoes worldwide (Baxter et al., 1999). The World Health Organization (WHO, 2001) has called for action to assess regional and local air pollution and the associated burden of disease. At the basaltic shield volcano Masaya, Nicaragua, Delmelle et al. (2002) mapped an increase in SO_2 in the gas plume with proximity to the vent, and concentrations were above WHO guidelines. Prevailing winds and local topography strongly affect plume dispersion. At Kilauea, little is known about the downwind dispersion of the plume's volcanic air pollutants or their effects on the human population. We present results from the first regional ground-level assessment of downwind air in the Kau district of the Big Island, Hawai`i (Figure 2.1), which was conducted as part of a study to measure chronic health effects.

Setting

Kilauea volcano's ongoing Pu`u `O`o–Kupaianaha East Rift eruption has been releasing a gaseous plume primarily composed of water, SO_2, and sulfate aerosols (Sutton et al., 2000). Degassing of SO_2 also occurs at Kilauea's summit both during eruption and in periods of quiescence (USGS, 1998).

The gas plume travels from the vent with prevailing northeastern Pacific trade winds through the marine boundary layer that is capped by a temperature inversion at ~1800 m above sea level (Figure 2.1). Below the inversion, humidity is high (70%–80%) and well distributed (WRCC, 2002). The plume travels southwesterly over the ocean around sloping Mauna Loa volcano and over South Point and eventually reaches the Kona Coast. In the Kau district, the trade winds blow to the southwest in the mornings and move inland and upslope by midday, bringing the plume over populated areas. Orographic effects produce afternoon rains in the upslope areas (Giambelluca &

Schroeder, 1998). Nighttime downslope winds carry the plume back over the ocean. The terrain in Kau is bare lava flows mixed with forest and farming and grazing lands.

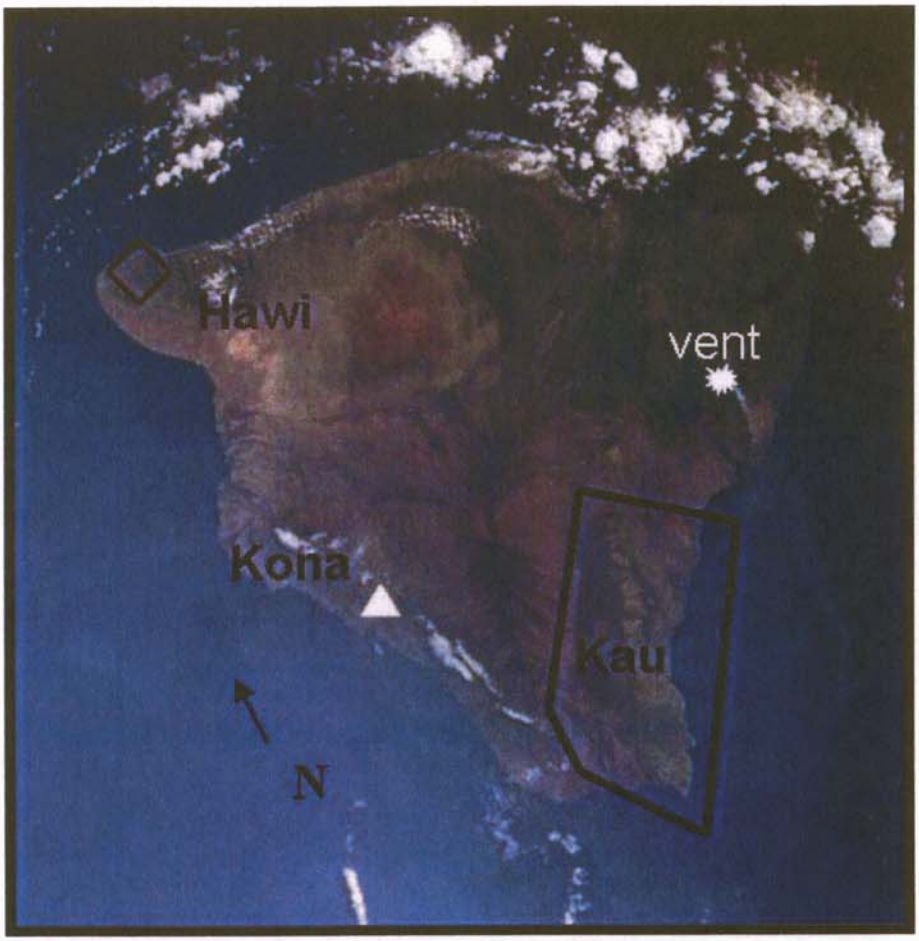

Figure 2.1 Location map of the Big Island (19°30′N, 155°30′W, 129 km wide east-west), Hawai`i, U.S.A. Exposed Kau cohort and unexposed Hawi cohort areas are outlined. The vent and plume are shown during trade-wind conditions. The white triangle marks the Kona air-monitor. Photograph credit: National Aeronautical and Space Administration, taken on STS-85 Space Shuttle mission August 1997.

Aircraft sampling of Kilauea's plume, using a laser optical counter, identified volcanic aerosol at ~0.3 μm; background marine aerosol was much larger at 2–3.0 μm (Clarke & Porter, 1991). Chuan (1995, 1997, 1998) characterized ground-based volcanic aerosols near the vent and at distal sites by using scanning electron microscopy and energy-dispersive X-ray analysis. Aqueous sulfuric acid aerosol (H_2SO_4), with geometric

mean diameters of 0.3 μm and 0.1 μm, comprised >80% of the total aerosol mass, and lesser elemental sulfur and silicates were measured at the Pu`u `O`o vent (Chuan, 1995). In the Kona Coast area, 130 km away, bimodal mass concentrations of volcanic aerosols peaked at 0.3 μm (H_2SO_4 and elemental sulfur) and at 1.7 μm (Na_2SO_4 and other sulfates), with background aerosols of NaCl (0.8 μm) and various silicates (>2 μm) (Chuan 1995, 1997, 1998). Aqueous HCl (0.8 μm) has been detected in Kona samples when lava-sea entry occurred (Chuan, 1995). SO_2 levels, monitored by the State of Hawai`i at a fixed site on the Kona Coast (Figure 2.1), are low. The lack of information on air quality in the vast Kau district, between the volcano and Kona, motivated this investigation.

Sampling Methodology and Conditions

SO_2 and fine volcanic aerosol data were collected during August and September 2003. We used a cohort model of exposed and unexposed areas with comparable geography and human populations. The exposed cohort lies 37–80 km downwind of the vent (Figure 2.1). The unexposed control cohort, Hawi, lies on the north side of the island. The sites have comparable rainfall, temperature, vegetation, and crops. Weather patterns during the three-week sampling period included typical Pacific trade winds (≤16 km/h), with the exception of a 48-h-long tropical storm that brought rains and winds up to 38 km/h in the Kau district. Inland areas were subject to afternoon rain showers on most days.

Lava flows erupted continuously during the sampling period from the base of Pu`u `O`o and tube breakouts. Lava did not enter the sea. Gas emissions for SO_2, by correlation spectrometer, averaged 1173 ± 335 t/d (metric tons per day) at the eruption site and 126 ± 25 t/d at the summit, in keeping with the recent 2 yr average of 1440 ± 470 t/d and 110 ± 30 t/d, respectively (USGS, unpublished HVO data from A.J. Sutton).

Sulfur dioxide sampling

SO_2 was measured with 70 SO_2-specific, passive diffusion tubes, made by Harwell Scientifics (Table 2.1). These tubes are used in urban air pollution and volcanology studies (Delmelle et al., 2002; Baxter et al., 1999; Nicholson et al., 1996) and are field verified for tropical climates. Cross sections of the vent plume and summit

degassing paths were captured by stratified sampling, using five gradient lines along the flank of Mauna Loa (Figure 2.2A) and six random sites. Six outdoor tubes served the control cohort. Outdoor tubes were placed 1.5–2.5 m above the ground, away from contamination sources or busy roads; exposure time ranged from 19 to 23 days. The method cannot resolve temporal variation of exposure.

Indoor tubes (N = 11) were placed in homes and facilities void of tobacco smoke, without air conditioning, and away from windows, doors, or stoves to measure indoor penetration of SO_2 on sensitive populations, such as children and medical patients. Two tubes for accuracy were placed for 20 days next to SO_2 pulse fluorescence monitors, and three sets of paired tubes in the cohorts were used to measure reliability (±5.5%). Outside the cohorts, two tubes were deployed near-source for 90 hours to capture SO_2 in the vent plume and summit path for mapping purposes.

Fine aerosol sampling

Aerosol samples (Table 2.2) were collected using a quartz crystal microbalance cascade impactor (QCM) with four geometric mean-diameter size ranges: ≥1.6 μm, 0.8 μm, 0.3 μm, and 0.1 μm (Chuan, 1995, 1997). Samples were collected at 1.5 m above ground for between 10 and 30 min; the QCM provides particle-size distribution and mass concentration of each size fraction with a precision of ±1 $\mu g/m^3$ within 5 min (Chuan, 1998). The method does not detect long-term exposure.

Concurrent with the SO_2 study, 54 fine aerosol samples were collected in the exposed cohort and 4 samples from the control cohort to use for background adjustment of exposed samples. To assess for a temporal pattern of plume migration with trade winds, samples were collected every 2 h for a 24 h period in the town of Pahala. During light variable wind conditions, 14 additional samples were collected in the exposed area.

Results

Both SO_2 and fine aerosol concentrations were elevated relative to background in the exposed cohort. Ambient SO_2 average concentration in the Kau district (17.8 ppbv, 45.2 $\mu g/m^3$) was 25 times that in control Hawi (0.7 ppbv, 1.8 $\mu g/m^3$) and ranged from 6 ppbv at Ocean View to 34 ppbv in the Na`alehu area (Table 2.1, Figure 2.2A). Aerosol findings reveal that adjusted concentrations of particles of ≤0.3 μm size ranged from 2 to

40 times greater in the Kau district (0.61–11.82 μg/m^3; Figure 2.2B) than in control Hawi (0.31 μg/m^3, Table 2.2). During variable winds, relatively higher concentrations of particles of ≤0.3 μm size were measured in Kau (Table 2.2).

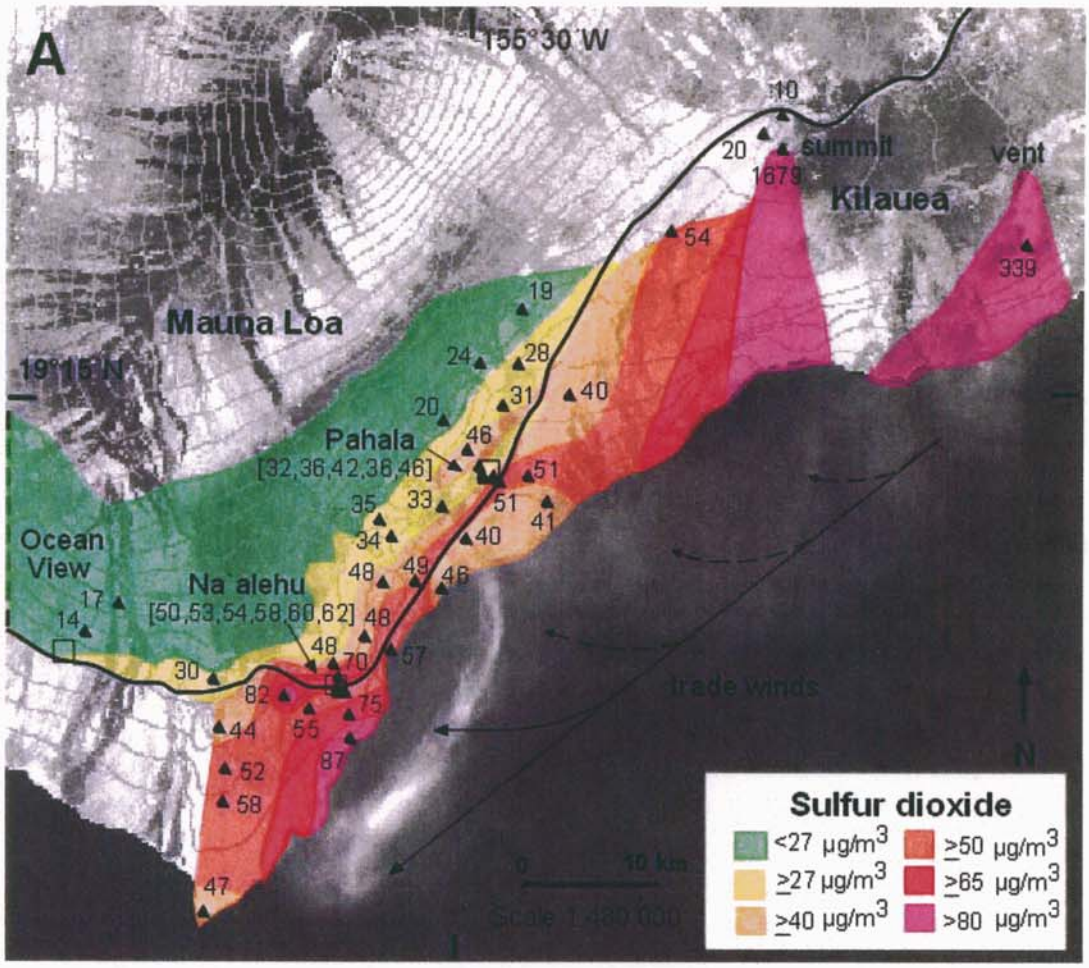

Figure 2.2A. Atmospheric SO_2 concentration shown via contour map of Kau District, Hawai`i, U.S.A. Colors and specific mass concentrations (in μg/m^3) are based on three-week exposure measurements taken in August–September 2003. Black triangles represent outdoor sample sites with corresponding concentration value. Base map uses elevation markers in 500 foot (152 m) intervals, provided by State of Hawai`i GIS (Geographic Information System) Program I-Map.

The concentration of SO_2 strongly decreases with altitude throughout the exposed cohort area (n = 43; Figure 2.2A) with and without accounting for distance from source

(partial correlation $r_{12,3} = -0.73$ and $r = -0.70$, $p < 0.001$, respectively). We considered instrument effects on SO_2 concentrations and used diffusion-coefficient corrections (up to –10% at highest altitude) and ppbv standardization for altitude (+2% to 4%); even for corrected data, altitude and concentration of SO_2 remained highly correlated. A high SO_2 measurement in the Na`alehu area (32 ppbv) occurs at a sharp topographic gradient, suggesting topographically induced stagnation of the plume (Figure 2.2A). Comparison of indoor and outdoor SO_2 testing yielded indoor/outdoor ratios ranging from 0.15 to 0.71, with a high value of 16.8 ppbv (Table 2.3). Locations with amounts >10 ppbv included the community hospital, grade school, and two residences of asthmatic individuals.

Volcanic aerosol has a pattern of peak concentrations at 0.3 and 0.1 μm; background aerosol has decreasing concentrations with decreasing size, as also noted by Chuan (1997, 1998). During trade winds ($n = 52$), concentration of aerosols (≤0.3 μm) and altitude were positively correlated, $r = +0.69$ ($p < 0.01$), even with accounting for distance, $r_{12,3} = +0.65$ ($p < 0.001$). Pahala was subject to an afternoon peak in ≤0.3 μm particles; the diurnal pattern of volcanic fine aerosol followed the trade-wind pattern for the windward slope of the Big Island (National Weather Service, 2003). Distal Ocean View had the highest concentrations of fine aerosols during dry and wet conditions, morning and afternoons, as well as during trade and variable wind periods. Aerosol sampling along coastal areas detected no volcanic aerosols during trade winds, similar to Chuan's finding in 1997.

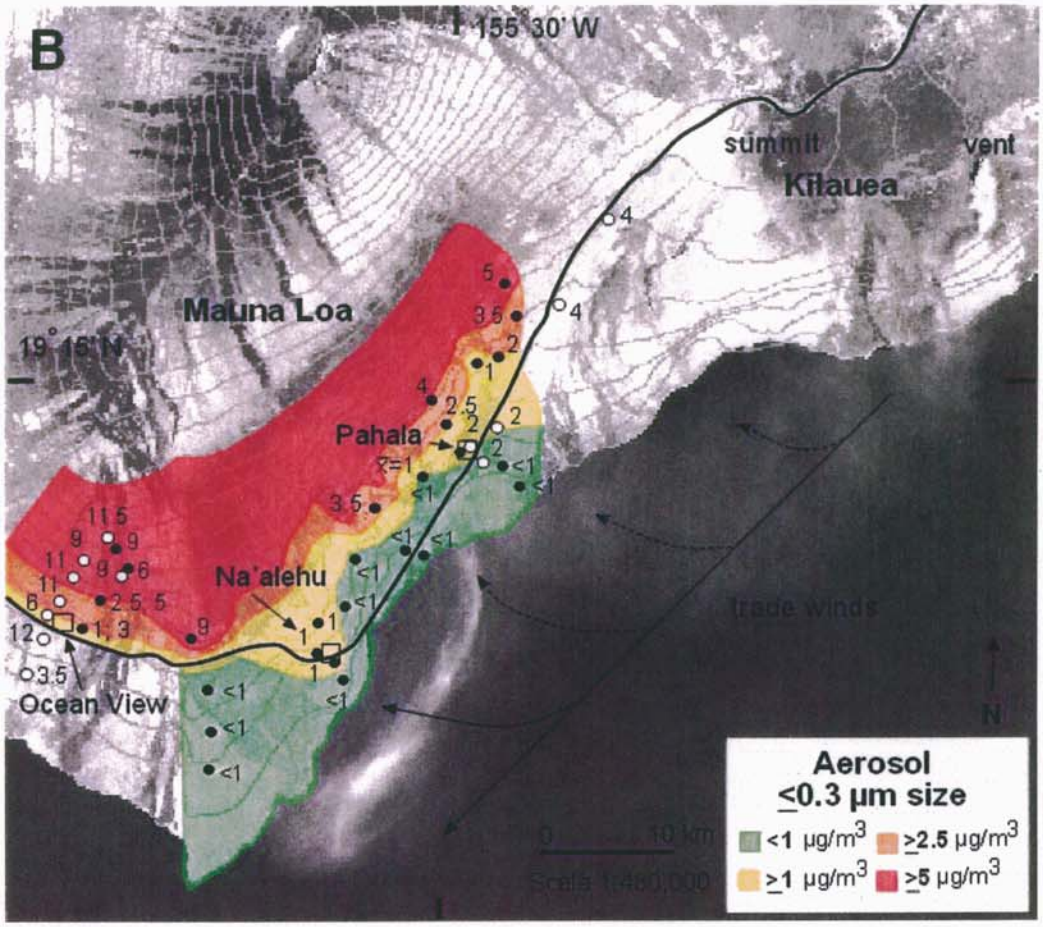

Figure 2.2B. Atmospheric fine aerosol (≤0.3 µm) concentration shown via contour map of Kau District, Hawai'i, U.S.A. Colors and specific concentrations (in µg/m^3) are based on grab sample measurements taken in September 2003. Black circles denote samples collected during trade-wind conditions. White circles denote samples during variable winds. Base map uses elevation markers in 500 foot (152 m) intervals, provided by State of Hawaii GIS Program I-Map.

Discussion

The results of SO_2 and fine aerosol measurements in the Kau district, downwind of Kilauea volcano, indicate that the area and population are exposed to volcanic air pollution. We first address the applicability of the study, the implications on human health, and finally the altitudinal variations of these data.

Applicability of the study

Sampling was done during conditions representative of typical weather and volcanic activity at Kilauea, thereby laying the groundwork for public health investigation. Assessment of the SO_2 concentrations is conservative, because there was rainfall, which scrubs SO_2 (e.g., Poas volcano, Nicholson et al., 1996), and no explosive lava fountaining occurred, which would increase SO_2 emissions. Similarly, aerosol assessment is conservative because we emphasize the exposure burden of fine aerosols ($\leq$0.3 μm) and not total exposure of particulate matter (<2.5 μm, $PM_{2.5}$). Ambient air likely also carries larger volcanic sulfates, between 0.8 μm and 2.5 μm (Chuan, 1997, 1998), thereby further exposing the population. High humidity at lower elevations may also hygroscopically enlarge fine aerosols beyond the range of the QCM instrument.

Air quality and health

Sulfur dioxide is a known respiratory irritant to sensitive populations (e.g., people with respiratory disease, asthma, or advanced in age; WHO, 1979, 2000). Sulfate aerosols, however, can negatively affect both sensitive and general populations by inducing respiratory tract irritation that can alter lung defenses, such as airway reactivity and mucociliary transport (Koenig, 2000; Holgate et al., 1999).

The two decades of eruption at Kilauea exceed the seven-year time frame used to define a chronic exposure. Comparisons to long-term exposure standards are justified, because typical exposure conditions prevailed during our study. Only two samples in the Na`alehu area exceeded the U.S. Environmental Protection Agency (EPA, 1990) annual standard for $SO_2$ (80 $\mu g/m^3$), but using the WHO annual guideline for $SO_2$ of 50 $\mu g/m^3$ (WHO, 2000), the Na`alehu area and most coastal areas are at or above the guideline (Figure 2.2). The summit tube placed 0.5 m above the ground at a common visitor's site recorded 1679 $\mu g/m^3 \pm 100$ $\mu g/m^3$, well above the WHO 10 minute SO_2 guideline of 500 $\mu g/m^3$ (WHO, 2000). Although specific for SO_2, H_2S gas may have contaminated the tube. Further work is warranted because small children may be most at risk.

Many populated areas in Kau, even indoors, are above the acute minimal risk level (MRL) for SO_2 (Fig. 2.2). The SO_2 MRL is 10 ppbv, or ~27 $\mu g/m^3$, set by the U.S. Agency for Toxic Substances and Disease Registry (ATSDR, 1998) for an acute

exposure of <14 days, a time frame covered by these data. An MRL is a public health guideline, set for sensitive members of the population, that estimates the daily human exposure to a hazardous substance that is likely to be without appreciable risk of adverse health effects over a specific time period. Exposure to concentration levels above an MRL do not necessarily mean that adverse health effects will occur.

In Ocean View, amounts of ≤0.3 μm aerosol as high as 9 $\mu g/m^3$ in trade winds and 11 $\mu g/m^3$ in variable winds were recorded (Figure 2.3). Lioy and Waldman (1989) defined a sulfate aerosol pollution "event" as a concentration of ≥5 $\mu g/m^3$. If H_2SO_4, at ≤0.3 μm, is assumed to be the major aerosol component of these samples (Chuan, 1995, 1997, 1998), then higher-altitude downwind areas may be undergoing concentrations above the 1 yr chronic reference exposure level of 1 $\mu g/m^3$ (California OEHHA, 2001).

Geographic variations of Kilauea's plume

The Kilauea plume affects the Kau district and is not restricted to oceanic terrain. SO_2 concentrations did not decrease strongly with distance from source as expected. Instead, the highest SO_2 concentrations were in the Na`alehu area, ~68 km from the source, where the plume passes over oceanic terrain. Sampling of a lateral part of the plume partially accounts for this $SO_2$ pattern. At Masaya volcano, Nicaragua, $SO_2$ concentrations are negligible at down-plume distances comparable to the distance Na`alehu is from the source, despite similar emission rates (Delmelle et al., 2002). Although wind-speed differences would influence this comparison, we argue that marine vs. land effects dominate.

A major mechanism for conversion of SO_2 is the hydroxyl radical (OH·), which readily reacts in the gas phase by photoinitiation to form H_2SO_4 (ATSDR, 1998; Seinfeld, 1986). Availability of OH· in ambient air depends on the presence of competitors. Oceanic terrain is not a major source for available OH· (Seinfeld & Pandis, 1998) because dimethyl sulfide reacts predominantly with OH·, limiting availability of OH· for oxidation of SO_2.

Aerosol increased with altitude regardless of distance from source. We propose that primary release of H_2SO_4 from the eruption site contributes to the downwind aerosol burden to combine with SO_2 oxidation mechanisms enhanced on land. At the Pu`u `O`o

vent, Chuan (1995) measured H_2SO_4 in ambient air samples. Moreover, primary released sulfates have been measured at other degassing basaltic volcanoes (Andres et al., 1993; Allen et al., 2002). At Kilauea, Porter et al. (2002) estimated the SO_2 oxidation half-life to be 6.0 hours, under the assumption that no H_2SO_4 was released. Therefore, an unknown percentage of primary sulfates are likely released.

When the diurnal trade winds move inland and upslope, dissipating the plume horizontally and vertically into new air masses under the 1800 m inversion, SO_2 oxidation may be enhanced with atmospheric water processes and available OH· fed by the photolysis of nitroxy anions NO_2^- and NO_3^- and H_2O_2 (Pasiuk-Bronikowska, 2002). Within clouds and fogs, hydrogen peroxide (H_2O_2) is an effective and fast oxidant of SO_2 independent of pH (Seinfeld & Pandis, 1998). SO_2 is absorbed into hydrosols (clouds, fog, or rain droplets) where aqueous-phase oxidation occurs by H_2O_2 producing H_2SO_4 (Seinfeld & Pandis, 1998). Concentrations of H_2O_2 are low near the surface and rise to a maximum at the top of the boundary layer (Seinfeld & Pandis, 1998), where cloud formation is common in Hawai`i.

Conclusions

After 22 years of eruption at Kilauea, this environmental investigation found volcanogenic SO_2 and fine aerosol at concentrations that justify public health concern for communities along the plume path. We posit that the striking decrease of SO_2 with altitude results as wind sweeps the plume landward to react with land-derived oxidants and upward to interact with atmospheric hydrosols. Increase of aerosol with altitude is likely from a primary emission from Kilauea and oxidation of SO_2. The strong geographic variability of pollutant concentrations underscores the need for regional sampling prior to point monitoring in exposure assessments. Further work is warranted to investigate oceanic vs. land interactions with the plume and potential adverse effects on the human population.

Acknowledgements

We thank the residents of Kau and Hawi, the Hawaiian Volcano Observatory, the Kau district schools, and the Kau Hospital for permission to sample. We thank the following contributors: P. Baxter, M.D., R. Bibilone, T. Elias, J. Green, M.D., A.J. Kimerling, A. Longo, C. Neumann, W.I. Rose, A.J. Sutton, R. Vong, and J.K. Yun.

Table 2.1. Atmospheric SO_2 Concentration Data. These data were obtained from Harwell Scientifics passive samplers during a three-week exposure in August - September, 2003. Field reliability tested by paired samples was ± 5.5%. An altitude flux correction (Larson and Vong, 1990) was made to the mass concentration lab data ($\mu g/m^3$); thereby considering the effects of changes in pressure and temperature on the tube diffusivity at each sample site. The estimated relative error was + 8% to11% to the criterion instrument (pulse fluorescence monitor) (U.S. National Park Service, 2004). ppbv =[(8.314E-2)*T/pMSO2)*(Fg/m^3 *103)]

SO_2 Diffusion Tube Data

Location	Altitude meters/feet		temp k	Diffusivity ratio pres. mb	D/D0	mass concentration Lab $\mu g/m^3$	$\mu g/m^3$ corrected	Gas mixing ratio ppbv ppbv altitude adjusted	Lab ppbv 1 atm. /20C	ppbv % change
Park SO_2 monitor (3.88 ppbv)	1215	3,986	289.28	872.06	**1.10**	11.3	**10.26**	**4.42**	4.3	2.76
HVO SO_2 monitor (7.69 ppbv)	1123	3,684	290.00	882.73	**1.09**	21.8	**19.95**	**8.51**	8.2	3.69
Summit plume – Halemaumau Crater	1110	3,642	290.12	884.24	**1.09**	1833.0	**1679.08**	**715.67**	688.0	3.87
Eruption plume – Chain of Craters Rd.	518	1,700	294.86	952.91	**1.04**	354.0	**339.42**	**136.43**	133.0	2.52
Mauna Iki's summit	924	3,032	291.61	905.82	**1.08**	58.4	**54.30**	**22.71**	22.0	3.12
Exposed cohort										
Kapapala trend	981	3,220	291.15	899.20	**1.08**	20.1	**18.60**	**7.83**	7.5	4.16
Kapapala trend	668	2,192	293.66	935.51	**1.05**	29.3	**27.78**	**11.33**	11.0	2.91
Kapapala trend	509	1,670	294.93	953.96	**1.04**	41.3	**39.63**	**15.91**	15.5	2.60
Wood Valley	750	2,460	293.00	926.00	**1.06**	25.5	**24.03**	**9.88**	9.6	2.81
Pahala/Wood Valley	549	1,800	294.61	949.32	**1.05**	32.0	**30.61**	**12.34**	12.0	2.77
Pahala trend	792	2,600	292.66	921.13	**1.06**	21.6	**20.29**	**8.37**	8.1	3.28
Pahala trend	500	1,640	295.00	955.00	**1.04**	47.7	**45.80**	**18.38**	17.9	2.59
Pahala trend house	366	1,200	296.07	970.54	**1.03**	32.9	**31.89**	**12.64**	12.3	2.68
Pahala trend school	287	940	296.70	979.71	**1.03**	37.1	**36.16**	**14.23**	13.9	2.30
Pahala trend house	274	900	296.81	981.22	**1.02**	42.9	**41.85**	**16.45**	16.1	2.11

Table 2.1. Atmospheric SO_2 Concentration Data (Continued).

Location (exposed)	Altitude meters / feet		temp k	pres. mb	D/D0	Lab µg/m³	µg/m³ corrected	ppbv altitude adjusted	Lab ppbv 1 atm. / 20C	ppbv % change
Pahala trend house	274	900	296.81	981.22	**1.02**	36.7	**35.81**	**14.07**	13.8	1.92
Pahala trend hospital	250	820	297.00	984.00	**1.02**	46.7	**45.64**	**17.89**	17.5	2.21
Pahala trend hospital	244	800	297.05	984.70	**1.02**	52.0	**50.84**	**19.92**	19.5	2.12
Pahala trend	229	750	297.17	986.44	**1.02**	51.9	**50.79**	**19.88**	19.5	1.90
Pahala trend	144	473	297.85	996.30	**1.02**	41.9	**41.25**	**16.02**	15.7	1.99
Pahala/Puna	396	1,300	295.83	967.06	**1.03**	34.3	**33.18**	**13.18**	12.9	2.16
Pahala/Puna	122	400	298.02	998.85	**1.01**	40.3	**39.73**	**15.40**	15.1	1.95
Punalu'u trend	549	1,800	294.61	949.32	**1.05**	36.5	**34.92**	**14.08**	13.7	2.68
Punalu'u trend	396	1,300	295.83	967.06	**1.03**	35.1	**33.95**	**13.49**	13.2	2.17
Punalu'u trend	90	296	298.28	1002.56	**1.01**	49.1	**48.51**	**18.75**	18.4	1.86
Punalu'u trend	42	139	298.66	1008.13	**1.01**	46.6	**46.19**	**17.78**	17.5	1.56
Punalu'u area	390	1,280	295.88	967.76	**1.03**	49.6	**48.00**	**19.06**	18.6	2.43
Honu'apo area	443	1,452	295.46	961.61	**1.04**	50.1	**48.30**	**19.28**	18.8	2.48
Honu'apo	60	197	298.52	1006.04	**1.01**	57.6	**57.03**	**21.98**	21.6	1.73
Na'alehu trend	572	1,877	294.42	946.65	**1.05**	49.7	**47.46**	**19.18**	18.6	3.01
Na'alehu trend house	232	760	297.14	986.09	**1.02**	70.8	**69.28**	**27.12**	26.6	1.91
Na'alehu trend house	213	700	297.30	988.29	**1.02**	51.0	**49.97**	**19.53**	19.1	2.19
Na'alehu trend house	207	680	297.34	988.99	**1.02**	60.9	**59.69**	**23.31**	22.8	2.21
Na'alehu trend school	195	640	297.44	990.38	**1.02**	63.3	**62.10**	**24.23**	23.7	2.17
Na'alehu trend school	195	640	297.44	990.38	**1.02**	54.0	**52.97**	**20.67**	20.2	2.26
Na'alehu trend clinic	195	640	297.44	990.38	**1.02**	55.2	**54.15**	**21.13**	20.7	2.02
Na'alehu trend clinic	195	640	297.44	990.38	**1.02**	59.4	**58.27**	**22.73**	22.3	1.91
Na'alehu trend	183	600	297.54	991.77	**1.02**	76.2	**74.81**	**29.16**	28.6	1.91
Na'alehu trend	152	500	297.78	995.37	**1.02**	88.0	**86.58**	**33.65**	33.0	1.93
Waiohinu Village	305	1,000	296.56	977.62	**1.03**	84.6	**82.36**	**32.46**	31.8	2.02
Kipuka Nahuaopala	238	780	297.10	985.39	**1.02**	56.2	**54.97**	**21.53**	21.1	1.99

Table 2.1. Atmospheric SO_2 Concentration Data (Continued).

Location (exposed)	Altitude meters / feet		temp k	pres. mb	D/D0	Lab µg/m³	µg/m³ corrected	ppbv altitude adjusted	Lab ppbv 1 atm. / 20C	ppbv % change
South point trend	742	2,434	293.06	926.93	**1.06**	31.4	**29.61**	**12.16**	11.8	2.97
South point trend	506	1,660	294.95	954.30	**1.04**	45.7	**43.86**	**17.61**	17.1	2.89
South point trend	378	1,240	295.98	969.15	**1.03**	54.0	**52.30**	**20.75**	20.0	3.61
South point trend	277	909	296.78	980.87	**1.03**	59.3	**57.84**	**22.74**	22.3	1.92
South point trend	15	50	298.88	1011.26	**1.01**	46.9	**46.57**	**17.88**	17.6	1.57
Ocean View	1244	4,082	289.05	868.70	**1.10**	18.4	**16.67**	**7.21**	7.0	2.85
Ocean View	866	2,842	292.07	912.54	**1.07**	14.8	**13.82**	**5.75**	5.6	2.57
Exposed cohort Average					**1.03**	46.48	**45.21**	**17.84**	17.43	2.35

Control Cohort Location	Altitude meters/feet		temp k	pres. mb	D/D0	Lab µg/m³	µg/m³ corrected	ppbv altitude adjusted
Hawi - north	146	480	297.83	996.06	1.02	<1.2		
Hawi - west	195	640	297.44	990.38	1.02	1.8	**1.77**	**0.69**
Hawi - south	268	880	296.86	981.91	1.02	1.2	**1.17**	**0.46**
Hawi - downtown	183	600	297.54	991.77	1.02	3.0	**2.95**	**1.15**
Hawi - east, pair	158	520	297.74	994.67	1.02	1.2	**1.18**	**0.46**
Hawi - east, pair	158	520	297.74	994.67	1.02	<1.2		
Control cohort Average						1.8	**1.77**	**0.69**

Table 2.2. Atmospheric Fine Particle Aerosol Data September, 2003. Precision is ± 1 μg/m^3.

AEROSOL SAMPLE LOCATION & ALTITUDE	DATE /TIME	SAMPLING CONDITIONS (wind, speed, climate, visual)	Count total	0.8 μm	0.3 μm	0.1 μm	≤ 0.3 μm	Adjusted ≤ 0.3 μm
Exposed Cohort Area			μg/m^3	μg/m^3	μg/m^3	μg/m^3	μg/m^3	μg/m^3
Kapapala 981 m	9/15/03, 1645	trades 5 swirls, overcast, pre-rain, haze	5.87	0.69	3.52	1.66	5.18	**4.87**
Kapapala 792 m	9/15/03, 1445	trades <5, overcast, pre-rain, haze	4.55	0.75	2.56	1.24	3.80	**3.49**
Kapapala 668 m	9/15/03, 1400	trades 5-10, overcast	2.78	0.63	1.75	0.38	2.13	**1.82**
Wood Valley 750 m	9/11/03, 0737	trades <5, clear sun	1.64	0.73	0.49	0.42	0.91	**0.60**
Pahala Trend 144 m	9/20/03, 1520	trades 5, overcast	1.42	0.69	0.57	0.14	0.71	**0.40**
Pahala Trend 229 m	9/20/03, 1422	trades <5, overcast	1.70	1.04	0.41	0.24	0.65	**0.34**
Pahala Trend Hospital 244 m	9/12/03, 2037	trades <5, partial clouds, dark	13.61	0.94	8.81	3.86	12.67	**12.36**
Pahala Trend Base 274 m	9/9/03, 0600	trades <5, sunrise, clear	1.61	0.47	1.10	0.03	1.13	**0.82**
	0815	trades <5, sun, clear	1.97	0.66	0.70	0.60	1.30	**0.99**
	1005	trades <5, partial clouds	1.46	0.58	0.32	0.56	0.88	**0.57**
	1400	trades 5-10, overcast, pre-rain	1.61	0.92	0.47	0.20	0.67	**0.36**
	1600	trades 5, overcast, post-rain	3.30	2.12	0.85	0.32	1.17	**0.86**
	1800	trades 5, overcast, spotty sun, pre-rain	2.17	1.23	0.61	0.32	0.93	**0.62**
	2000	trades <5, overcast, dark, no rain	1.11	0.46	0.42	0.22	0.64	**0.33**
	2200	trades 5, overcast, dark, no rain	4.67	0.75	3.44	0.47	3.91	**3.60**
	2300	trades <5, overcast, dark, no rain	2.15	0.00	1.45	0.70	2.15	**1.84**
	0300	trades <5, overcast, dark, no rain	1.95	1.19	0.51	0.24	0.75	**0.44**
Average for 24-hour sample		low trades with rain	**2.20**	**0.84**	**0.99**	**0.37**	**1.35**	**1.04**
	9/10/03, 2008	trades calm, overcast, dark, post-rain	5.41	0.92	3.34	1.14	4.48	**4.17**
	9/10/03, 2210	trades calm, moonbeams, partial cloud	1.87	0.71	1.00	0.16	1.16	**0.85**
	9/12/03, 1530	trades 5-10, overcast, pre-rain	1.53	0.78	0.57	0.17	0.74	**0.43**
	9/12/03, 1838	trades 5-10, overcast, sunset, post-rain	6.41	1.75	3.43	1.22	4.65	**4.34**
	9/12/03, 2002	trades <5, partial clouds, dark	6.71	0.92	3.56	2.21	5.77	**5.46**

Table 2.2. Atmospheric Fine Particle Aerosol Data, September 2003 (Continued).

AEROSOL SAMPLE LOCATION & ALTITUDE		DATE /TIME	SAMPLING CONDITIONS (wind, speed, climate, visual)	Count total	0.8 µm	0.3 µm	0.1 µm	≤ 0.3 µm	Adjusted ≤ 0.3 µm
Exposed Cohort Area				µg/m3	µg/m3	µg/m3	µg/m3	µg/m3	µg/m3
Pahala (continued)	274 m	9/13/03, 2308	trades <5, moon & stars, clear night	4.27	1.72	2.21	0.34	2.55	**2.24**
		9/14/03, 1830	trades 5-10, overcast, sunset, no rain	0.95	0.25	0.40	0.30	0.70	**0.39**
		9/14/03, 2030	trades <5, overcast, dark, no rain	2.69	1.58	0.76	0.34	1.10	**0.79**
		9/15/03, 2030	trades calm, stars clear, dark	1.96	0.56	0.96	0.44	1.40	**1.09**
		9/16/03, 1800	trades <5, overcast, no rain	1.34	0.65	0.51	0.18	0.69	**0.38**
		9/17/03, 1949	trades <5, clear night	3.11	1.05	1.21	0.84	2.05	**1.74**
Average of evening samples			trades, some rain, typical evenings	**3.30**	**0.99**	**1.63**	**0.67**	**2.30**	**1.99**
Pahala Trend	500 m	9/11/03, 0837	trades 5, sun, haze	3.25	0.58	1.25	1.42	2.67	**2.36**
		9/11/03, 1345	trades 5-10, overcast, clear	1.35	0.11	1.11	0.11	1.22	**0.91**
Pahala Trend Upper	792 m	9/18/03, 1007	trades, <5, overcast, pre-rain, haze	5.41	1.30	2.40	1.71	4.11	**3.80**
Pahala/Punalu'u	396 m	9/11/03, 1157	trades <5, overcast	1.04	0.20	0.51	0.32	0.83	**0.52**
Punalu'u Trend	42 m	9/10/03, 0950	trades <5, partial clouds	<.01	0.00	0.00	0.00	0.00	**0.00**
Punalu'u Trend	90 m	9/10/03, 1025	trades 5-10, sun, clouds area	0.50	0.23	0.06	0.21	0.27	**0.00**
Punalu'u Trend	396 m	9/11/03, 0944	trades 5-10, partial sun, haze	4.48	0.75	1.79	1.93	3.72	**3.41**
Punalu'u area	390 m	9/11/03, 1132	trades <5, partial clouds, pre-rain, haze	1.29	0.57	0.41	0.29	0.70	**0.39**
Honu'apo area	443 m	9/11/03, 1029	trades 10, clear sun	1.61	0.52	0.63	0.44	1.07	**0.76**
Na'alehu Trend	152 m	9/18/03, 1236	trades 10, overcast	1.69	1.04	0.41	0.23	0.64	**0.33**
Na'alehu Trend school	195 m	9/12/03, 1708	trades <5, overcast	3.31	1.95	0.59	0.76	1.35	**1.04**
Na'alehu (end of town)	259 m	9/12/03, 1637	trades 5, overcast	2.75	1.45	0.70	0.60	1.30	**0.99**
		9/22/03, 1515	trades <5, partial clouds	1.05	0.95	0.06	0.02	0.08	**0.00**
Na'alehu Trend Upper	572 m	9/11/03, 1053	trades 10, sun, partial clouds	1.64	0.52	0.67	0.44	1.11	**0.80**
South point Trend	277 m	9/10/03, 1526	trades 15, partial clouds, clear	1.75	0.79	0.48	0.47	0.95	**0.64**
South point Trend	378 m	9/10/03, 1452	trades 10, partial clouds, clear	1.25	0.63	0.29	0.32	0.61	**0.30**
South point Trend	506 m	9/10/03, 1426	trades 5-10, sun, partial clouds, clear	1.09	0.48	0.21	0.40	0.61	**0.30**

Table 2.2. Atmospheric Fine Particle Aerosol Data, September 2003 (Continued).

AEROSOLSAMPLE LOCATION & ALTITUDE		DATE /TIME	SAMPLING CONDITIONS (wind, speed, climate, visual)	Count total	0.8 µm	0.3 µm	0.1 µm	≤ 0.3 µm	Adjusted ≤ 0.3 µm
Exposed Cohort Area				µg/m3	µg/m3	µg/m3	µg/m3	µg/m3	µg/m3
South point Trend	742 m	9/17/03, 1739	trades 5-10, overcast, haze	9.31	0.31	8.09	0.89	8.98	**8.67**
		9/20/03, 1041	trades 5, partial clouds, haze	9.16	0.72	4.03	4.40	8.43	**8.12**
Ocean View	634 m	9/10/03, 1645	trades 5-10, pre-rain, clear	2.12	0.68	1.07	0.37	1.44	**1.13**
		9/12/03, 1017	trades 5-10, partial clouds, clear	3.79	0.40	1.66	1.72	3.38	**3.07**
Ocean View	930 m	9/10/03, 1720	trades 5-10, pre-rain	4.93	2.00	2.33	0.59	2.92	**2.61**
		9/12/03, 1045	trades 5, partial clouds, clear	5.71	0.58	3.07	2.06	5.13	**4.82**
Ocean View	1302 m	9/10/03, 1805	trades 5-10, overcast, pre-rain, haze	8.54	6.37	1.95	0.20	2.15	**1.84**
		9/12/03, 1115	trades 5-10, partial clouds, haze	6.88	0.30	2.88	3.70	6.58	**6.27**
Ocean View	1393 m	9/12/03, 1140	trades 5 circular, partial clouds, haze	10.70	1.23	5.63	3.84	9.47	**9.16**
Exposed Cohort Area samples during variable winds									
Ocean View	1487 m	9/23/03, 1524	Variables 5, upslope, sun, haze	13.04	1.21	10.75	1.07	11.82	**11.51**
Ocean View	1244 m	9/23/03, 1502	Variables 5, trade-like, overcast, haze	10.39	1.04	8.06	1.28	9.34	**9.03**
Ocean View	1243 m	9/23/03, 1347	Variables 5, upslope, sun, clouds, haze	10.35	1.36	7.58	1.40	8.98	**8.67**
Ocean View	1049 m	9/23/03, 1607	Variables 5, upslope, sun, clouds	12.33	1.07	9.72	1.53	11.25	**10.94**
Ocean View	866 m	9/23/03, 1658	Variables <5, sun, distal haze	12.81	1.39	10.4	1.02	11.42	**11.11**
Ocean View	698 m	9/23/03, 1632	Variables <5, upslope, sun, wispy, haze	7.32	1.07	5.47	0.77	6.24	**5.93**
		9/23/03, 1807	Variables calm, sun, haze & sunset color	10.50	1.59	8.09	0.81	8.90	**8.59**
Ocean View	561 m	9/23/03, 1720	Variables 5, trade-like to west, sun, haze	12.95	1.39	10.71	0.83	11.54	**11.23**
Ocean View	305 m	9/23/03, 1742	Variables 5-10, trade-like, sun, haze	4.62	0.69	3.32	0.59	3.91	**3.60**
Kapapala Highway	762 m	9/24/03, 1306	Variables 5 inland, overcast	5.43	0.94	3.39	1.10	4.49	**4.18**
Kapapala trend Hwy	549 m	9/24/03, 1240	Variables 5 inland upslope, overcast	5.03	0.79	3.58	0.66	4.24	**3.93**
North of Pahala Hwy	305 m	9/24/03, 1341	Variables 5-10 inland, overcast	3.03	0.52	1.87	0.64	2.51	**2.20**
Pahala Trend Hwy	244 m	9/24/03, 1408	Variables <5 upslope & northerly, traffic	3.57	1.15	1.27	1.13	2.40	**2.09**
Pahala Trend (Base)	274 m	9/24/03, 1152	Variables 5 inland, overcast, haze	2.79	0.52	1.79	0.48	2.27	**1.96**

Table 2.2. Atmospheric Fine Particle Aerosol Data, September 2003 (Continued).

AEROSOL SAMPLE LOCATION & ALTITUDE	DATE /TIME	SAMPLING CONDITIONS (wind, speed, climate, visual)	Count total	0.8 µm	0.3 µm	0.1 µm	≤ 0.3µm	Adjusted ≤ 0.3µm
Hawi – downtown 183 m	9/19/03, 1107	trades 10-15, clear sun	1.10	0.69	0.25	0.15	0.40	
Hawi - end of town 195 m	9/19/03, 1419	trades 10-15, clear sun	1.02	0.63	0.20	0.18	0.38	
Hawi - north street 146 m	9/19/03, 1155	trades 10-15, clear sun	0.77	0.46	0.14	0.16	0.30	
Hawi - south high elev. 268 m	9/19/03, 1232	trades 10-15, patchy clouds	0.70	0.56	0.02	0.12	0.14	
Average for Control site			**0.90**	**0.59**	**0.15**	**0.15**	**0.31**	
Kona Area								
Captain Cook 561 m	9/17/03, 1547	trades <5, overcast, pre-rain, haze	3.55	0.63	2.13	0.78	2.91	**2.60**
Kipahoehoe reserve	9/17/03, 1656	trades <5, overcast, pre-rain, haze	7.62	1.04	5.50	1.07	6.57	**6.26**

Table 2.3. Indoor/Outdoor (I/O) Ratios of SO_2 in the Kau District of the Big Island, Hawai`i, U.S.A. Sulfur Dioxide concentration was measured by Harwell Scientifics passive diffusion tube samplers exposed for three weeks in August-September, 2003.

I/O RATIO	INDOOR $\mu g/m^3$	OUTDOOR $\mu g/m^3$	INDOOR ppbv	LOCATION DESCRIPTION
0.69	43.0	62.1	16.8	School cafeteria
0.59	31.4	53.0	12.3	School classroom
0.56	33.6	59.7	13.1	Plantation house
0.68	34.0	50.0	13.3	Plantation house
0.15	8.1	55.0	3.2	House
0.71	36.1	50.8	14.1	Hospital dayroom
0.65	29.8	45.6	11.7	Hospital clinic
0.69	24.9	36.2	9.8	School classroom
0.23	7.2	31.9	2.8	House
No data				2 tubes disturbed

Field Observation Notes

August – September 2003

Visible harmful effects attributed to the sulfurous air pollution were observed in the environment. Street signs in Ocean View had increasing corrosion with a rise in altitude. Rusting of metal roofs and machinery was noted throughout the exposed cohort area. Leaf damage was observed on coffee plants in the upper Pahala area.

Interviews with local residents revealed conflicting experiences. A farmer in Pahala reported abundant crops from a variety of vegetables, whereas the macadamia nut production in the area was felt to have a decreased yield since the eruption. Other farmers of vegetables and coffee described high yields and no detrimental effects on crops. Residents from the Na`alehu area stated that flora was affected by a decreased ability to produce or early drop of fruit or nuts, chlorosis on foliage, and parasite infestation in certain areas. A long-time resident of Kau District described indicator plants as yellow/white ginger and blackberries. The author confirmed this by field observation.

Local ranchers in the Pahala area described the plume's behavior as moving inland and swirling every afternoon during typical trade winds. Effects of burning eyes and breathing irritation were reported by ranchers, whose outdoor exposure averaged 12 hours a day. Farmers in the upper Punalu`u area described the plume as passing westerly through high altitude hill areas each day, rapid rusting of their machinery as compared to other Big Island areas, and significant respiratory and eye irritation when lava-sea entry occurs (likely HCl aerosol from laze).

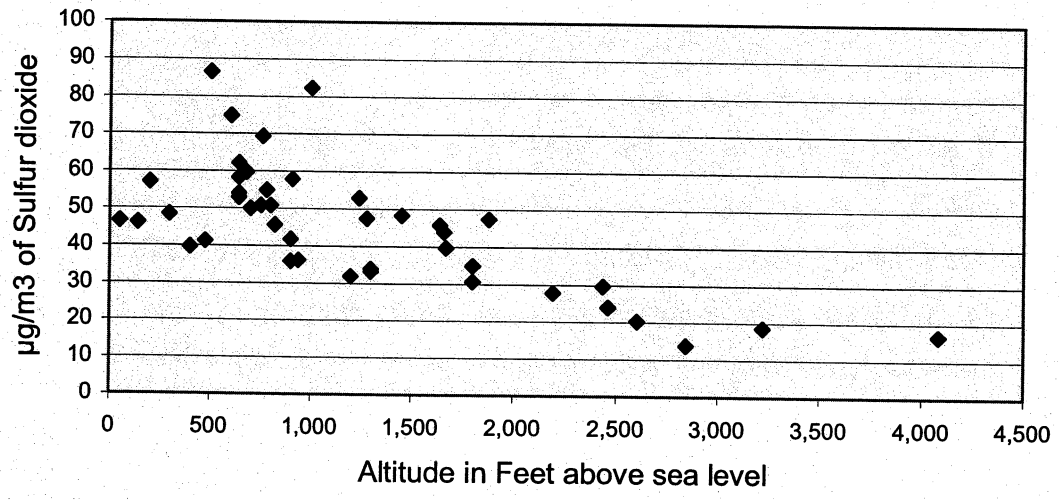

Figure 2.3. Correlation scatter plot of SO_2 mass concentration ($\mu g/m^3$) and altitude. ($r = -.70$, $p < 0.01$, $N = 43$)

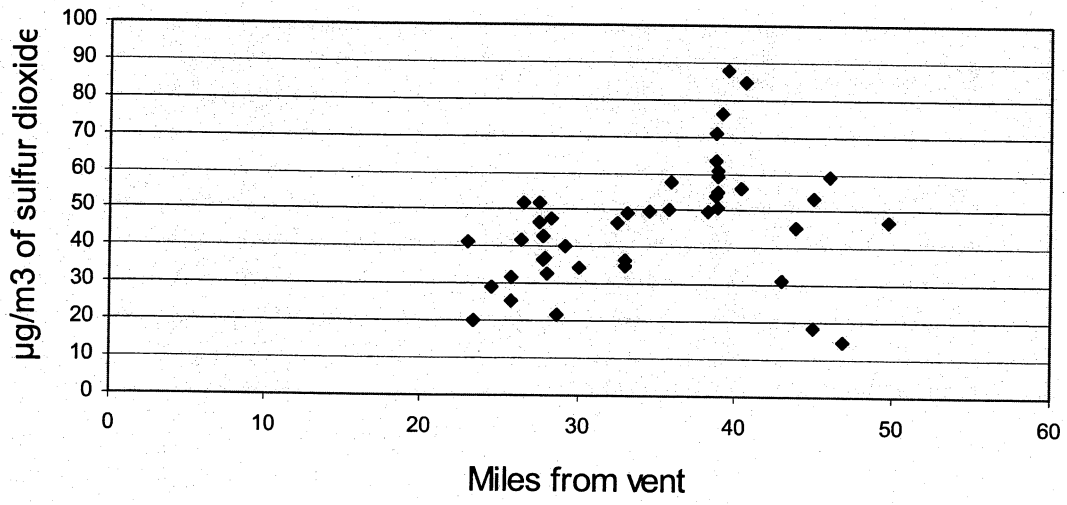

Figure 2.4. Correlation scatter plot of SO_2 mass concentration ($\mu g/m^3$) and distance from source. ($r = +.35$, $p < 0.05$, $N = 43$)

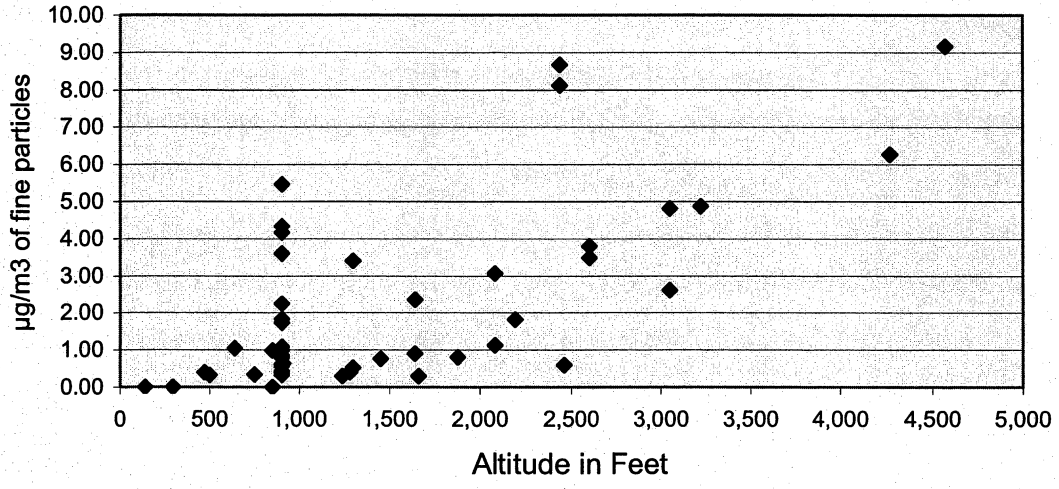

Figure 2.5. Correlation scatter plot for fine particles (≤0.3 µm) and altitude during trade winds. (r = +.69, p <0.01, N = 52)

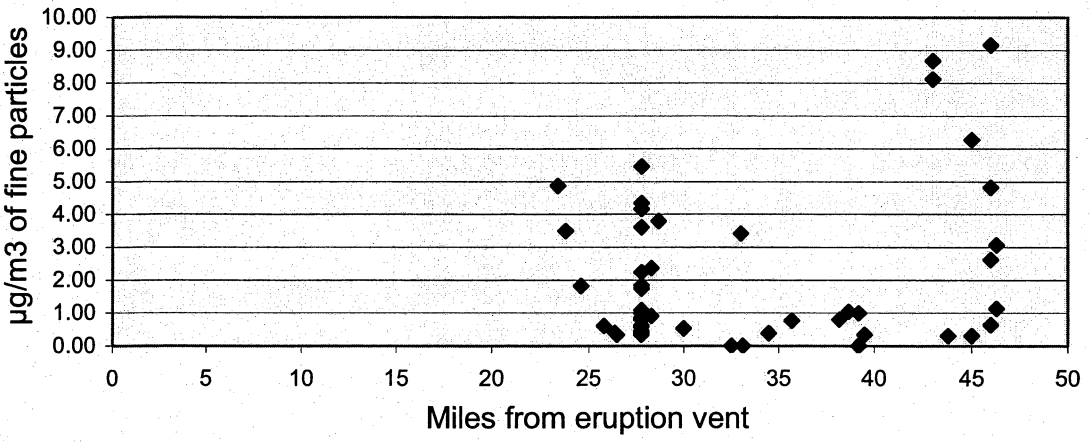

Figure 2.6. Correlation scatter plot of fine particles (≤0.3 µm) and distance from source during trade winds. (r = +.30, p <0.05, N = 52)

REFERENCES CITED

Allen, A.G., Oppenheimer, C., Ferm, M., Baxter, P.J., Horrocks, L.A., Galle, B., McGonigle, A., and Duffell, H.J., 2002, Primary sulfate aerosol and associated emissions from Masaya volcano, Nicaragua: Journal of Geophysical Research, v. 107, p. (5)1–8.

Andres, R.J., Kyle, P.R., and Chuan, R.L., 1993, Sulfur dioxide, particle and elemental emissions from Mt. Etna, Italy during July 1987: Geologische Rundschau, v. 82, p. 687–695.

ATSDR (Agency for Toxic Substances and Disease Registry), 1998, Toxicological profile for sulfur dioxide: CAS# 7446-09-5, Atlanta, GA: U.S. Department of Health and Human Services, Public Health Service, 223 p., www.atsdr.cdc.gov/toxprofiles/tp116.html (accessed November 2004).

Baxter, J.P., Baubron, J.C., and Coutinho, R., 1999, Health hazards and disaster potential of ground gas emissions at Furnas volcano, Sao Miguel, Azores: Journal of Volcanology and Geothermal Research, v. 92, p. 95–106.

California OEHHA (Office of Environmental Health Hazard Assessment), 2001, Chronic toxicity summary, sulfuric acid: CAS Registry No. 7664-93-9, 10 p., http://www.oehha.org/air/chronic_rels/AllChrels.html (accessed November 2004).

Chuan, R., 1995, Characteristics of "VOG" from Kilauea volcano, Hawai'i, *in* Andres, R.J., ed., Proceedings, Volcano-Atmosphere Interactions Symposium: International Chemical Congress, Honolulu, Hawaii, p. 36-49.

Chuan, R., 1997, Physical/chemical characterization of atmospheric aerosols around the island of Hawaii: Hawaii State Department of Health Research Report, Clean Air Branch, 11 p.

Chuan, R., 1998, Physical/chemical characterization of atmospheric aerosols around the island of Hawaii: Further investigation on the characteristics of volcanic smog: Hawaii State Department of Health Research Report, Clean Air Branch, 8 p.

Clarke, A.D., and Porter, J.N., 1991, Volcanic haze—Physiochemistry and transport, *in* Vog and Laze Seminar [abs.]: Hilo, University of Hawaii, Center for the Study of Active Volcanoes.

Delmelle, P., Stix, J., Baxter, P., Garcia-Alvarez, J., and Barquero, J., 2002, Atmospheric dispersion, environmental effects and potential health hazard associated with the low-altitude gas plume of Masaya volcano, Nicaragua: Bulletin of Volcanology, v. 64, no. 6, p. 423–434.

EPA (U.S. Environmental Protection Agency), 1990, Sulfur dioxide primary standards: National ambient air quality standards, 1 p., http://www.epa.gov/air/criteria.html (accessed November 2004).

Giambelluca, T.W., and Schroeder, T.A., 1998, Climate, *in* Juvik, S., and Juvik, J., eds., Atlas of Hawai'i: Hilo, University of Hawai'i, Department of Geography, p. 49–59.

Holgate, S.T., Samet, J., Koren, H., and Maynard, R., eds., 1999, Air pollution and health: London, Academic Press, 1065 p.

Koenig, J., 2000, Health effects of ambient air pollution: How safe is the air we breathe?: Norwell, Massachusetts, Kluwer Academic Publishers, 249 p.

Lioy, P.J., and Waldman, J.M., 1989, Acidic sulfate aerosols: Characterization and exposure: Environmental Health Perspectives, v. 79, p. 15–34.

National Weather Service, 2003, Forecast service model output 10 meter winds, Hawaii, September: http://www.prh.noaa.gov/hnl/pages/model.php (accessed September 2003).

Nicholson, R.A., Roberts, P., and Baxter, P., 1996, Preliminary studies of acid and gas contamination at Poas volcano, Costa Rica: Environmental geochemistry and health with special reference to developing countries: Geological Society [London] Special Publication, 113, p. 239–244.

Pasiuk-Bronikowska, W., 2002, Atmosphere-related aspects of the aqueous phase oxidation of sulfur dioxide, *in* Barnes, I., ed., Global atmospheric change and its impact on regional air quality: Netherlands, Kluwer Academic Publishers, p. 121–127.

Porter, J.N., Horton, K.A., Mouginis-Mark, P.J., Lienert, B., Sharma, S., Lau, E., Sutton, A.J., Elias, T., and Oppenheimer, C., 2002, Sun photometer and lidar measurements of the plume from the Hawai'i Kilauea volcano Pu'u O'o vent aerosol flux and SO_2 lifetime: Geophysical Research Letters, v. 29, n. 16, p. 30-1 to 30-4.

Seinfeld, J.H., 1986, Atmospheric chemistry and physics of air pollution: New York, John Wiley and Sons, 738 p.

Seinfeld, J.H., and Pandis, S.N., 1998, Atmospheric chemistry and physics: New York, John Wiley and Sons, 1326 p.

Sutton, A.J., and Elias, T., 2002, Twenty years of continuous gas release at Kilauea: Effusive lessons in a volatile time [abs.]: Eos (Transactions, American Geophysical Union), v. 83, no. 47, Fall meeting abstracts, abstract no. V62C-06.

Sutton, A.J., Elias, T., Hendley, J.W., II, and Stauffer, P.H., 2000, Volcanic air pollution—A hazard in Hawaii: U.S. Geological Survey Fact Sheet No. 169-97, 2 p., http://pubs.usgs.gov/fs/fs169–97/ (version 1.1) (accessed November 2004).

USGS (U.S. Geological Survey), 1998, "COSPEC" helps observatory scientists study volcanic air pollution and processes: Volcano Watch, June 25, 2 p., http://hvo.wr.usgs.gov/volcanowatch/1998/98_06_25.html (accessed July 2004).

WHO (World Health Organization), 1979, Sulfur oxides and suspended particulate matter: Geneva, Environmental Health Criteria, v. 8, 107 p.

WHO (World Health Organization), 2000, Sulfur dioxide 7.4: WHO Air quality guidelines for Europe 2nd Ed.: Copenhagen, WHO Regional Office for Europe, 107 p., http://www.euro.who.int/document/aiq/7_4sulfurdioxide.pdf (accessed November 2004).

WHO (World Health Organization), 2001, WHO strategy on air quality and health: Geneva, 12 p., www.who.int/peh/air/Strategy.pdf (accessed March 2003).

WRCC (Western Regional Climate Center), 2002, The climate of Hawaii, 15 p., http://www.wrcc.dri.edu/narratives/HAWAII.htm (accessed July 2004).

The "Clean Air" Layer at Sea Level along the Kona Coast

Steven Ryan
Mauna Loa Observatory
P.O. Box 275 Hilo, HI 96721 Steve.C.Ryan@noaa.gov

Abstract. Volcanic pollution (vog) coming from the Kilauea eruption is commonly observed along the leeward Kona slopes on the island of Hawaii. Recent measurements of particle (condensation nuclei) concentrations at three locations in Kona show that there is a persistent layer of relatively clean air that extends from sea level to about 100 meters (330 ft.) above sea level near the shoreline. The particle concentration in the "clean air" layer generally remains below 1000 particles per cc throughout the day while concentrations of several thousand to tens of thousand per cc are measured in the vog layer above this at elevations between 200 meters and 1400 meters (4500 ft.) on the slope.

1. INTRODUCTION

Condensation nuclei (submicron particles) in the atmosphere have been measured continuously at seven sites on Hawaii since early 2002 by the VOGNET program. VOGNET is a collaboration between the National Oceanic and Atmospheric Administration (NOAA) Mauna Loa Observatory and several public and private high schools that was created to monitor the distribution of volcanic pollution (vog) coming from the eruption of Kilauea volcano. The prevailing northeasterly trade winds bring the volcanic plume from its source at the Pu'u O'o eruption near Hawaii Volcanoes National Park around the southern tip of the island to the leeward Kona coast.

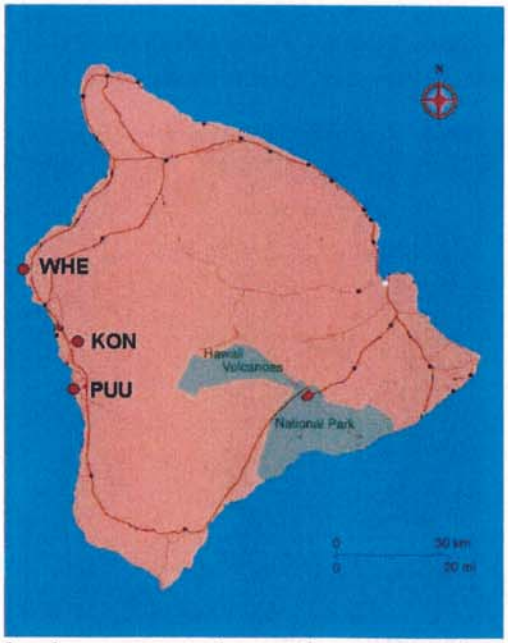

Figure 1. Location of the three sites in this study. WHE and PUU are at sea level, and KON is at 518 meters (1700 ft.) above sea level.

Network measurements at Konawaena High School (KON) at 518 meters (1700 ft) above sea level in Kealakekua have shown that particle concentrations were typically below 1000 particles per cc at night and increased to about 10,000 per cc at midday, which was attributed to the presence of the vog layer on the Kona Coast (Figure 1). At the same time, particle concentrations usually remained below 1000 particles per cc throughout the day at the West Hawaii Explorations Academy (WHE) school located at sea level on Keahole point, except for a few hours centered around 6 to 7 AM. A special field experiment was run in July-August 2002 in which all seven particle counters were deployed from sea level to 1370 meters (4490 ft.) on the slope above Keahole point. This experiment showed that on average the midday vog layer had a broad maximum particle concentration between 220 meters and 980 meters (720 and 3200 ft.). There were no sites between sea level and 220 meters in that experiment.

In September, 2003, the network particle counter at the windward Pahoa High School site was relocated to the Pu'uhonua o Honaunau National Historic Park (PUU) which is located at sea level on the Kona coast (Figure 1). This site was chosen to investigate if the relatively clean air observed at WHE during the day extended further south down the coast, and to see if the particle concentration increases observed around 7 AM at WHE was due to manmade pollution from a nearby highway and power plant or to incursions of vog. This study reports on findings from the first three weeks of measurements at PUU, compared to simultaneous measurements at WHE and KON.

2. INSTRUMENT DESCRIPTION

The VOGNET condensation nuclei counters (Figure 2) were designed by the author in 2000 and built by high school students and teachers from the VOGNET schools. They are built with inexpensive hardware and communicate with a laptop computer via a serial port.

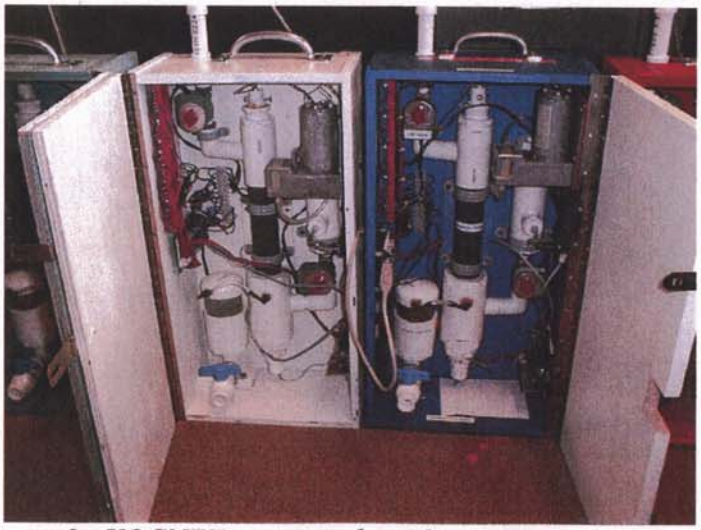

Figure 2. VOGNET automated condensation nuclei counters

The counters measure the total number of particles larger than about 0.01 microns in a cubic centimeter of air once every minute. Many of these particles are too small to be seen in visible light (which has a wavelength of around 0.5 microns). They are detected by causing a water droplet to form around each particle inside of a chamber. A laser diode light beam shines through the chamber onto a detector. The instrument records the fraction of light which is scattered by the water droplet fog, and uses a calibration table to calculate the particle concentration from this ratio. The measurement technique is unable to distinguish between types of particles, their chemical composition, or their size distribution.

Calibrations of each instrument were most recently made in August, 2003 by comparison with a standard instrument (the Mauna Loa Observatory "Pollak Counter" replica #13) using solder flux smoke particles over a concentration range of 50 to 200,000 particles per cc. The calculated concentrations are accurate at a 95% confidence level to within a factor of two from 1000 particles per cc to 100,000 particles per cc.

3. RESULTS

The study ran from September 27 to October 17, 2003. The data from October 6 is shown in Figure 3 in the 1-minute resolution at which it was acquired. There were extended periods when the particle concentration varied slowly over timescales of tens of minutes. This indicates that the air upwind of the site had a fairly uniform particle concentration over a spatial scale of more than a kilometer at typical wind speeds of over 10 km/hr. There were also brief increases in concentration lasting for one or several minutes, which we attribute to emissions from nearby and intermittent manmade pollution sources such as passing vehicles.

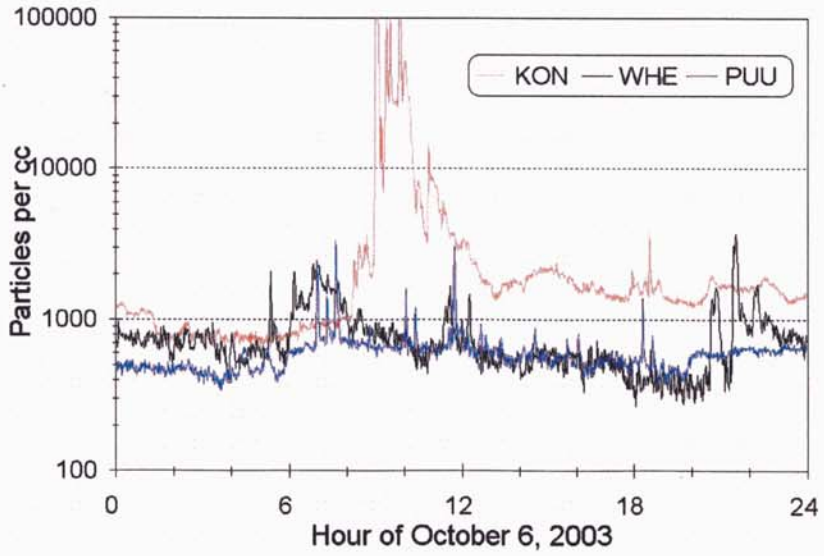

Figure 3. Particle concentrations taken at 1-minute intervals during one day of the study.

At the two sea level sites of PUU and WHE, the concentration generally ranged between 400 and 800 particles per cc for the entire 24 hour period on October 6. This is similar to what we have measured in rural, mostly unpolluted air at windward Hawaii VOGNET sites. The 1-minute scale variability was greater at WHE than at PUU, and WHE had more frequent episodes when the concentration exceeded 1000 particles per cc. These differences were probably caused by the greater amount of manmade pollution within a few km of WHE (including a major highway, power plant, and airport), compared to rural PUU (a lightly traveled road and picnic area).

At KON, the particle concentration increased on October 6 from minimally polluted nighttime levels to tens of thousands per cc at after 8 AM, about the time when the wind usually switches direction from downslope/offshore to upslope/onshore. Starting at 9 AM, there was a 1 ½ hour period when the concentration remained above 30,000 per cc and occasionally exceeded 100,000 per cc. A similar concentration range is often measured at the VOGNET site in Pahala (40 km downwind of the volcano) when vog is present, and at Hilo (35 km from the volcano) during vog episodes in southerly winds.

The diurnal patterns seen on October 6 were typical of what occurred throughout the three week study (Figure 4 shows a 1 week period). The several hour period of increased particle concentration centered at around 7 AM was seen almost every day at WHE. At PUU, there were occasional 1 to 2 hour episodes around noon or early afternoon when the median concentration reached a few thousand per cc. These may have been caused by smoke from cooking fires in the nearby picnic area or by incursions of vog.

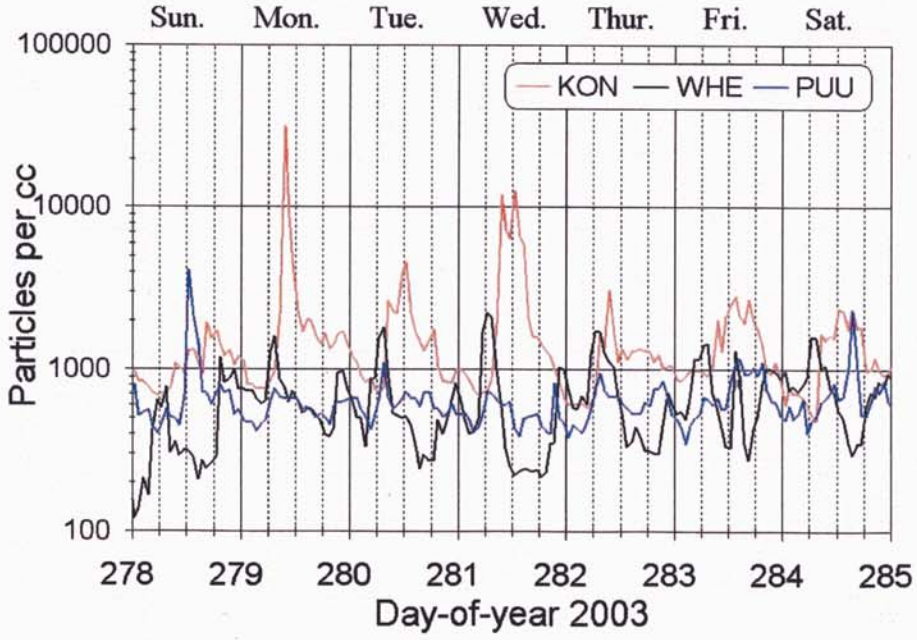

Figure 4. Hourly median particle concentrations from October 5 to 11, 2003. Midnight occurs at the solid vertical lines. The dashed lines are at 6 hour intervals.

The averaged hourly medians throughout the three week study are shown in Figure 5. At KON, which is within the visible vog layer at 518 meters above sea level, the average hourly median particle concentration remained above a thousand particles per cc between 9 AM and 7 PM, which coincides with the period when upslope/onshore winds are blowing. At sea level PUU, the average remained between 400 and 800 particles per cc over 24 hours, which is within the range measured in unpolluted air at windward Hawaii sites. The same was true at WHE, except for a three hour period of increase centered on 7 AM. Since a similar increase did not occur at PUU (which is 30 km closer to the volcano) it was probably not due to a regular daily incursion of vog at sea level. We attribute this feature to pollution from State Highway 19 and the Keahole power plant, which are upwind of WHE during this time of downslope/offshore winds. If this interpretation is correct, it means that both PUU and WHE are almost completely free of vog particles for 24 hours per day, and that there is a persistent "clean air" layer at sea level all along the Kona coast between these two locations.

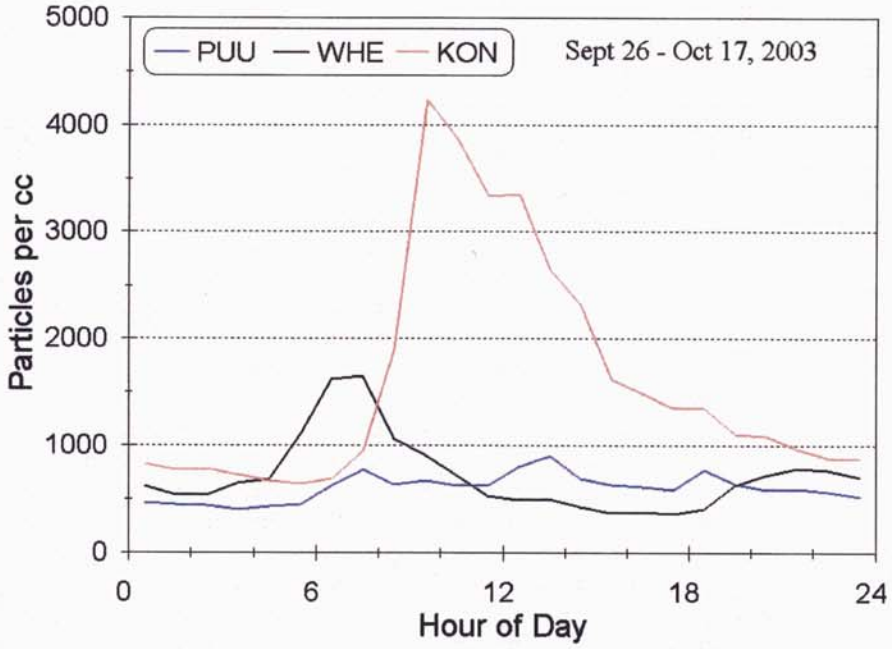

Figure 5. Averages of hourly median particle concentrations.

On the final day of the study, a series of particle concentration measurements were made along the road that leads from sea level at the Pu'uhonua o Honaunau National Historic Park to the junction with State Highway 11 at about 245 meters (800 feet) elevation. The readings were taken with a Gardner Counter, which is a hand operated condensation nuclei counter which was developed in the 1960's. At each point of measurement, the elevation was determined from an altimeter watch with a resolution of 20 feet that had been previously zeroed at sea level in the Park.

These measurements are shown in Figure 6. They show that at this time the "clean air" layer was about 100 meters (330 feet) thick. The transition from low concentration (400 to 900 particles per cc) to high concentration (above 4000 particles per cc) was fairly abrupt, occurring over an elevation interval of about 50 meters. Median hourly concentrations measured by the VOGNET counters at PUU, WHE, and KON are consistent with measurements made along the road at similar altitudes at this time (square symbols in Figure 6).

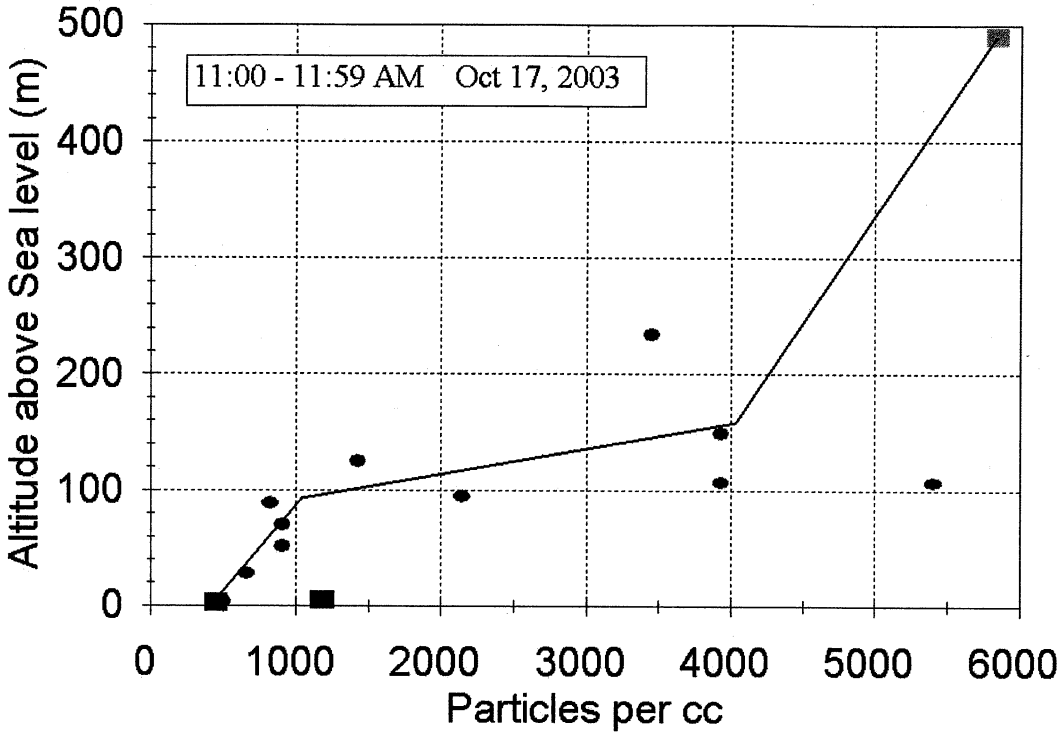

Figure 6. Particle concentrations on the road above Pu'uhonua o Honaunau National Historic Park compared with median hourly concentrations at PUU (blue square), WHE (black square) and KON (orange square). The points between 90 and 150 meters were taken on two trips up and down the road over a period of 20 minutes.

4. VERTICAL EXTENT OF THE VOG LAYER

From July 19 to August 14, 2002, all seven VOGNET condensation nuclei counters were deployed on the slope above Keahole Point in the "Kaloko Road Experiment". The sea level site was WHE, and the remaining counters were put at 220, 350, 460, 850, 980, and 1370 meters above sea level near homes in residential areas. The data from this experiment was edited to remove brief one-to-several minute increases in concentration caused mostly by nearby vehicle traffic, and hourly average concentrations were calculated from the edited data. These are shown in Figure 7.

The Kaloko Road Experiment results agree with the findings of this study (Figure 6). Both studies show that there were relatively high particle concentrations at and above 220 meters and low concentrations at sea level during the day. The Kaloko experiment found that high concentrations persisted all the way up to 980 meters and then dropped off above that. The onset time of the morning increase in particle concentration was later with increasing altitude, with a 1 hour difference between the 220 meter site and the 980 meter site. Since these locations are 7 km apart, this implies that a vog "front" moved up the slope at about 7 km/hr (4.3 miles/hour), which may be similar to the speed of the developing upslope wind at that time. In the late afternoon, the elevation of the peak concentration dropped from 850 meters to 400 meters. By 6 PM, elevated concentrations were confined to a layer between 220 and 460 meters, with background concentrations at 850 meters and above.

The 3 hour period of higher concentration seen at WHE (red line Figure 7) in the early morning only extended as high as 460 meters, and was weaker at increasing elevations. This is consistent with the assumption that it was caused by pollution from the highway and power plant located at 40 to 50 meters above sea level.

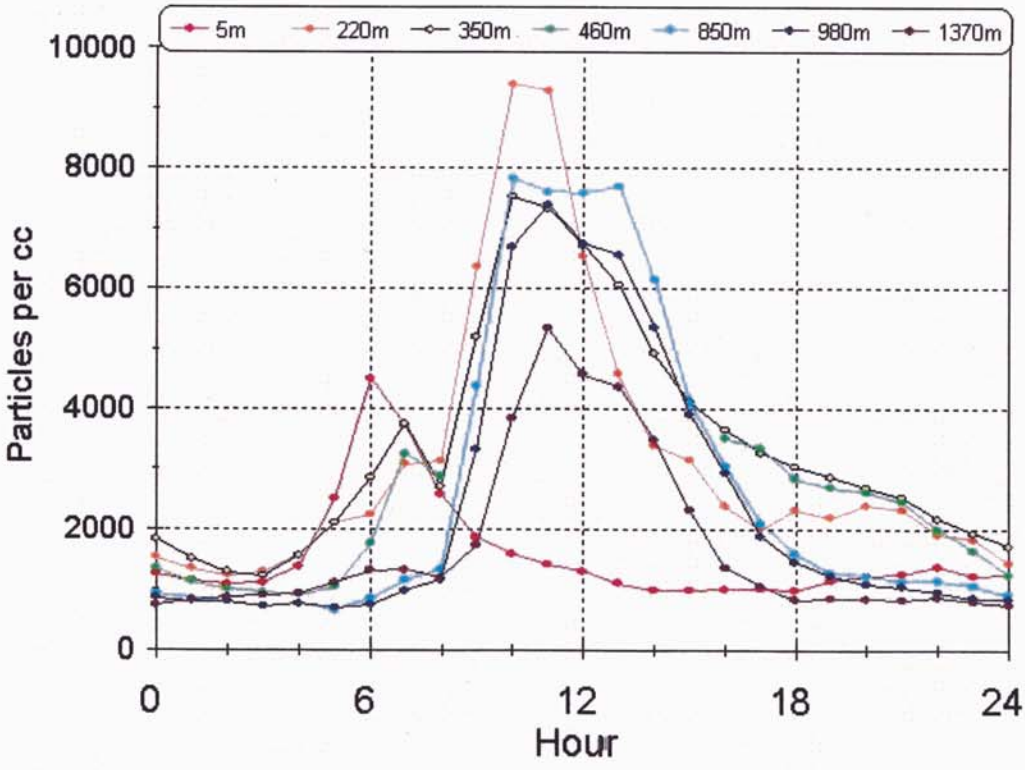

Figure 7. Hourly average concentration at seven locations in subdivisions above Keahole Point between July 19 and August 14, 2002. Daytime averages for the 460 meter site are omitted because of excessive pollution from a nearby major highway.

5. DISCUSSION AND FUTURE WORK.

We suggest two possible mechanisms for the formation a "clean air" boundary layer at sea level along the coast. One is that clean air is transported along the surface from some distance offshore and never mixes with the vog layer aloft. The second is that the sea level air layer can sometimes be contaminated with vog particles, but these are subsequently removed by interaction with the ocean surface before the air reaches the coast. Both of these mechanisms (isolation and particle removal) could be active to varying degrees. Both require that the surface boundary layer does not substantially mix with the vog layer above it. This suggests that there may be a temperature inversion in the atmosphere right above the ocean surface, which would prevent convective mixing with polluted air aloft during the day.

We are planning on making captive balloon flights using a radiosonde to measure the temperature profile throughout the day right at the coastline. When onshore winds blow during the day, the profile measured near the beach should be the same as that over the open ocean just offshore.

We will also make more Gardner counter measurements at and above sea level at Na'alehu, Miloli'i , and Keahole point, as well as repeating the measurements at Honaunau. This will show the extent and thickness of the "clean air" layer along most of the coast that is affected by vog at higher elevations during trade winds.

6. CONCLUSION

Above the leeward central Kona coastline of Hawaii there is a persistent layer extending from sea level to about 100 meters above sea level which has very few or no volcanic particles. The condensation nuclei concentration in this layer averages 400-1000 particles per cc consistently over 24 hours, which is similar to the concentration found in unpolluted air on the windward coast of Hawaii. Above this "clean air" layer, a vog layer forms during the day with a broad maximum peak extending to about 900 meters above sea level with condensation nuclei concentrations averaging 4000 to 10,000 particles per cc. Above this up to the maximum elevation of our measurements, about 1400 meters, the concentration decreases with height. Between midnight and 4 AM, the average concentration is usually less than 1500 particles per cc at all elevations.

The Distribution of Volcanic Aerosols in Hawaii from VOGNET

Steven Ryan
Mauna Loa Observatory
P.O. Box 275, Hilo, HI 96721
(808) 933-6965 (voice) -6967 (fax) ryan@mloha.mlo.hawaii.gov

ABSTRACT

Measurements of condensation nuclei concentration in two size ranges and aerosol optical depth at two wavelengths have been made by VOGNET, a network of high schools located around the island of Hawaii. Between October 1996 and May, 1999 over 6000 measurements were made by students at five locations: Pahala, Kealakekua, Waimea, Hilo, and Pahoa. These data show how the particle concentration, size distribution, and aerosol optical depth varies around the island as a function of the prevailing wind direction and altitude above sea level. An automated condensation nuclei counter built for VOGNET measured the diurnal cycle of particle concentration at these sites.

INTRODUCTION

Kilauea volcano on the Big Island of Hawaii has been in nearly continuous eruption from the Pu'u O'o and Kupaianaha vents on its east rift zone since 1983. During the period of this study, SO_2 emissions from these sites have ranged from less than a few hundred to over 7000 metric tones per day, while emissions from the Kilauea summit have varied from 40 to 240 metric tones per day [1]. The average SO_2 emission rate from Kilauea volcano was greater than that from any EPA-listed anthropogenic source in the United States.

Aerosol particles are produced from volcanic SO_2 ("vog") and by the interaction of molten lava and sea water where lava enters the ocean ("laze"). Vog consists mostly of sulfuric acid and sulfates, while laze contains hydrochloric acid [2]. In normal easterly trade wind conditions, the leeward southern and western sides of the Big Island suffer from reduced visibility, crop damage, and health complaints due to the persistent presence of vog and laze.

VOGNET was organized in September 1996 in a partnership between Mauna Loa Observatory (MLO), a baseline climate monitoring station of the National Oceanic and Atmospheric Administration (NOAA), and teachers from several Big Island public and private high schools. NOAA provided surplus and obsolete instruments, MLO trained volunteer high school teachers to make observations and reduce data, and the teachers supervised students in taking measurements during school hours. The measurements were archived by students at one of the schools (HPA-Hawaii Preparatory Academy), and used in classroom exercises and science fair projects. HPA maintains a VOGNET web page at http://vognet.hpa.edu that gives a description the program and provides public access to the complete database.

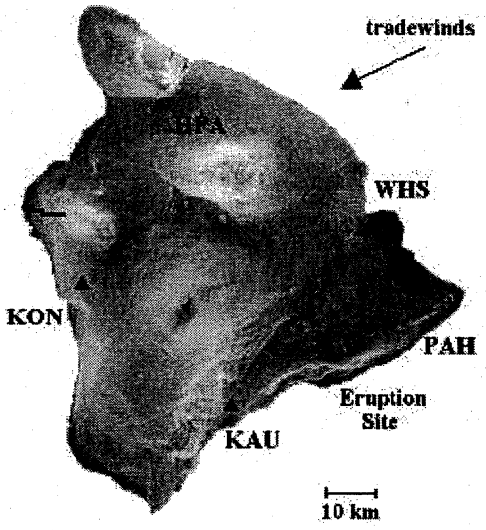

Figure 1. Location of VOGNET sites on Hawaii

METHODS

Daytime measurements were made at Kau High School in Pahala (KAU), Konawaena High School in Kealakekua (KON), Hawaii Preparatory Academy in Waimea (HPA), Waiakea High School in Hilo (WHS), and Pahoa High School in Pahoa (PAH). These sites are shown in Figure 1 along with the location of the Kilauea volcano eruption site.

Aerosol optical depth was calculated from observations using NOAA J-Series handheld sunphotometers with 380nm and 500nm narrow-bandpass interference filters [3]. Calibrations were made at MLO on 9/96, 1/97, 7/97, 11/97 and 11/98 using the Langley method. The instrument response decreased by an average of 18% per year due to degradation of the filters. Observations were reduced using linearly interpolated calibration constants.

Condensation nuclei (CN) were measured with Gardner Counters [4]. In a Gardner Counter, a saturated air sample is subject to a rapid underpressure which causes water vapor to condense on the particles, forming a water droplet fog. The light transmission through the fog is measured and this is converted to particle concentration using a calibration curve for each instrument. The minimum particle size detected by the Gardner Counter can be adjusted by changing the amount of underpressure applied to the air sample. Routine VOGNET measurements were made at the two extreme settings of the instrument, >0.26 microns and >0.002 microns. CN counters experience a loss of counting efficiency for

particles smaller than 0.01 microns [5]. All of the VOGNET Gardner Counters were calibrated relative to the MLO CN standard Pollak Counter on two separate occasions by making simultaneous measurements of a smoke aerosol in a $1m^3$ box.

In July 1998 a continuous CN counter was built on the operating principle of a Gardner Counter. This continuous counter used standard plumbing hardware, solenoid valves, a laser diode light source, and a personal computer for control and data acquisition. It made one measurement every minute of >0.01 micron particles and was calibrated relative to the MLO Pollak standard. The continuous counter was deployed for 1-3 months at a time at each of the VOGNET schools.

RESULTS

The long-term average CN concentration and aerosol optical depth at the five sites is shown in Figure 2. Optical depth measurements were stopped at several schools after May, 1997 because of frequent cloudiness at windward sites, problems with filter degradation, and data quality concerns.

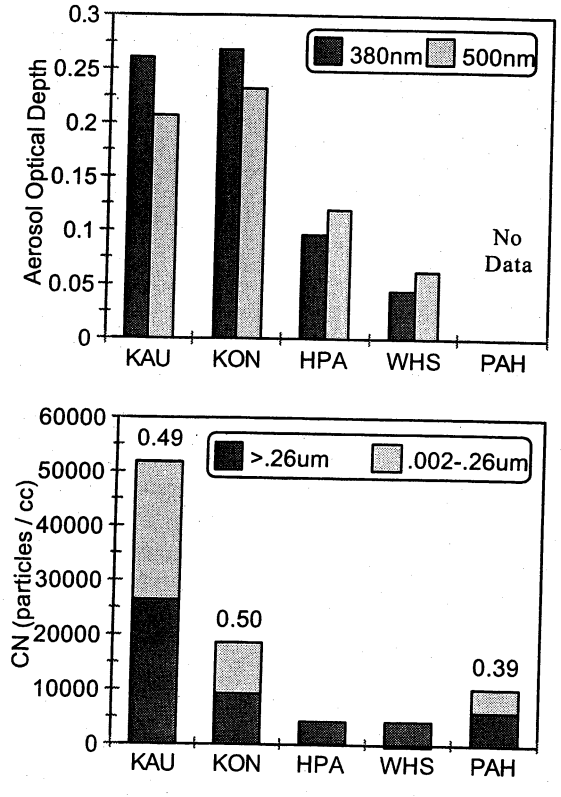

Figure 2. TOP Aerosol optical depth at two wavelengths between October 1996 and February 1997. BOTTOM Condensation nuclei in two size ranges between October 1996 and May 1999, with the fraction of small particles indicated.

The sites in Figure 2 are arranged in clockwise order of their coastal distance from the volcano. The average optical depth was greatest and similar at the leeward sites of KAU and KON then decreased clockwise around the island to a minimum at windward WHS. Average condensation nuclei concentrations were greatest at KAU (30 km downwind of the eruption site), significantly less at leeward KON, and equally low at windward/rural HPA and windward/suburban WHS.

At the downwind sites of KAU and KON, about 50% of the particles were smaller in diameter than 0.26 um, while the windward sites of HPA and WHS had virtually no <0.26 um particles. This feature was also seen in the optical depth measurements. Leeward KAU and KON had a greater average optical depth at 380 nm than at 500 nm, while the inverse was true at windward HPA and WHS. Measurements of particle size distributions using a laser optical particle counter aboard an aircraft by Clarke and Porter [6] have shown that the volcanic plume aerosol is centered around 0.3 um diameter, while the background marine aerosol has a distribution centered around 2-3 um.

PAH is only 15 km upwind of the eruption site and is located near the geothermally active Kilauea east rift zone. The average fraction of <0.26 um diameter particles at PAH was about 40%.

In 1997 students from West Hawaii Explorations Academy made CN measurements at altitudes from sea level to 910 meters along a road between Keahole Point and the top of Kaloko Drive (located on the WNW coast, Figure 1). Twenty five transects were averaged to produce the vertical profiles shown in Figure 3. The aerosol layer at this location has a maximum concentration at an altitude of 500-600 meters, which happens to be about the same as the 520 meter elevation of KON, 15 km to the south. At sea level, the average concentration was near the marine boundary layer background level.

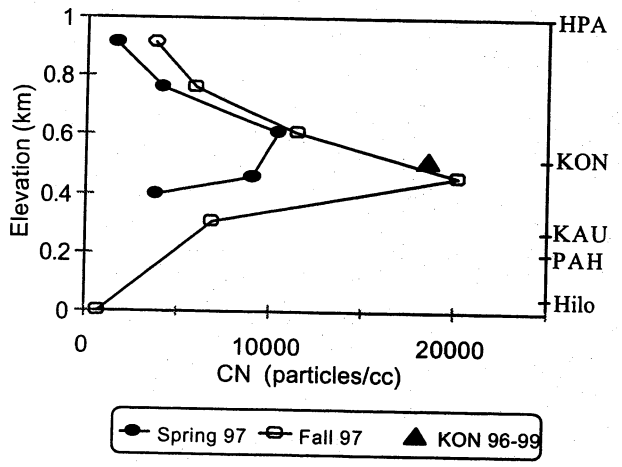

Figure 3. Average condensation nuclei concentration between 11 AM and 1 PM at several elevations along a road on the western slope of Hualalai volcano. Elevations of the VOGNET school sites are shown on the right for comparison.

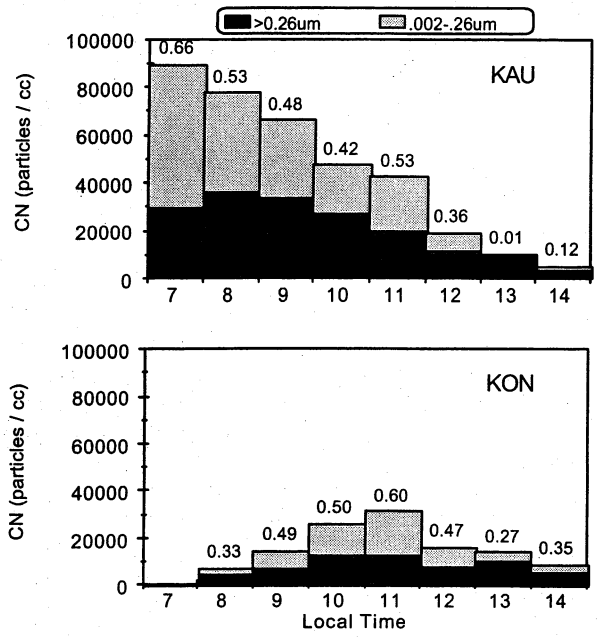

Figure 4. Average particle concentration during the day at KAU and KON between October 1996 and May 1999. The numbers above the bar give the fraction of particles <0.26 um in diameter.

At KAU the fraction of <0.26 um particles remained near 50% throughout the morning, then dropped to near zero by 1 PM (Figure 4). At KON, both the total concentration and fraction of <0.26 um particles were greatest at 11 AM. The average small particle fraction at KON did not drop below about 30% during the day.

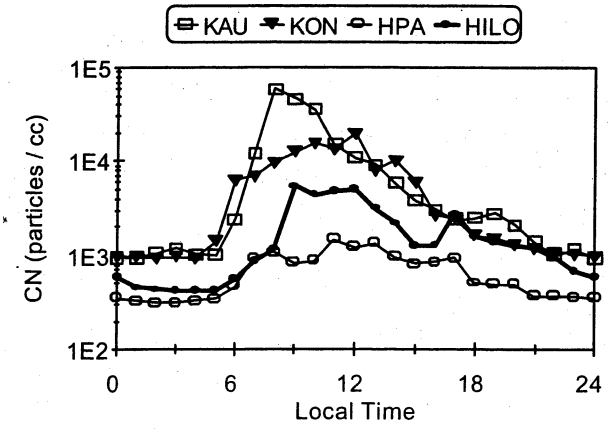

Figure 5. Hourly average concentration of >0.01 um particles at four sites. KAU: 1/29/99-4/9/99, KON: 4/22/99-5/22/99, HPA: 10/3/98-1/4/99, HILO: 5/28/99-6/23/99. The Hilo site was in the Kaumana residential neighborhood.

The automated CN counter was deployed at various sites in 1998-1999 (Figure 5). All sites had minimum particle concentrations between midnight and 5 AM, a period when surface temperature inversions and downslope/land breeze winds are well developed. At windward locations (HPA and suburban Hilo) the average minimum concentration was 300-400 particles per cc, similar to that measured in unpolluted marine air [6]. At leeward sites (KAU and KON) the average minimum was about 1000 particles per cc.

The particle concentration began rising at 6 AM at all four locations. At KON, HPA, and Hilo, maximum particle concentrations occurred just before noon, while at KAU, there was a sharp maximum at 8 AM.

Although the eastern coast generally experiences relatively clean air, westerly or southerly winds can bring high concentrations of volcanic aerosols to these locations. The maximum concentration of >0.002 micron particles measured at each site (with Gardner Counters and the continuous counter) between October 1996 and May 1999, in particles/cc were: KAU 800,000; KON 348,000; HPA 48,000; WHS/Hilo 316,000; PAH 140,000. Higher concentrations at PAH were probably missed because of poor temporal coverage.

ACKNOWLEDGMENTS

The following teachers have generously volunteered their time in and out of the classroom to make VOGNET a success: Deighton Emmons; Hawaii Preparatory Academy, Renwick Bibilone; Kau High School, Jim Wiley; Konawaena High School, Anne Caldwell; Pahoa High School, Bill Woerner; East Hawaii Explorations Academy, Mary Heaton; St. Joseph High School, Mary Kern; Waiakea High School

REFERENCES

[1] T. Elias, A.J. Sutton, J.B. Stokes, and T.J. Casadevall, "Sulfur dioxide emission rates of Kilauea Volcano, Hawaii, 1979-1997", U.S. Geological Survey Open-File Report 98-462, 1998.

[2] R. L. Chuan, "Characteristics of "vog" from Kilauea Volcano, Hawaii", Proceedings from a Symposium on Volcano-Atmosphere Interactions. Honolulu, HI, December 1995, pp 36-49.

[3] E. G. Dutton, P. Reddy, S. Ryan, and J.J. DeLuisi, "Features and effects of aerosol optical depth observed at Mauna Loa, Hawaii: 1982-1992", J. Geophys. Res., Vol 99 No. D4, 1994, pp 8295-8306.

[4] T. A. Rich, "A photo-electric nucleus counter with size discrimination", Geofis. Pura Appl. Vol. 31, 1955, pp60-65.

[5] B. Y. H. Liu and C. S. Kim "On the counting efficiency of condensation nuclei counters", Atmos. Environ. Vol 11, 1977, pp. 1097-1100.

[6] A. D. Clarke and J. N. Porter, "Volcanic haze – physiochemistry and transport" (abstract), Vog and Laze Seminar, Hilo, Hawaii, July 1991.

Appendix 5

Airflow Over the Island of Hawaii

Yi-Leng Chen
Department of Meteorology
University of Hawaii
Honolulu, HI 96822

1. Introduction

Pertubations induced by the airflow past single isolated mountains include a variety of phenomena: flow splitting and flow deceleration on the windward side, mountain wakes in the lee side and etc. In addition, the airflow is also affected by the diurnal heating cycle. During 11 July - 24 August 1990, the Hawaiian Rainband Project (HaRP) was conducted over the island of Hawaii to study the mesocale airflow around the island and the dynamics of early morning rainbands offshore of Hilo. The mesoscale airflow over the island summarized in this report is based on the data collected from surface stations and aircraft observations during HaRP.

2. Airflow over the island

(a) Island blocking as revealed by the mean surface airflow

The mean tradwind sounding taken by aircraft over the ocean east of Hilo during HaRP exhibits east-northeast trade winds on the order of 6 - 9 meters per second (not shown). Along the windward coast, flow splitting occurs in the Hilo Bay area (Fig. 1). The airflow moves around the island with northeasterlies along the northeastern coast and southeasterlies along the northeastern coast. In addition to northern and southern tips of the island, strong surface winds are also found in the Humu'ula Saddle between Mauna Loa and Mauna Kea and in the Waimea Saddle between Kohala Mountains and Mauna Kea. In both regions, the airflow moves around the mountains and channels through the saddle. On the windward slope the incoming flow is decelerated significantly as it approaches the island. In the lee side, the trade winds are completely blocked by the Mauna Kea and Mauna Loa with calm winds.

(b) Nighttime and daytime flow regimes

The surface airflow is strongly modulated by the diurnal heating cycle. At night, much of the island has a downslope wind component except in the high wind regions: northern tip, southern tip, Waimea Saddle, and Humu'ula Saddle (Fig. 2). The flow direction along the northeastern and southeastern coasts shows that the trade winds are being forced to move around the island.

On the windward slopes west of Hilo, on the Kona coast and along the Waikoloa coast downstream of the Waimea Saddle, the wind direction of the daytime flow regime is about 180 out of phase with the nighttime flow regime (Fig. 3). In these regions, the

wind flow has a large upslope component during the day. Pronounced upslope flow is also observed at Mauna Loa Observatory, on the southeastern flank of Mauna Loa and along the Kona coast as a result of solar heating.

(c) Wake vortices

The wake consists of two elongated counterrotating quasi-steady eddies that give rise to a wide region of strong reverse flow along the wake axis (Fig. 4). THe reverse flow extends westward from the west coast of Hawaii a distance of about 200 km. A cloud line extends along the wake axis and sometime broadens considerably farther downstream (Fig. 5). Aerosol concentration in the southerly eddy is elevated due to the entrainment of Kilauea plume. Strong shear zones, trailing westward from the northern and southern tips of the island, delineate the accelerated trade winds and air trapped in the recirculating wake.

References

Chen, Y.-L. and A. J. Nash, 1994: Diurnal variation of surface airflow and rainfall frequencies on the island of Hawaii. Mon. Wea Rev., 122, 34-56.

Smith, R. B. and V. Grubisic, 1993: Aerial observsations of Hawaii's wake. J. Atmos. Sci., 50, 3728-3750.

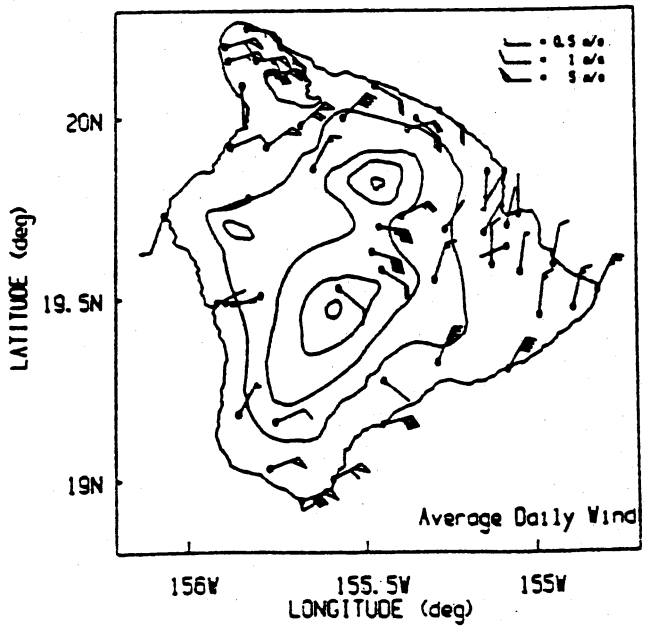

FIG. 4. Averaged wind for the period of 11 July–24 August 1990.

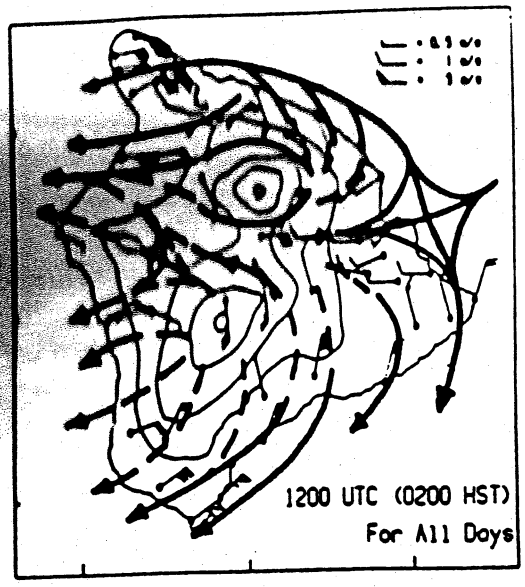

Fig. 2 Surface streamline analysis for averaged winds at 0200 HST.

The solid (broken) streamlines indicated regions where air at the surface does (not) stay at the surface for the entire path as it moves upslope–downslope.

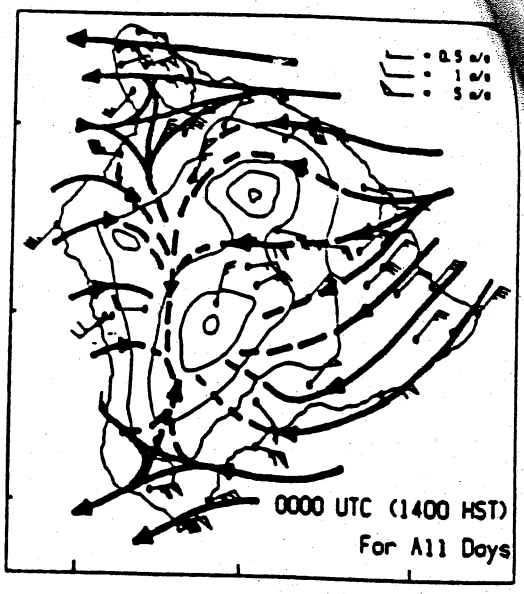

Fig. 3

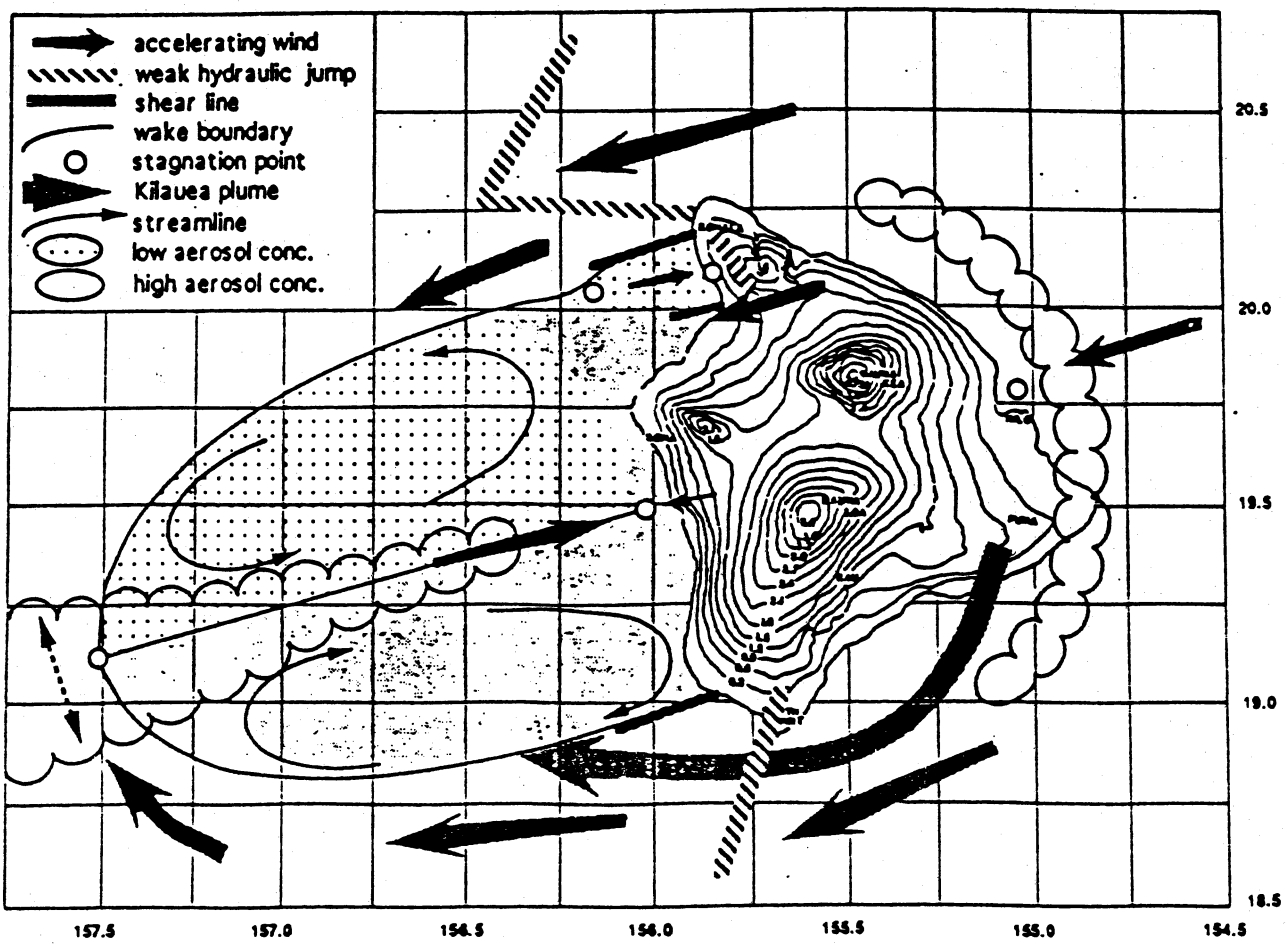

FIG. 4 Summary diagram depicting features observed in Hawaii's wake. Dashed two-way arrow at the downstream end of the wake is suggesting the existence of a north to south drift. The upstream rainband and "centerline" cloud are also outlined.

Smith & Grubisic

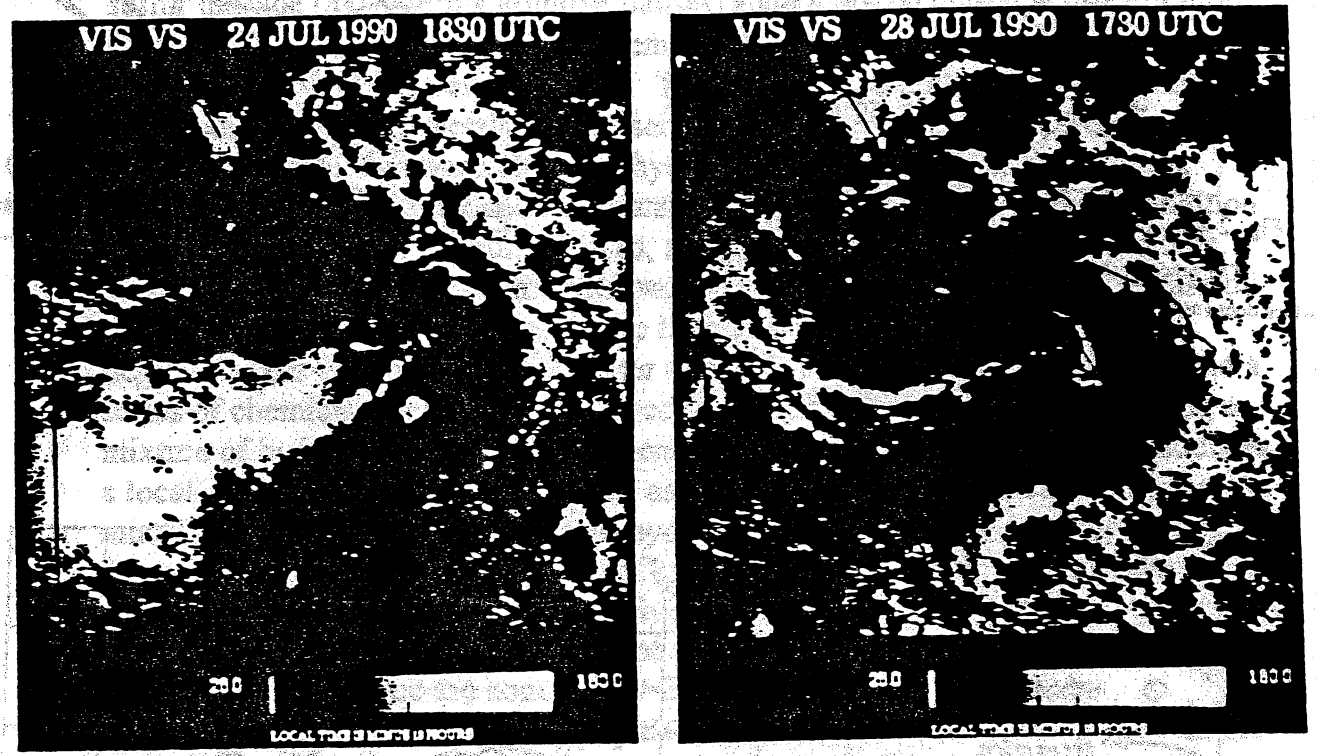

FIG. 5. (a) One kilometer resolution GOES visible satellite image at 1830 UTC 24 July 1990. At the time of the image the aircraft was flying along the third wake leg where it encountered the wake cloud. The orographic clouds on Maui, Molokai, and Ko'olau Range on Oahu are noticeable. (b) 1-km resolution GOES visible satellite image at 1730 UTC 28 July 1990. A sharp boundary between the bright southern portion of the wake and clear region to the south of it is barely evident about 40 km south of the central cloud line. Note convective clouds developing on the Kona Coast as a result of diurnal upslope, onshore circulation.

Diurnal Variation of Surface Airflow and Rainfall Frequencies on the Island of Hawaii

YI-LENG CHEN AND ANDREW J. NASH*

Department of Meteorology, School of Ocean and Earth Science and Technology, University of Hawaii, Honolulu, Hawaii

(Manuscript received 3 February 1993, in final form 9 July 1993)

ABSTRACT

The high-resolution Portable Automated Mesonet data from the Hawaiian Rainband Project are used to document the circulation over the entire island of Hawaii for the first time. It is shown that the surface airflow and rainfall occurrences over the island are strongly modulated by the diurnal heating cycle.

Most areas over the island show daytime upslope and nighttime downslope components separated by morning and evening transitions. On the windward slope, the onset of the downslope (upslope) wind during the evening (morning) transition starts on the slopes and progresses downward. The effects of island blocking are also evident. On the windward slopes of Mauna Kea and Mauna Loa, the mean winds are weak ($\sim$1 m s^{-1}) due to flow deceleration. Flow splitting occurs in the Hilo Bay area as the trade winds are forced to move around the island. On the lee side, the trade winds are absent. For stronger trade-wind days, the island blocking is more significant with a higher surface pressure (0.2–0.5 hPa) on the windward slopes and lower pressure in the lee side than weak trade-wind days. Along the windward coast, it is much easier for the land breeze to overcome weaker trade winds. For weaker trade-wind days, the onset (cessation) of land breeze there is earlier (later) in the evening (morning).

At night, the area of maximum rainfall frequency is over the windward lowland west of Hilo. Most of the nocturnal precipitation there starts in situ. The effects of orographic lifting aloft are enhanced by the nighttime convergence west of Hilo due to the interaction between the katabatic–land-breeze flow and the trade winds. In the early morning, the rainfall frequency has a maximum along the windward coast due to the inland drifting of the frequently observed rainbands offshore.

1. Introduction

It is well known that the trade-wind belt has a minimum in the global distribution of rainfall. Nevertheless, over the Hawaiian islands, trade-wind showers are frequent. The island of Hawaii is the largest island in the Hawaiian chain. It is roughly 140 km in diameter, extending over 10 000 km^2 in area. Its topography is dominated by the two volcanic mountains of Mauna Loa and Mauna Kea, both of which exceed 4100 m in elevation (Fig. 1), well above the typical height of the trade-wind inversion (approximately 2 km at Hilo). Northeasterly trade winds of 5–10 m s^{-1} are persistent especially during the summer months.

The orographic clouds and local showers are typical for such an isolated subtropical island characterized by steep topography and abundant low-level moisture. The mountains provide lifting by direct means (e.g., orographic lifting) and by more indirect means, such as blocking or acting as a high-level heat source (sink) during the day (night) resulting from the temperature contrasts between the elevated topography and adjacent areas (Banta 1990). Local circulations may focus the precipitation in certain locations and suppress cloud growth in others. Rainfall patterns over the island of Hawaii show a wide degree of spatial variability that is clearly linked to the terrain and local winds (Giambelluca et al. 1986).

During 11 July–24 August 1990, the Hawaiian Rainband Project (HaRP) was conducted over the island of Hawaii. Prior to HaRP, three major field experiments were conducted over the island: Project Shower (1954), the Warm Rain Project (1965), and the Joint Hawaii Warm Rain Project (1985). These studies focused on the microphysical studies of rain showers. HaRP (1990) sought to extend our understanding by emphasizing mesoscale airflow around the island and the dynamics of rainbands. Previous studies on the mesoscale airflow over the island were primarily based on very limited surface data (e.g., Garrett 1980; Schroeder 1981) or single station soundings (e.g., Lavoie 1967a; Mendonca 1969). Garrett and Schroeder used the surface data collected during Project Ahupua'a (1978) conducted by the University of Hawaii. During the Joint Hawaii Warm Project (1985), only limited airflow mapping by aircraft was made in the Hilo Bay area (Rasmussen et al. 1989). Airflow in the lee side

* Present affiliation: National Weather Service, NOAA, U.S. Department of Commerce, Montgomery, Alabama.

Corresponding author address: Dr. Yi-Leng Chen, Department of Meteorology, University of Hawaii at Manoa, School of Ocean and Earth Science and Technology, Honolulu, HI 96822.

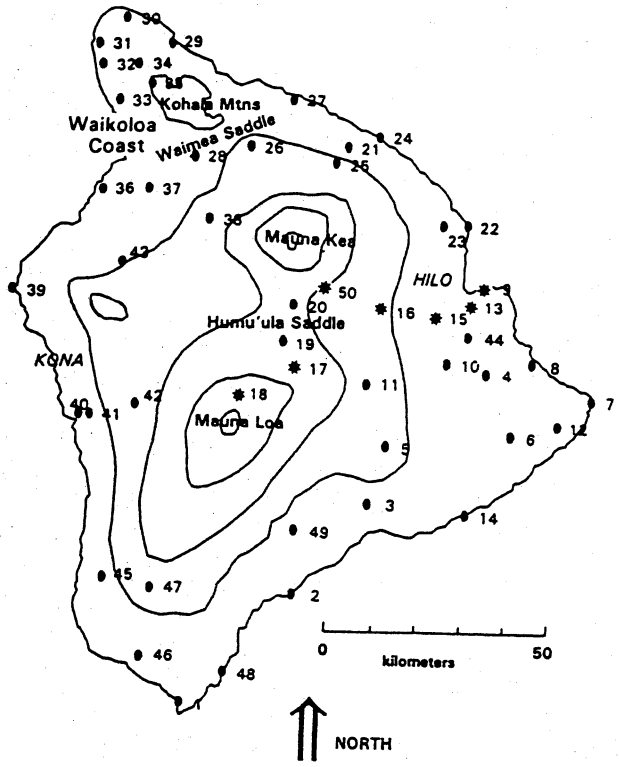

FIG. 1. The island of Hawaii with PAM sites. Contours are for every 1000-m elevation.

of the island was studied by Nickerson and Dias (1981) and Fett and Burk (1981). They used the satellite and P-3 aircraft data collected during the Hawaii Mesoscale Energy and Climate Project conducted by the National Oceanic and Atmospheric Administration (NOAA) in 1980. Information on the mesoscale airflow from these studies is incomplete. High-resolution data on the airflow and thermodynamic structure over and upstream of the island of Hawaii were collected with the deployment of 50 Portable Automated Mesonet (PAM) stations, tethersondes, a low-level wind profiler radar, supplement Hilo rawinsonde observations, two Dopplar radars, an instrumented aircraft, and a chaff aircraft during HaRP 1990. This was the first field experiment that emphasized the mesoscale airflow over a subtropical island. The deployment of 50 PAMs around the island (Table 1) allows us to document the surface circulation over the entire island for the first time.

2. Knowledge prior to HaRP

a. Existing climatologies of rainfall and airflow

Rainfall observations in Hawaii date from the 1840s and have been studied for a variety of meteorological, hydrological, and agricultural purposes (Taliaferro 1959; Schroeder et al. 1977; Meisner 1979; Lyons 1982; Giambelluca et al. 1986; and others). An early monograph published by the American Meteorological Society (Leopold et al. 1951) was devoted to Hawaii rainfall. The most recent rainfall atlas of isohyetal maps depicting the patterns of median and mean monthly and annual rainfall for the six largest islands of Hawaii was compiled by Giambelluca et al. (1986) using data updated through 1983. In general, rainfall maximum areas correspond to regions of persistent orographic lifting of moisture-laden northeast trade winds up the windward slopes. Areas of low rainfall areas are found in leeward areas and atop the highest mountains. High mountain dry areas occur because the upslope flow of moist air is prevented from reaching this elevation due to the presence of trade-wind inversion. In addition, thermally driven diurnal circulations, (e.g., land breeze–sea breeze systems and mountain–valley winds) may contribute to rainfall by reinforcing trade–orographic lifting, generating areas of low-level convergence with interaction with the prevailing trade winds or producing orographic lifting in areas not exposed to trade winds (Leopold 1949; Garrett 1980). Schroeder et al. (1977) presented time series of hourly rainfall frequency during the diurnal cycle for various stations over the island of Hawaii based on rainfall records for the period of March 1965–December 1973 and showed that windward coastal stations have a nocturnal maximum in rainfall occurrences. With increasing elevation, the maximum rainfall frequency shifts to the afternoon. On the leeward slopes, the sea-breeze circulations produce afternoon rainfall maxima. Harmonic analysis of the rainfall data shows that the diurnal cycle accounted for 64%–90% of the variance in the rainfall frequency. The large diurnal cycle in rainfall occurrences over the island suggests that local winds may play an important role in the development of local showers (Leopold 1949; Schroeder et al. 1977).

In the past, most observational studies of the island-induced wind regimes focused on the combined effects of the sea (land) breeze, mountain (valley) breeze, and the trade winds (e.g., Leopold 1949; Eber 1957; Lavoie 1967a; Mendonca 1969; Garrett 1980; and Schroeder 1981). The flow splitting of the trade wind by the island of Hawaii has long been recognized in the literature (e.g., Leopold 1949; Fellbaum 1984; Nickerson 1979; and others). Leopold noted that the trade-wind inversion acts as a lid above the trade winds, forcing them to split around the island; however, these studies focused on the surface thermal forcing as the primary cause for the development of downslope wind and the observed nocturnal rainfall along the windward coast. The early morning rainbands offshore are viewed as one component of the overall windward-slope circulation cell driven by the nocturnal cooling on the slopes. Because of low heat capacity of the bare lava soils and clear sky above the inversion, the katabatic flow can become quite significant and is a regular nighttime feature. Lavoie (1967a) used Hilo rawinsonde data to

TABLE 1. PAM stations during HaRP. An asterisk next to a PAM station number denotes a station on the Hilo to Mauna Loa transect.

PAM number	PAM name	Latitude (°N)	Longitude (°W)	Elevation (m)
1	South Point	18.941	155.685	91
2	Palima Point	19.159	155.454	26
3	Hilina Pali	19.323	155.295	863
4	Hawaiian Acres	19.575	155.043	202
5	Volcano Park	19.433	155.259	1215
6	Pahoa	19.458	154.988	432
7	Cape Kumukahi	19.520	154.814	12
8	Paradise Park	19.598	154.946	17
9*	Hilo	19.730	155.047	5
10	North Kulani Road	19.593	155.130	506
11	Kulani Prison	19.555	155.303	1579
12	Hawaiian Geothermal Project A (HGPA)	19.474	154.887	195
13*	UH Hilo	19.706	155.083	32
14	Lae'apuki	19.303	155.082	23
15*	Kaumana	19.688	155.154	405
16*	Lower Saddle Road	19.691	155.273	1128
17*	Upper Stainback Highway	19.586	155.457	2529
18*	Mauna Loa Observatory	19.539	155.578	3393
19*	Upper Saddle Road	19.634	155.484	2150
20*	Humu'ula Sheep Station	19.704	155.464	2042
21	Hamakua Upper	20.006	155.355	622
22	Pep'ekeo	19.853	155.089	18
23	Honomu Mauka	19.853	155.143	320
24	O'okala	20.020	155.286	107
25	Mauna Kea Ranch	19.979	155.381	1076
26	Mana	20.002	155.564	1052
27	Haina	20.097	155.474	133
28	Waimea	19.981	155.684	768
29	Land's End	20.208	155.738	148
30	Hawi	20.255	155.836	111
31	Mahukona 1	20.208	155.893	110
32	Mahukona 2	20.166	155.885	45
33	Kohala Ranch	20.095	155.848	245
34	Pu'u Hue Ranch	20.166	155.089	768
35	Kahua Ranch	20.129	155.780	1166
36	Waikoloa	19.922	155.880	12
37	Waikoloa Mauka	19.920	155.781	358
38	Waiki'i Ranch	19.868	155.649	1480
39	Keahole Point	19.732	156.064	5
40	Captain Cook	19.495	155.920	402
41	Captain Cook Mauka	19.499	155.896	729
42	Papa'aloa	19.510	155.798	1555
43	Pu'u Wa'awa'a	19.783	155.833	878
44	Waiakea	19.647	155.084	186
45	Ho'omau Ranch	19.184	155.860	573
46	Lower Ocean View	19.039	155.775	213
47	Ocean View Mauka	19.160	155.757	1476
48	Kahilipali	19.001	155.595	12
49	Kapapala Ranch	19.279	155.452	632
50*	Pu'u O'o	19.733	155.399	2125

show that the land breeze–sea breeze circulation extends to 3 km or more and is composed of a 1-km-deep lower part with 2–3 m s^{-1} winds and a 2-km-deep return-flow layer with 1–1.5 m s^{-1} winds. He suggested that the coastal land–sea breezes merge with the inland mountain–valley winds to form one diurnal oscillating cell. Mendonca (1969) used balloon measurements to show that the daytime upslope flow at the Mauna Loa Observatory was roughly 600 m deep, compared to 50 m for the nighttime downslope flow. Along the coast, the downslope flow is rather deep with a depth roughly 200 m (Garrett 1980). Integrating his own observations with those of earlier investigations, Garrett presents a conceptual model for the well-developed island circulations over the eastern slopes of Mauna Loa. By day, differential heating between land and sea drives the combined mountain anabatic and sea-breeze winds, causing orographic clouds to develop

along the windward slope. At night, radiational cooling initiates the combined katabatic and land-breeze winds. The katabatic winds, which are strongest just before sunrise, clear most of the island's orographic clouds and meet the trade winds well offshore. The resulting convergence zone usually generates a cloud band or rainband below the inversion (Leopold 1949). After rain begins, these bands often drift inland and, as a result, windward coastal stations exhibit a nocturnal rainfall maximum (Takahashi 1977; Schroeder et al. 1977; Matsumoto 1982). Takahashi (1986) suggests that wind shear within the trade-wind layer is important to rainband formation in the early morning and that long-lasting rainbands develop in the convergence zone when the wind profile is parabolic.

b. *Review of modeling studies*

The modeling and observation studies by Smolarkiewicz et al. (1988), Rasmussen et al. (1989), and Rasmussen and Smolarkiewicz (1993) have emphasized rainband formation offshore in terms of the interaction of the trade-wind flow with the island barrier (Hunt and Snyder 1980) in addition to the thermal effect. They suggest that the arc-shape rainband upstream of the island is frequently observed throughout the diurnal cycle. The Froude number ($\mathrm{Fr} = U/Nz$), where U is the far upstream wind speed, N is the Brünt–Väsälä frequency, and z is the height of the obstacle, is shown to characterize the behavior of the flow as it interacts with the island. For typical trade-wind conditions ($\sim$7.5 m s^{-1}), the Froude number has a value of 0.15 and most of the flow goes around the island. Along the upwind side of the island, the low-level trade winds are predicted to reverse direction in their model. This results in a separation line and associated stagnation point, along which low-level convergence and upward motion occur. Band clouds were periodically initiated within this convergence zone (Rasmussen and Smolarkiewicz 1993) but tended to move with the mean cloud wind, whereas the low-level convergence zone remained stationary. The flow reversal is dynamically induced by the interaction of the trade wind with the island barrier, and it does not require a downslope density current or thermally driven land breeze. Below a Froude number of 0.1, the effects of nocturnal cooling became increasingly important and eventually dominated the formation of downslope flow in agreement with Garrett's (1980) results for a weak trade-wind flow case ($\mathrm{Fr} \sim 0.08$). These studies argued that the basic flow behavior at night for $0.1 < \mathrm{Fr} < 0.3$ can be understood in terms of the interaction of the flow with the barrier; however, the nocturnal cooling can modify the strength and location of the dynamically driven flow.

Another parameter that exerts control over low-Froude-number flow is the cross-shear horizontal scale of the obstacle. Because the trade winds in Hawaii exhibit directional variations (northeast to east), different horizontal scales will be encountered by the flow due to the asymmetry of the island. As the wind direction changes from easterly to northerly, the flow experiences a progressively narrow island. Rasmussen et al. (1989) suggest that the cloud band is located significantly farther onshore for the more northerly wind cases, with little change in the strength of the convergence zone and the resulting clouds. It is important to note, however, that the case presented by Rasmussen et al. (1989) and Rasmussen and Smolarkiewicz (1993) was obtained under very strong trade-wind conditions that were not frequently observed over the Hawaiian Islands. They initialized their model based on a strong trade-wind case with easterly winds of 10 m s^{-1} with no directional or speed shear from the surface to nearly the 650-hPa level.

In summary, previous mesoscale observational studies over the island emphasized the evolution of the island-induced wind regimes in terms of the thermal forcing with very limited observations over the island (Leopold 1949; Lavoie 1967a; Garrett 1980; and others). The early morning rainband offshore is thought to be generated in the convergence zone where the katabatic flow meets the opposing trade-wind flow. Modeling studies (Smolarkiewicz et al. 1988; Rasmussen et al. 1989; Rasmussen and Smolarkiewicz 1993) suggest that the Froude number characterizes the behavior of the flow at night as the trade winds interact with the island. The downslope flow on the windward slopes is thought to be forced by pressure gradients arising from blocking rather than by the nocturnal cooling. This controversy is one of the main scientific problems for HaRP.

In this study, to assess the effects of the diurnal heating cycle on the surface airflow, PAM data during the entire period of HaRP (11 July–24 August 1990) were composited on the basis of the time of the day to yield the diurnal evolution of surface weather patterns. This is the first time that the climatologies of surface airflow and spatial distribution of rainfall patterns over the entire island are analyzed throughout the diurnal cycle. The effects of blocking will be examined based on the comparison of the surface airflow and pressure distributions for the 12 strongest and 12 weakest trade-wind days during HaRP. With small day-to-day variations in thermal stability, the wind speed is the primary parameter determining the daily variations in Froude number under trade-wind flow. For stronger days, we expect the blocking effect to be more significant. To assess the difference in the blocking effects caused by the difference in the wind speed, we need a large sample size to reduce the sampling problems. HaRP lasted for 45 days. The largest sample size we could have for both the strong and weak trade-wind cases is 22 days. By choosing the 12 strongest and the 12 weakest trade-wind days we used only about 25% of the strongest

and weakest cases in our sample size and discarded cases with wind speed values close to the mean value.

3. Data analysis

Pressure, temperature, wet-bulb temperature, winds, and rainfall amount were measured by PAMs at 1-min intervals. From these measurements, six additional parameters were derived: dewpoint, relative humidity, mixing ratio, rainfall rate, potential temperature, and equivalent potential temperature. The equivalent potential temperature was calculated from Bolton's formula (1980). This study also used the data from radiosondes launched consistently three times daily at 1400, 0200, and 0800 HST (Hawaiian standard time) from the Hilo National Weather Service (NWS) office. The information available is temperature, relative humidity, pressure, altitude, and u- and v-component winds. Additional sources of information include aircraft soundings and tethersondes.

The high-resolution PAM data for the period of 11 July–24 August were averaged into centered 15-min means for each day. These daily data were then averaged into a composite for the 45-day period. Also, the 12 strongest and 12 weakest trade-wind days were averaged into strong and weak trade-wind composites, respectively, to examine differences in the circulation due to changes in the strength of the trade-wind flow.

To remove spikes in the data record, the following error checking procedure was followed. From the original 1-min data, median values were found for the observed PAM values of pressure, temperature, wet-bulb temperature, and u- and v-component winds for the particular centered 15-min period (e.g., 15 min past the hour consisted of minutes 8–23). These 15 individual values were then checked in relation to the median. Because large fluctuations over such a short time period are unlikely, any value outside the designated ranges was discarded. The ranges specified are ±3°C for temperature and wet-bulb temperature; ±1 hPa for pressure: and ±4 m s^{-1} for u- and v-component winds. These bounds were chosen based on careful review of the raw data. Time series plots of the 15-min averages with and without data checking procedure were compared with the raw data to ensure that these bounds are chosen properly to remove spikes.

If a value was discarded, all derived parameters from that value were also discarded. From the acceptable values, the averages of all the observed and derived values were calculated. If the number of acceptable values was less than 8 for the 15-min period, the average was not calculated. For rainfall, a consistency check to see that the rainfall rate and rainfall accumulation were the same was performed to assure that the occasional accumulation errors due to the counter being reset and resulting in unrealistic 15-min accumulations were not affecting the data.

During the next phase of data treatment, the daily 15-min data were compiled into the various 15-min averages. Again, a similar error checking routine was performed. A median of all the values of a particular time was found. Values outside of a designated range were discarded and the average of the remaining values was calculated. For this phase, the extreme values were examined and a reasonable range within which the values should fall was determined. The ranges specified were ±5°C for temperature and wet-bulb temperature; ±5 hPa for pressure; and ±9 m s^{-1} for u- and v-component winds. This procedure would remove apparent bad data due to instrument problems or errors. It is very unlikely that we would discard useful information by this procedure. For example, surface wind speeds in Hawaii are usually less than 8 m s^{-1} except by a few corner locations (Fig. 2). A departure in 15-min averaged wind speed from the median greater than 9 m s^{-1} is very unlikely in the trade-wind flow regime during the summer even during the period of rain showers. Time series of the composited data with and without this error checking procedure were plotted and carefully reviewed for each station to ensure that the apparent erroneous data were removed.

All stations suffer from occasional periods of missing data, either due to equipment failure or as a result of the error checking. The problem stations with overall recovery rates of less than 75% were the Pahoa (station 6), Lower Saddle Road (station 16), and the Upper Saddle Road (station 50) sites. Other more serious errors that have been noted are incorrect height or location references or both for the Pu'u O'o station (station 16). For this study, the height of the station was estimated to be 2125 m, as the location given did not match the original elevation from detailed U.S. Geo-

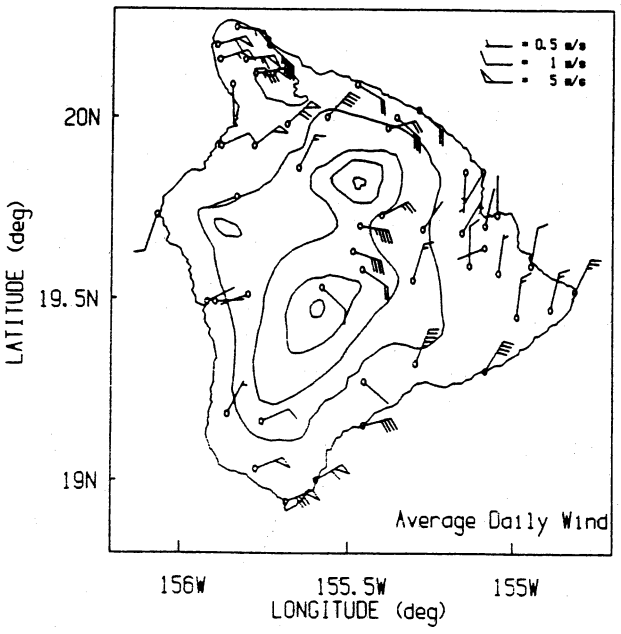

FIG. 2. Averaged wind for the period of 11 July–24 August 1990.

logical Survey charts. Another major problem was that the Hawaii Volcanoes National Park station (station 5) had poor wind exposure. No wind-based analyses incorporate this station.

Ideally, one would want to determine the 12 strongest and 12 weakest trade-wind days using the wind speeds of the trade wind upstream of the island without the influence of the island-induced circulations. Unfortunately, such data from the aircraft soundings are not available on a daily basis. The best estimate of trade-wind strength is to use the wind speeds at the south and north ends of the island. The mean surface airflow for the entire period of HaRP exhibits strongest surface winds ($\sim$6–8 m s^{-1}) at those sites (Fig. 2) as the incoming trade-wind flow is forced to move around the island. Stations at South Point (station 1) on the southern tip and Hawi (station 30) on the northern tip also have a very high correlation of 0.67. The 12 strongest and 12 weakest days were determined on the basis of the average daily (0000–2400 UTC) resultant wind speeds for these two stations. Based on the daily resultant winds at South Point and Hawi, the dataset of the strong trade-wind days are 11, 13, 24, 25, 28 July and 8, 9, 12, 13, 16, 18, 23 August. The weak trade-wind days consist of 15, 20, 21, 27, 29, 30 July and 3, 5, 7, 19, 20, 21 August. An examination of the wind data from the rawinsonde data from Lihue on the island of Kauai along with the daily weather charts showed that trade winds occurred for the above days. Surface winds at Honolulu International Airport also corroborated the strong and weak trade-winds breakdown.

Based on the available morning aircraft soundings, the wind speeds were about 6 and 8 m s^{-1} on average for weak and strong trade-wind days. With $z \sim 3130$ m (Rasmussen et al. 1989) and $N \sim 0.013$ s^{-1}, the corresponding Froude number is 0.15 and 0.18, respectively. These values are lower than 0.2 used by Smolarkiewicz et al. (1988) and Rasmussen et al. (1989). During HaRP the Froude number has a small range ($\sim$0.1–0.2) due to the fact that the trade winds were persistent.

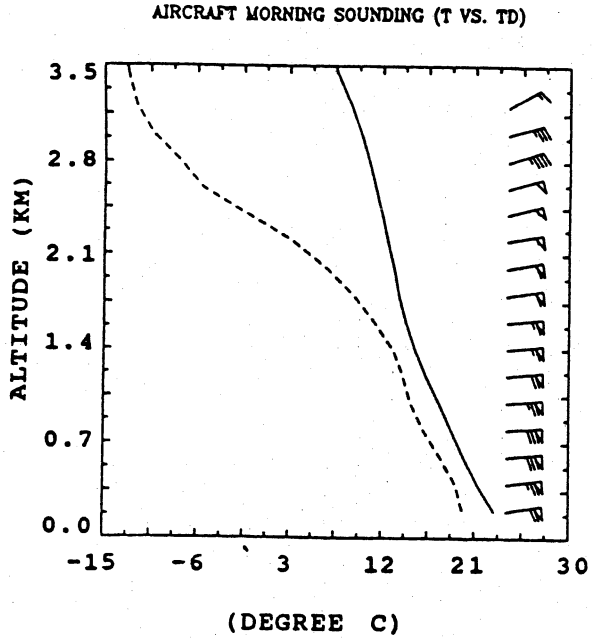

FIG. 3. Mean upstream aircraft early morning sounding during HaRP. Wind (m s^{-1}) with one pennant, full barb, and half barb representing 5, 1, and 0.5 m s^{-1}, respectively.

4. Characteristics of surface airflow

a. Mean surface airflow

On the eastern slopes of Mauna Kea and Mauna Loa, the mean winds ($\sim$1 m s^{-1}) (Fig. 2) are considerably weaker than those of the mean upstream aircraft during HaRP (Fig. 3). The mean upstream sounding exhibits east-northeast trade winds on the order of 6–9 m s^{-1} beneath the trade-wind inversion ($\sim$2.1 km), with strongest winds in the layer between 500 and 850 m (Fig. 3). It is apparent that, on the windward slopes, the incoming flow is decelerated significantly as it approaches the island. The decelerated airflow moves around the topography with weak northerlies ($\sim$1 m s^{-1}) south of Hilo and weak southerlies ($\sim$1 m s^{-1}) north of it. Along the windward coast, flow splitting occurs in the Hilo Bay area. The airflow moves around the island with strong northeasterlies ($\sim$4 m s^{-1}) along the southeastern coast and strong southeasterlies ($\sim$3–4 m s^{-1}) along the northeastern coast. In addition to northern and southern tips of the island, strong winds are also found in the Humu'ula Saddle ($\sim$4 m s^{-1}) between Mauna Loa and Mauna Kea and in the Waimea Saddle ($\sim$7 m s^{-1}) between the Kohala Mountains and Mauna Kea. Flow deceleration due to island blocking in both regions is less significant than that over the windward slopes. The airflow moves around the mountains and channels through the saddle. However, wind data from both regions are not used as trade-wind index, because winds in these areas are generally weaker than winds at the northern and southern tips of the island (7–8 m s^{-1}) and show considerable diurnal variations due to the influences of the underlying land surface (section 3). In the lee side, the trade winds are completely blocked by the Mauna Kea and Mauna Loa with calm winds. In general, the trade-wind flow is interrupted by the island obstacle with splitting airflow along the windward coast, weak winds on the windward slopes due to flow deceleration, and the absence of trade winds in the lee side.

b. Nighttime flow regime

At night, the linear transect on the windward slopes and within the valley between Mauna Kea and Mauna Loa shows westerly katabatic flow (Fig. 4). At Mauna

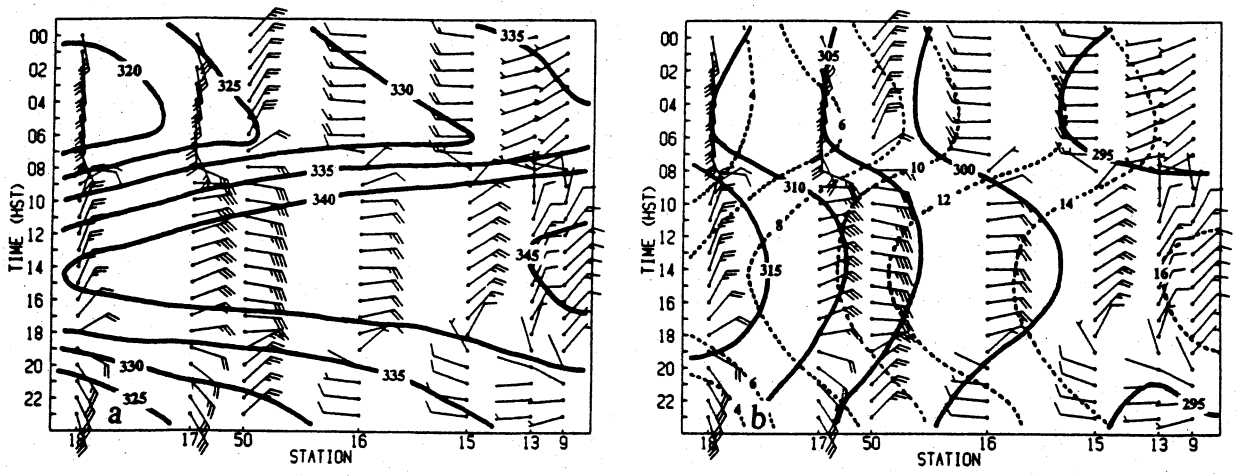

FIG. 4. (a) Time series of the averaged surface winds and equivalent potential temperature (K) at stations along the transect. Winds (m s^{-1}) with one pennant, full barb, and half barb representing 5, 1, and 0.5 m s^{-1}, respectively. (b) Same as (a) but for the potential temperature (K) (solid) and the mixing ratio (dashed).

Loa Observatory, which is on the northern flank of Mauna Loa, the winds are southerlies and almost perpendicular to the topographic contours. Pu'u O'o (station 50) is on the southeastern flank of Mauna Kea (Fig. 1)—the winds have a northerly component. Stations between Lower Saddle Road (station 16) and Hilo exhibit westerly flow throughout the night. The distance between the Humu'ula Saddle and Hilo is approximately 40 km (Fig. 1). If the air moves down the slope along the terrain with a speed of 1 m s^{-1} (Fig. 4a), it would take about 12 h for the air from Humu'ula Saddle to reach the Hilo coast. In other words, the downward-moving air from Humu'ula Saddle cannot reach the Hilo coast. Since the potential temperature is generally much higher at the upper elevations (Fig. 4b), without sufficient cooling, it is unlikely that the air moves completely downslope from higher elevation to the windward coast. In addition to radiative cooling and heat loss to the underlying surface, the air on the windward slope may also be modified by precipitation and evapotranspiration from the surface. The moist static energy (or equivalent potential temperature) is conserved for an adiabatic process as well as during the phase change between water vapor and liquid. If this air were to be advected down the slope following the terrain, assuming no turbulent mixing and no eddy fluxes from the surface, the moist static energy of the downward-moving air would be lower than its original value on the slopes due to the effect of radiational cooling. Nash (1992) estimates the change in moist static energy due to radiational cooling following the downward-moving air for the portion of the windward transect in which westerly downslope occurs. Knowing the horizontal distance and average resultant wind speed between stations allows an estimate of the time for air to be advected down the slope from one station to the next to be made. With the estimated radiational cooling rate on the order of about 0.5 K based upon the outgoing longwave radiation observed by the PAM at Kaumana (station 15), he shows that the observed moist static energy typically is about 1.3 J g^{-1} higher than the estimated values of the assumed downward-moving air. This indicates that the low moist static energy air from the higher elevations may not reach the lower elevations. Because the rate of latent heat flux from the surface and the extent of mixing of the downslope-moving air with the ambient air farther down are not known, how far the air could have moved along the terrain down the slope is relatively uncertain and may vary from one case to another depending on the amount of cooling experienced by the downward-moving air.

Much of the island has a downslope wind component at 0200 HST (Fig. 5a) except in the high-wind regions: northern tip, southern tip, Waimea Saddle, and Humu'ula Saddle (Fig. 2). The flow direction along the northeastern and southeastern coasts shows that

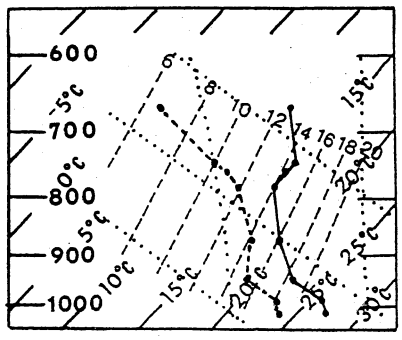

FIG. 5. The temperature and dewpoint curves of surface conditions at 1400 HST along the windward transect. Diagonal dashed lines are saturated mixing ratio (g kg^{-1}). Dotted curves are selected dry and moist adiabats.

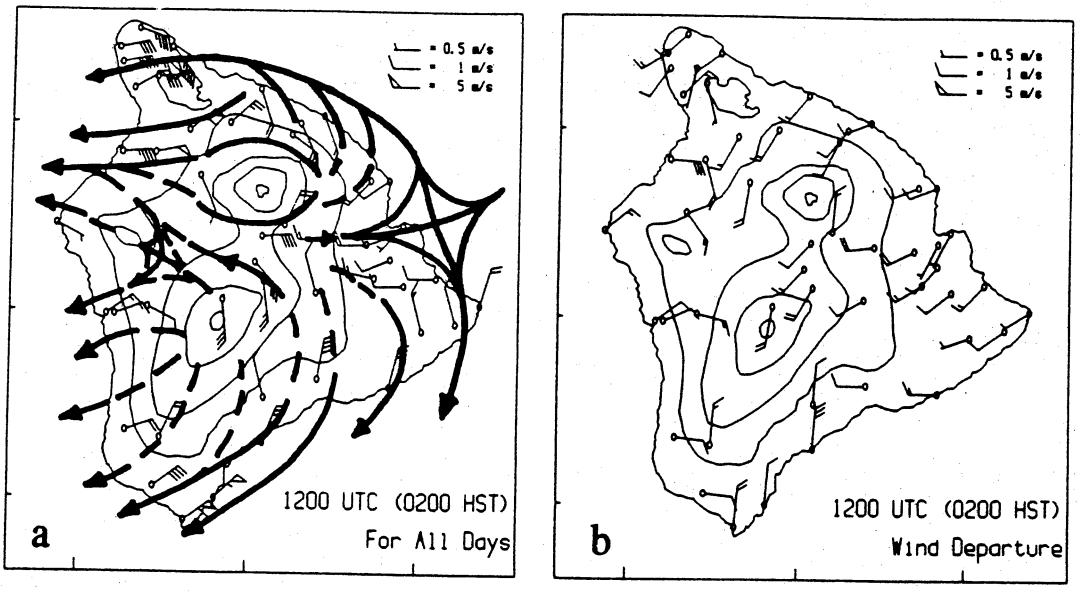

FIG. 6. (a) Surface streamline analysis for averaged winds at 0200 HST. The solid (broken) streamlines indicated regions where air at the surface does (not) stay at the surface for the entire path as it moves upslope–downslope. (b) Wind departure at 0200 HST from the daily averaged wind.

the trade winds are being forced around the island. Cape Kumukahi (station 7) located at the eastern tip of the island does not exhibit offshore flow until nearly 0400 HST and is in general agreement with Fitzjarrald's (1984) study of katabatic wind in opposing flow and the linear sea breeze–land breeze theory of Rotunno (1983), which predicts that flow reversal occurs roughly six hours following sunset. Within both saddles and at the northern tip, the deviations of surface winds from the mean flow (Fig. 2) exhibit a westerly wind component (Fig. 6b) at this time, suggesting weaker trade winds at night in these high-wind regions. Along the northeastern (southeastern) coast, the winds show a large southerly (northerly) component. The winds along the northeastern and southeastern coasts are a mix of nighttime katabatic flow and splitting airflow as the trade-wind flow is forced around the island. The rest of the island shows that the wind departure from the mean flow is dominated by a downslope component that is nearly perpendicular to the topographic contours

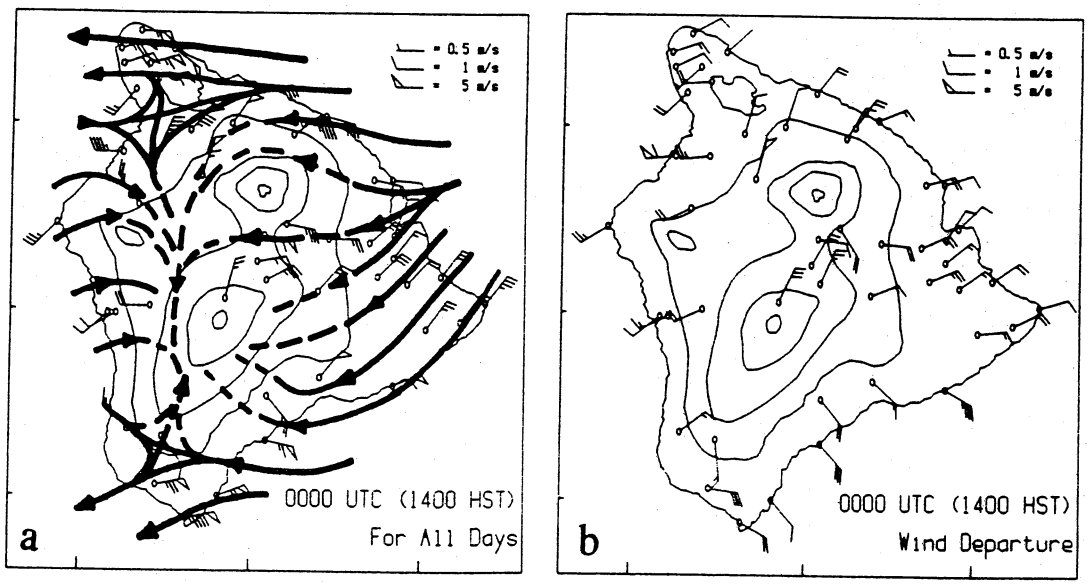

FIG. 7. Same as Fig. 6 but for 1400 HST.

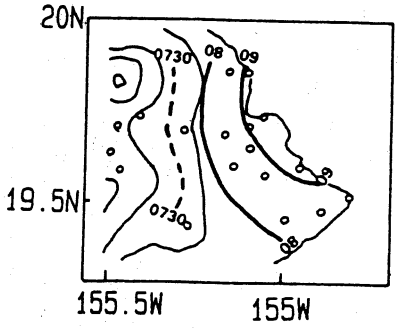

FIG. 9. Isochrone analysis of time (HST) of upslope flow onset for the windward side.

which indicated that the majority of the air below the balloon level was not moving up the slope but instead was being deflected around the mountain. The balloon showed only a substantial vertical motion when it was within approximately 500 m of the slope surface.

The 1400 HST wind flow patterns are those of the fully developed daytime circulations (Fig. 7a). On the windward side of the island, the surface flow is an anabatic flow combined with trade winds. Furthermore, north (south) of the valley between Mauna Kea and Mauna Loa, the wind flow has a southerly (northerly) component suggesting a splitting of the airflow by the island. Similar to the nighttime flow regime, strong winds are found in the following regions: northern tip, southern tip, Waimea Saddle, and Humu'ula Saddle. On the windward slopes west of Hilo, on the Kona coast and along the Waikoloa coast downstream of the Waimea Saddle, the wind direction of the daytime flow regime is about 180° out of phase with the nighttime flow regime. In these regions, the wind flow has a large upslope component. Pronounced upslope flow is also observed at Mauna Loa Observatory and on the southeastern flank of Mauna Loa as a result of solar heating.

The deviations of the 1400 HST airflow from the mean (Fig. 7b) show an onshore (or upslope) component for most of the island except in the following areas: northern tip, Waimea Saddle, and Humu'ula Saddle. In these regions, the wind departure shows a northeasterly component for the daytime flow regime (Fig. 7b) and a southwesterly component for the nighttime flow regime (Fig. 6b), indicating stronger trade winds during the day for these high-wind regions. The upstream mean aircraft sounding shows that the ambient trade-wind speed at the same level is generally higher than surface wind speed in these regions. It appears that stronger trade-wind flow in these regions at the surface may be related to the downward transport of trade-wind momentum as a result of turbulent mixing in the afternoon hours caused by solar heating (Schroeder 1981). On the windward slopes as well as in the lee of Mauna Kea and Mauna Loa, the speed of wind departure from the mean is quite strong at 1400 HST (Fig. 7b). In both regions, in contrast to modeling studies (Smolarkiewicz et al. 1988; Rasmussen et al. 1989), the surface airflow is dominated by the daytime anabatic winds and the nighttime katabatic winds. The mean winds are weak (Fig. 2). It is apparent that in regions with weak winds caused by island blocking the thermally driven diurnal winds become significant.

d. The morning transition

At 0700 HST, an hour after sunrise (Fig. 8a), the surface airflow remained dominated by the nighttime flow regime, remarkably similar to the airflow at 0200 HST. With continued solar heating, the katabatic winds at higher elevation shift to upslope flow at 0800 HST (Fig. 8b). At the windward coast, offshore flow still exists at this time. In the Kona region, the daytime sea breeze is developing; winds are weak and nearly parallel to the coast. Along the Waikoloa coast, the winds are a mix of katabatic flow and trade winds, as the airflow moves through the Waimea Saddle and descends in the lee side.

At 0900 HST, upslope flow is found on the windward slopes (Fig. 8c). Stations in the windward lowland south (north) of the valley show a northerly (southerly) wind component due to flow splitting in the Hilo Bay region. Along the northeastern coast, the winds are southeasterlies. After sunrise with the disappearance of the nocturnal inversion and the cold air at the surface (Chen et al. 1991), the thermal contrasts between the island surface and the adjacent areas decrease. The flow splitting due to blocking is pronounced in low levels. At the Kona coast, the sea breeze develops with continued heating at the surface. Along the Waikoloa coast, sea breeze is developing under the opposing trade winds.

After sunrise, the upslope–sea-breeze transition is progressing downslope (Fig. 9) on the windward side in contrast with previous observational studies (e.g., Garrett 1980), which, with limited data, suggest that the onset of the upslope flow occurs at the same time

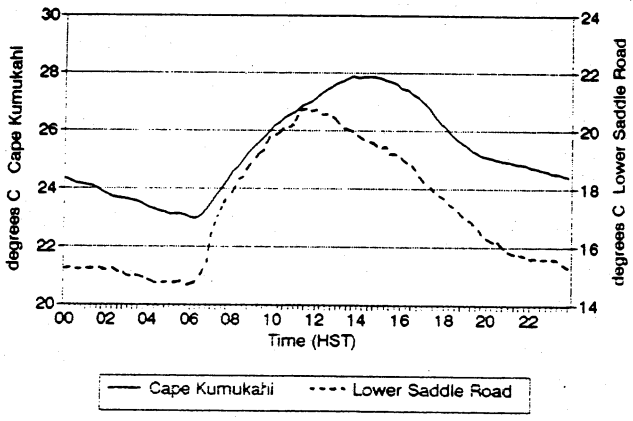

FIG. 10. Time series of temperature at Cape Kumukahi (station 7) (solid) and Lower Saddle Road (station 16) (dotted).

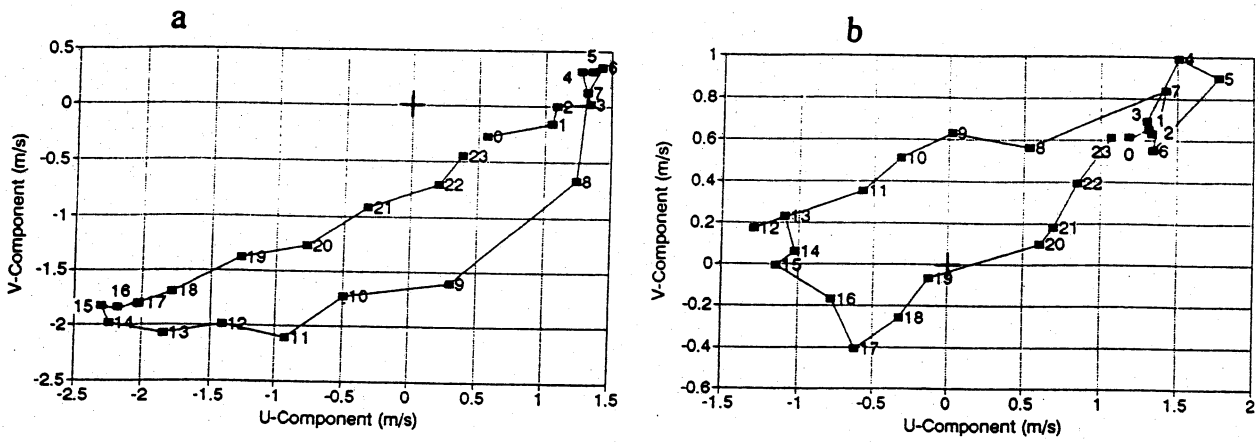

FIG. 11. Wind hodographs for (a) Paradise Park (station 8) and (b) Pepe'ekeo (station 22).

over the windward slope. The turning from katabatic to upslope flow occurs sooner on the higher slopes as the insolation is hitting the slopes at a more direct angle and quickly destroying the shallow nocturnal inversion. The morning temperature increase is earlier and larger for a station on the slope than at a coastal station. This increase can be clearly seen by a comparison of the diurnal temperatures between Cape Kumukahi (station 7) at the eastern tip of the island and the Lower Saddle Road (station 16) on the slope (Fig. 10). In addition, the nocturnal inversion is shallower on the slope than along the coast. Near the Mauna Loa observatory, the inversion is at about 55 m above the surface (Mendonca 1969). Tethersonde observations of katabatic flow at Kaumana (station 15) and the UH Agriculture Experiment Station (station 44) show a deeper (~120 m) nocturnal inversion with a nocturnal jet (Chen et al. 1991). Farther down the slope, the inversion is deep with a height of approximately 200 m at Hilo (station 9) (Garrett 1980). At the coast, it takes longer for the solar heating to destroy the thick nocturnal inversion. Furthermore, the solar heating in the coastal region may be reduced by the presence of offshore clouds and precipitation. As will be discussed later (section 5), during the early mornings the maximum rainfall occurrences were found along the windward coast.

During the morning transition, the winds turn clockwise (counterclockwise) with respect to time on the windward lowland south (north) of the valley between Mauna Kea and Mauna Loa (Fig. 11). South (north) of the valley, the winds have a large westerly component at night, turn to northwesterlies (southwesterlies) during the morning transition, and become northeasterlies (southeasterlies) in the morning. In general, the turning of winds with time during the diurnal cycle is due to a complex interaction among advection of horizontal momentum, the mesoscale pressure gradient force, frictional force, and the Coriolis force; however, the mesoscale pressure gradient force may be the most influential (Kusuda and Alpert 1983). From model predictions (Rasmussen et al. 1989), the windward lowland within the valley between Mauna Kea and Mauna Loa is the favored region for the dynamically induced high pressure center. As will be shown later, this feature has been confirmed in our analysis of PAM data based on a comparison of surface pressure between the strong and weak trade-wind cases. It is probable that this stationary feature interacting with the changing thermally induced pressure gradient produces the observed hodographs.

e. *The evening transition*

During the evening transition, the katabatic flow starts on the windward lowland at 1830 HST just before sunset (~1900 HST) and progresses toward the coast (Figs. 12 and 13). The progression of the onset of katabatic flow down the slope is held up near the coast because the region is more exposed to the trade-wind flow. Cape Kumukahi (station 7) does not get the offshore flow until around 0400 HST (Fig. 13). The speed of the progression during the first two hours, roughly 2.5–3 m s^{-1}, is faster than the speed of katabatic flow. Thus, the progression is not due to simple advection of the surface airflow along the surface.

Without significant heating or cooling during sunset, flow splitting on the windward lowland is evident with a northerly (southerly) wind component south (north) of the valley between Mauna Kea and Mauna Loa (Fig. 12a). The airflow on the windward slopes has a large component parallel to the topographic contours because of blocking. During the morning transition, the splitting airflow has an upslope component on the slopes and an offshore component at the coast (Fig. 8). In contrast, during the evening transition, the splitting airflow has a downslope component on the slopes and an onshore component at the eastern part of the island (Fig. 12). The delay in the onset of katabatic wind at the coast during the evening transition may be related to 1) exposure of

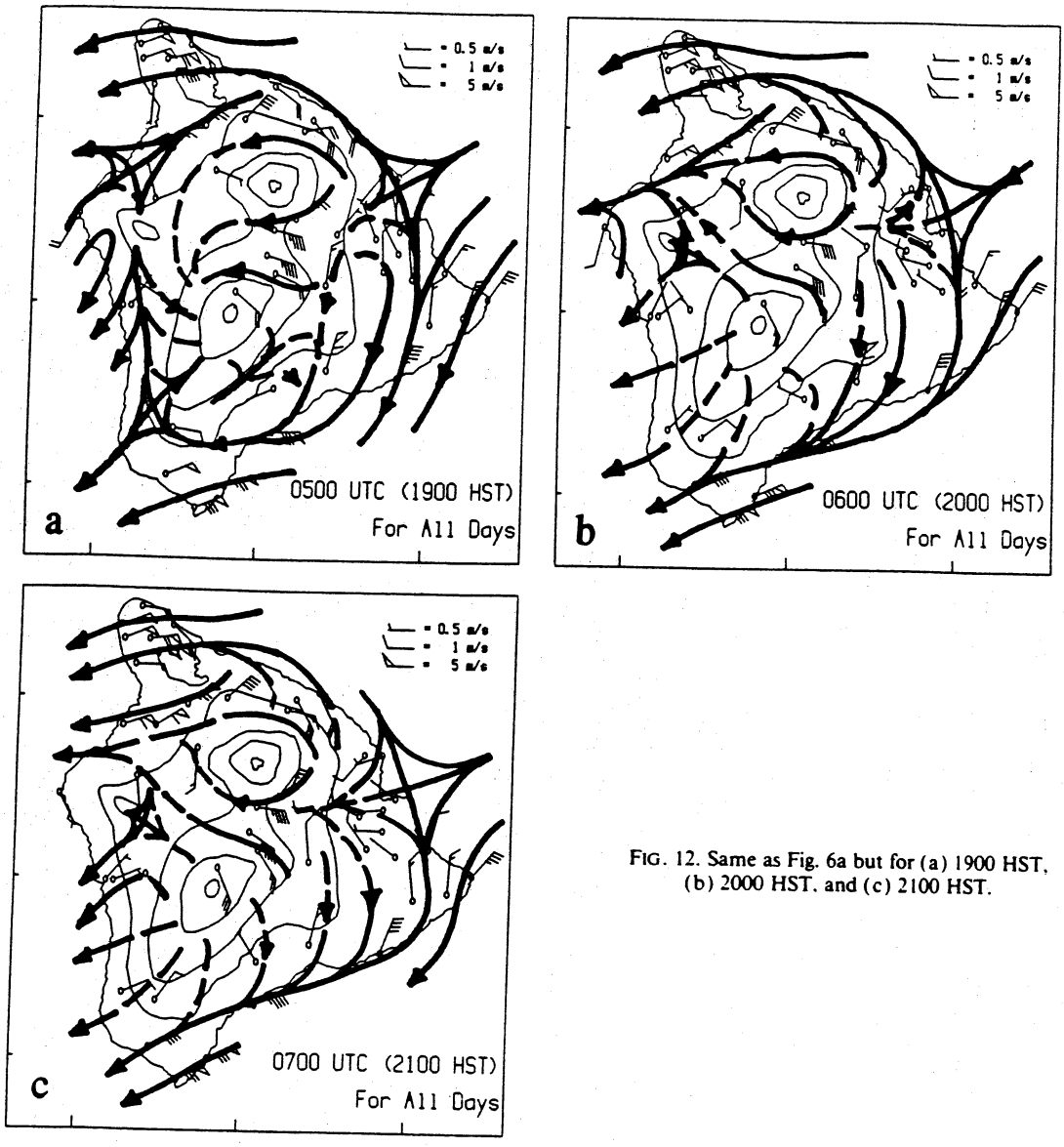

FIG. 12. Same as Fig. 6a but for (a) 1900 HST, (b) 2000 HST, and (c) 2100 HST.

the coastal region to the opposing trade-wind flow, 2) the gradual decrease in the surface temperature along the coast during the late afternoon hours (Fig. 10), and 3) frequent observed showers occurring on the slope (see section 5) in the late afternoon. On the slopes, the daily temperature maximum occurs around noon, closely in phase with the daily heating cycle. Windward coastal stations, however, which are under the influences of prevailing trade winds, recorded maximum temperature in the early afternoon (Fig. 10). These stations also show smaller diurnal temperature fluctuations because of oceanic influences. Frequent showers on the slopes at this time may cause the air temperature to drop due to evaporative cooling and help the initiation of downslope flow.

On the lee side, the evening transition commences at 1900 HST and the sea breezes along the Kona and Waikoloa coasts weaken (Fig. 12a). In the Kona region, the sea-breeze flow has become more parallel with the coast. Note that the cessation of sea breezes over Waikoloa, which is downstream of the Waimea Saddle, occurs earlier than along the Kona coast (Fig. 12). Along the Waikoloa coast, the sea breeze has to overcome the opposing trade winds. In contrast, trade winds are absent in the Kona region because they are completely blocked by the volcanoes. At 2000 HST (Fig. 12b), Keahole Point (station 39) located at the western tip of the island still has light onshore flow. By 2100 HST, land breeze is well established on the west coast (Fig. 12c).

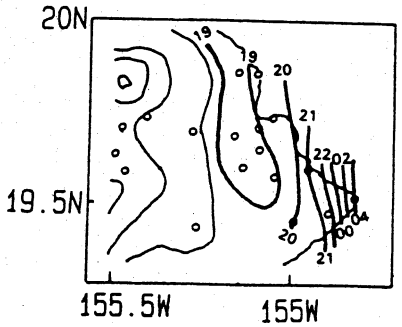

FIG. 13. Isochrone analysis of time (HST) of downslope flow onset for the windward side.

5. Strong and weak trade winds

The blocking of the low-level air is one of the most important ways in which mountains affect the airflow (Smith 1979). The flow deceleration upstream is due to the difficulty the potentially colder surface air has in moving upslope (Smith 1990). As the stable, low-level air is pushed up the windward slope, it becomes potentially colder than the air at the same level. This creates relatively high pressure next to the slope, which decelerates the incoming flow (Hunt and Snyder 1980; Smolarkiewicz et al. 1988; Smith 1990). For strong trade-wind days, we anticipate the effect of blocking to be more significant.

In this study, we compare the surface pressure between the 12 strongest and the 12 weakest trade-wind days during HaRP based on the pressure measurements from PAM stations. For the weak trade-wind days, the synoptic-scale surface pressure is generally higher—because the subtropical high is closer to the island—than for the strong trade-wind days. To isolate the topographic-induced pressure differences due to blocking, the small synoptic-scale pressure difference of 0.25 hPa between the weak and strong trade-wind days was removed. This value was computed from the pressure observations from a buoy located at 17.5°N, 152.6°W. This is about 300 km southeast of the island of Hawaii. The results show that there is a positive topographic-induced pressure anomaly on the order of about 0.2–0.5 hPa on the windward slopes just west of Hilo (Fig. 14) between the 12 strongest and the 12 weakest trade-wind days during HaRP. The maximum anomaly is within the valley between Mauna Kea and Mauna Loa. In the lee side, the surface pressure is generally lower for the strong than for weak trade-wind days. This pattern of pressure difference is observed for both the daytime and nighttime flow regimes. It is apparent that the blocking effect is more significant under strong trade-wind conditions.

For the strong trade-wind days, the flow deceleration on the slopes due to blocking is expected to be more significant. An examination of the u-component difference, $U_{strong} - U_{weak}$, between the strong and weak trade-wind days shows a small positive difference in the u component (≥ 1 m s^{-1}) on the windward slopes for both the daytime and nighttime flow regimes (Fig. 15). The difference indicates that on the windward slopes, the upslope flow during the day is slightly weaker and the katabatic wind at night is slightly stronger for the strong than for the weak trade-wind days, consistent with the observed pressure difference.

The general patterns of the nighttime (Fig. 16a) and daytime (Fig. 16b) surface flow under the strong and weak trade-wind conditions are very similar to the

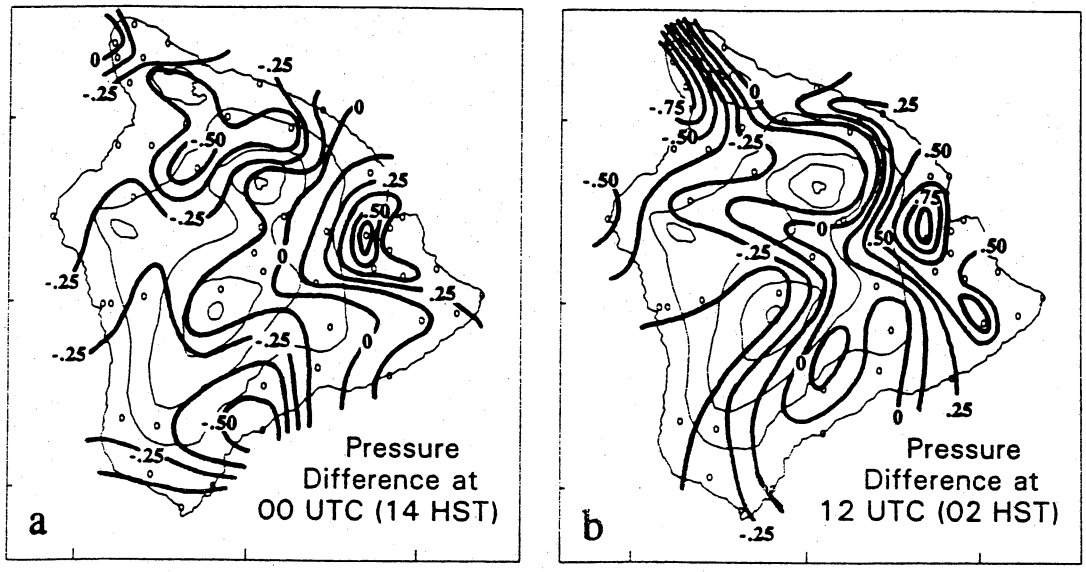

FIG. 14. Observed pressure difference (hPa) between the strong and weak trade-wind days. The contour interval is 0.125 hPa: (a) 1400 HST; (b) 0200 HST.

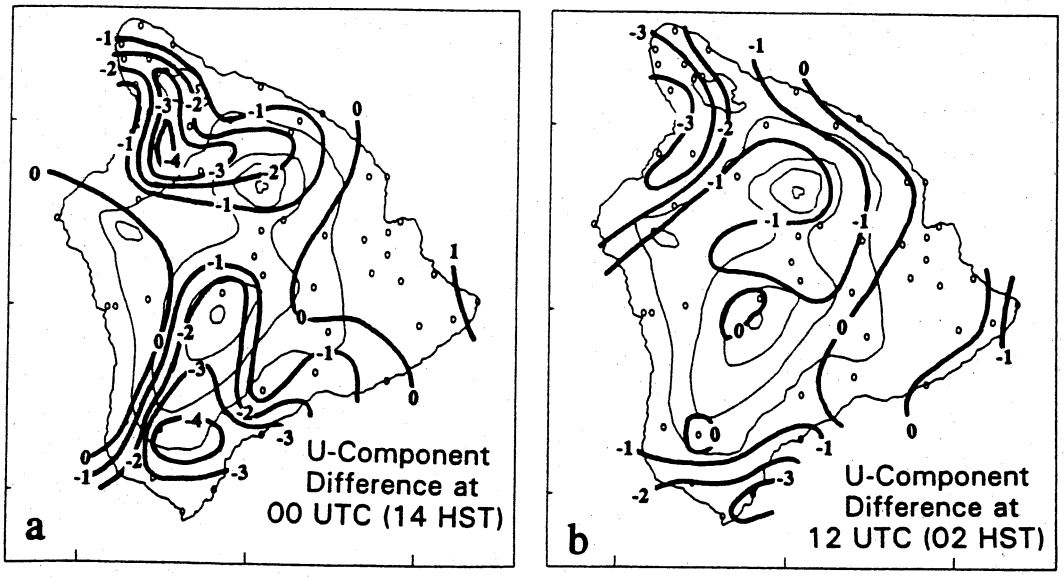

FIG. 15. The u-component difference between strong and weak trade-wind days. The contour interval is 1 m s^{-1}: (a) 1400 HST; (b) 0200 HST.

mean nighttime (Fig. 6a) and daytime (Fig. 7a) flow. In the regions well exposed to trade-wind flow, stronger easterlies were found for the strong trade-wind days as compared to the weak trade-wind days (Fig. 14). These areas are located at the northern and southern parts of the island and in the northwestern part of the island downstream of the Waimea Saddle. In general, easterly anomalies in these regions are slightly larger during the day than at night as a result of downward transport of trade-wind momentum due to vertical mixing in the afternoon hours.

In addition, there are time differences of the onset times of the downslope–offshore and upslope–onshore flow between the strong and weak trade-wind days, especially in the areas where the diurnal wind flow blows in the direction opposing the trade-wind flow. For the weak trade-wind cases, the sea breeze along the Waikoloa coast downstream of the Waimea Saddle starts earlier in the morning and ends later in the late afternoon (Fig. 17a). The sea breeze in this region can overcome the weaker trade winds for a long period. It has become established at 0900 HST in the morning (Fig. 16c). In contrast, for the strong trade-wind days, the sea breeze is observed in the area until more than an hour later (not shown), as the sea breeze cannot easily form against the stronger trade winds blowing through the saddle. In the late afternoon, the sea breeze is still blowing in this region at 1800 HST for the weak trade-wind cases (Fig. 16d). For the strong trade-wind cases, however, winds have already shifted to offshore flow at this time. At the Kona coast, the differences in the onset and cessation times of sea breeze observed between the strong and weak trade-wind days are not evident. The trade winds are absent in this area.

Along the windward coast and in the Hilo area, the katabatic wind starts earlier in the evening and ends later in the morning for the weak trade-wind cases than for the strong trade-wind cases (Fig. 17b). For the strong trade-wind days, the downward progression of the katabatic flow in the evening transition is held up more by strong winds. Cape Kumukahi (station 7), located at the eastern tip of the island, shows that the winds exhibit an onshore component nearly all night for the strong trade-wind cases except for a short period (<1 h) before sunrise. For the weak trade-wind cases, the katabatic flow lasts longer than 5 h (Fig. 17c). High up on the slope, the onset and cessation times of the katabatic wind occur nearly at the same time for the weak and strong trade-wind cases (Fig. 17d). At 0900 HST, winds still exhibit an offshore component in the Hilo area for the weak trade-wind cases (Fig. 16c). As a comparison, by this time, the onshore flow is established along the windward coast for the strong trade-wind cases. It is apparent that it is easier for the katabatic wind to overcome trade winds along the windward coast under weak trade-wind conditions.

6. Diurnal rainfall patterns

The overall patterns on the total rainfall accumulation during HaRP (Fig. 18) are remarkably similar to the summer climatological patterns reported by Giambelluca et al. (1986). Most of the rainfall fell on the windward side of the island, with a maximum below the 1000-m elevation west of Hilo. A maximum rainfall axis is also found along the northeastern coast with a local maximum on the windward side of the Kohala Mountains. On the lee side, the rainfall accumulation

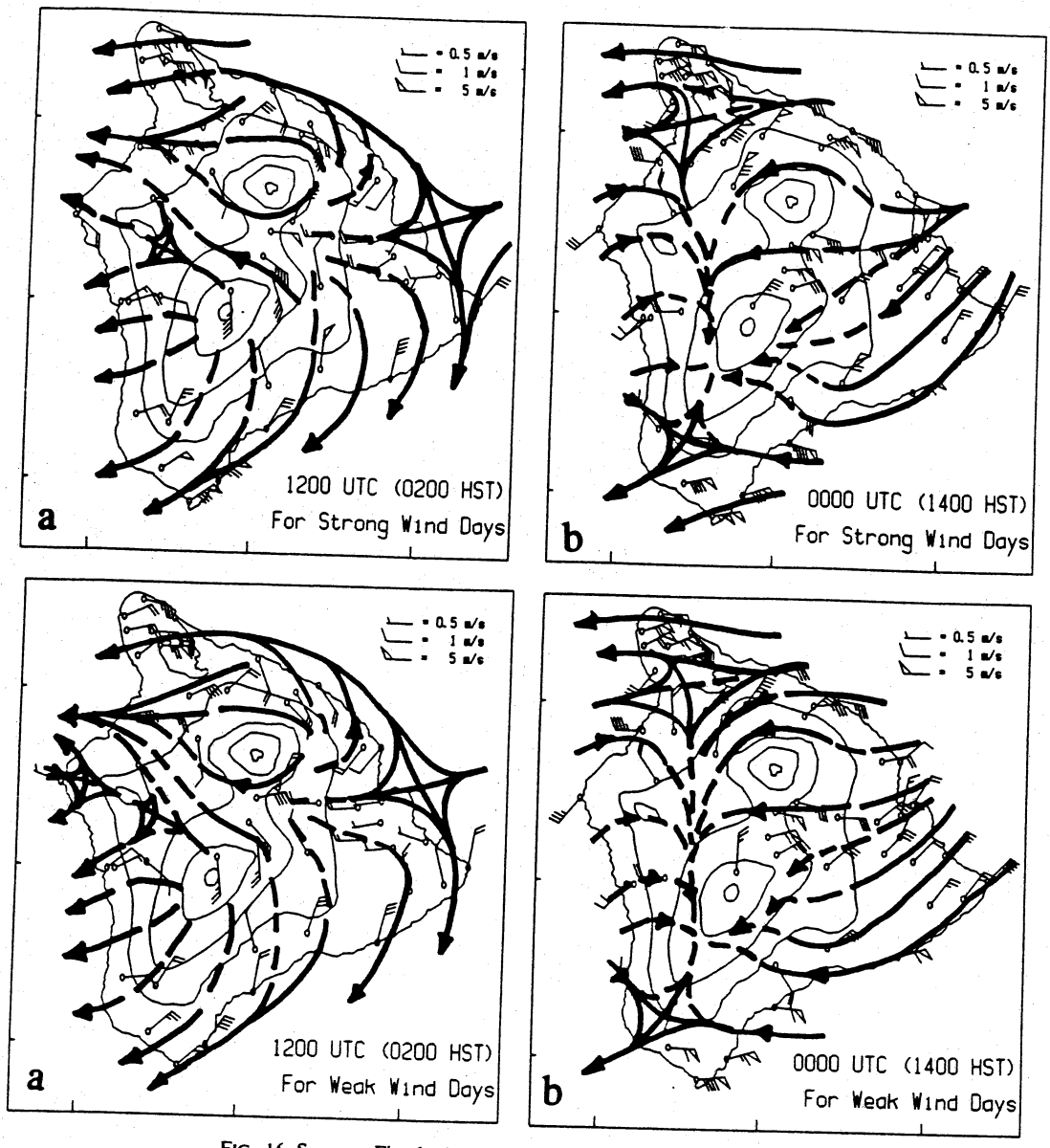

FIG. 16. Same as Fig. 6a, but for strong and weak trade-wind days: (a) 0200 HST, (b) 1400 HST, (c) 0900 HST, and (d) 1800 HST.

is generally much less except in the Kona region where more than 200 mm of rainfall was recorded. The driest areas (<50 mm) are found over the summits of Mauna Loa and Mauna Kea, northwestern Hawaii downstream of the Waimea Saddle, southwestern Hawaii, and along the southeastern coast.

In addition to large spatial variations in rainfall accumulation, the timing of rainfall occurrences also shows large diurnal variations. The hourly rainfall frequency (%) during HaRP, the percentages of days that rainfall occurs within the hour for the entire 42 days, has been computed for all PAM stations. On the lee side, the trade winds are absent with less rainfall (Fig. 18). The rainfall occurrences there are closely related to local circulations. During the night and in the early morning, rainfall occurrences in the lee side are rare as the circulations are dominated by katabatic–land-breeze flow. With the development of anabatic–sea-breeze winds during the day, orographic showers are more frequent on the leeside slopes in the late afternoon hours (Fig. 19) in agreement with previous studies (Leopold 1949; Schroeder et al. 1977). As the anabatic–sea-breeze flow dissipates in the evening, rain showers diminish. Rainfall frequencies at Waikoloa Mauka (station 37) over northwestern Hawaii also show the late afternoon maximum (Fig. 19b). This is the time of the closest approach of the Waikoloa sea breeze. This area is very dry with less than 100-mm

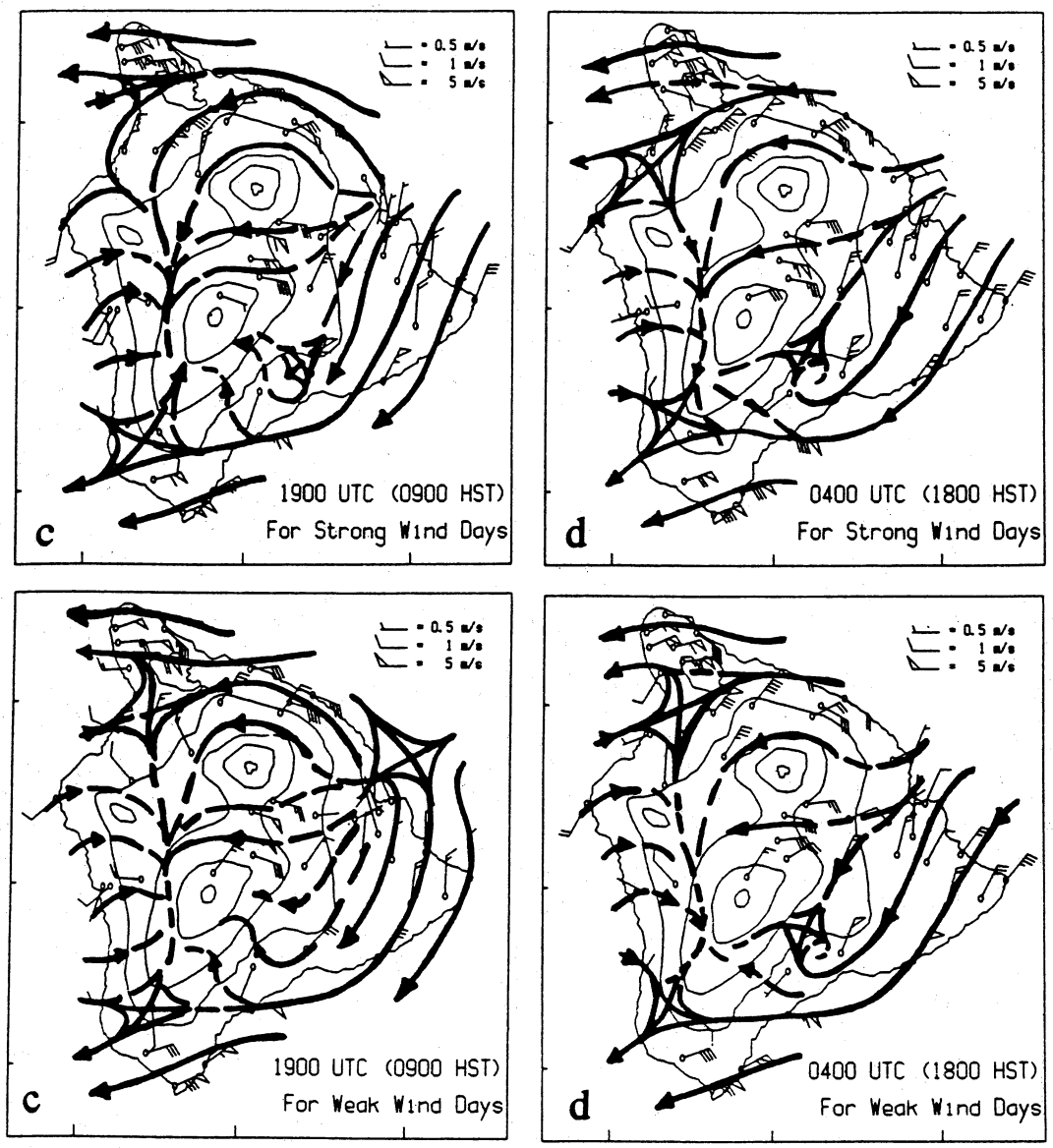

FIG. 16. (*Continued*)

total rainfall during HaRP (Fig. 18). This is because it is downstream of the Waimea Saddle. The trade winds blow through the saddle (Fig. 7a) and descend in the lee side. The late afternoon maximum in this region is related to the interaction between the sea breeze and the opposing trade winds as found by Schroeder (1981). There is a larger area-averaged (Fig. 20) convergence value of nearly 5×10^{-4} s^{-1} in the late afternoon (Fig. 21a).

On the windward side, the rainfall frequencies vary substantially during the diurnal cycle (Fig. 22). At 1400 HST, the area of maximum rainfall frequency is on the windward slopes (Fig. 22a). Showers in this area form by orographic lifting provided by the anabatic–trade-wind flow rising up the mountain slopes as found by Leopold (1949). During the day, the windward lowland exhibits divergence (Fig. 21b) caused by splitting airflow there (Fig. 7a). During the evening transition, the daytime divergence over the Hilo region turns to nighttime convergence as a result of the interaction between the katabatic flow and the opposing trade winds (Fig. 21b). The rainfall frequencies over the windward lowland increase. As a result, the area of maximum rainfall frequency moves seaward (Figs. 22b–d). These showers may enhance the katabatic flow by cooling the air by precipitation.

At night, the area of maximum rainfall frequency is over the windward lowland west of Hilo (Figs. 22e,f), suggesting that most of the observed nocturnal precipitation over the windward lowland starts in situ. Our

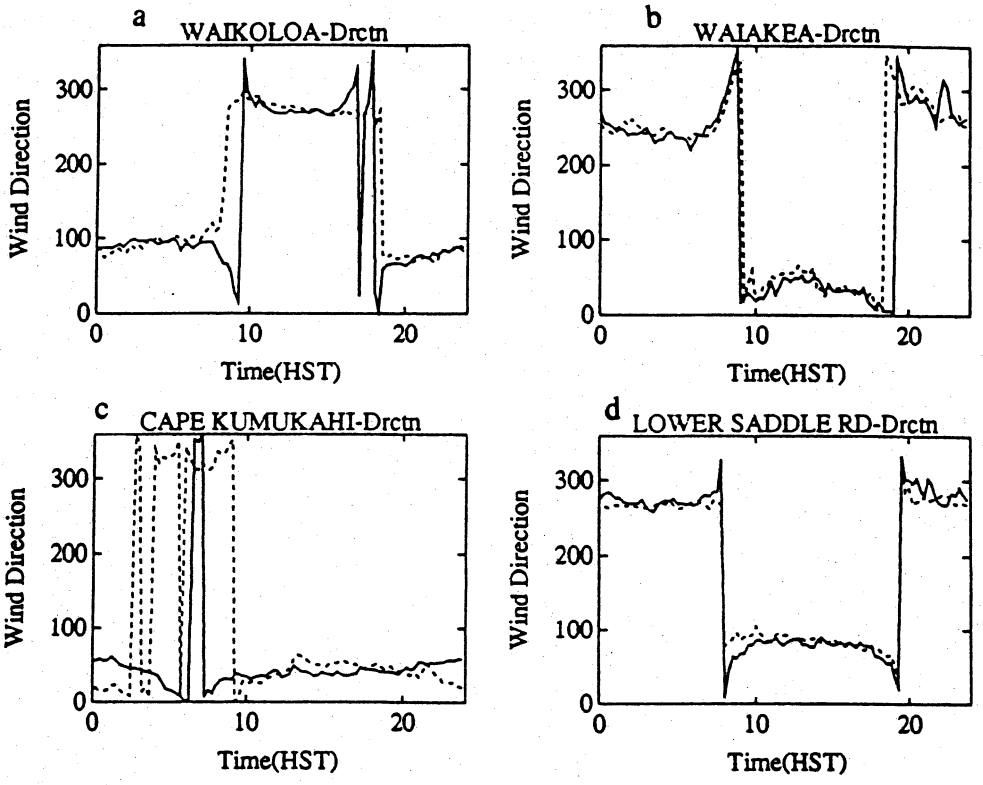

FIG. 17. Time series of wind direction for strong (solid) and weak (dotted) trade-wind days at (a) Waikoloa Mauka (station 37), (b) Waiakea (station 44), (c) Cape Kumukahi (station 7), and (d) Lower Saddle Road (station 16).

results are in contrast to previous studies (Leopold 1949; Garrett 1980; and others), which with limited data suggest that nocturnal precipitation develops off-

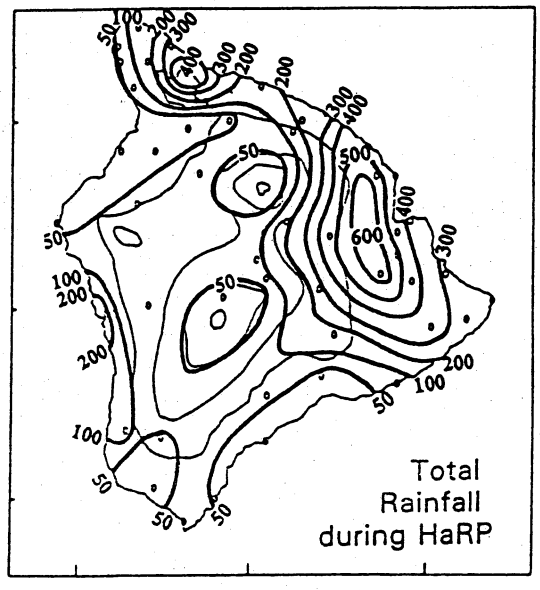

FIG. 18. Total rainfall accumulation (mm) during HaRP.

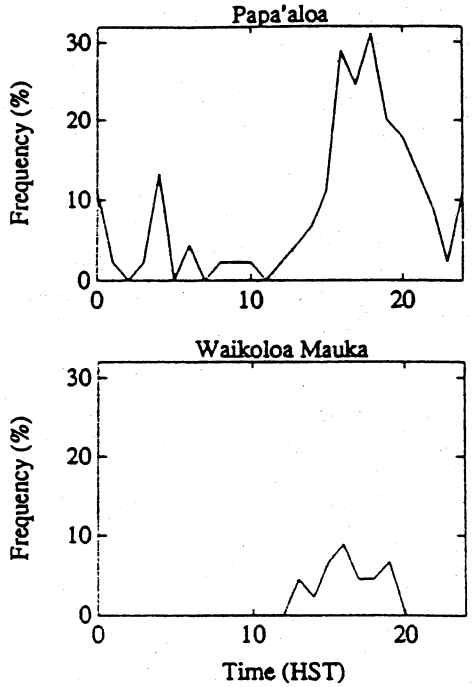

FIG. 19. Time series of rainfall frequency (%) for (a) Papa'aloa (station 42) and (b) Waikoloa Mauka (station 37).

shore and drifts inland. Note that rain showers occur primarily on the windward side (Figs. 22e,f). It is also interesting to note that the magnitude of convergence at night west of Hilo is less than half of that of the afternoon convergence observed at the Waikoloa region, and yet, the nocturnal precipitation is frequent over the Hilo area compared to the dry condition over the Waikoloa coast (Fig. 19). It is apparent that over the windward lowland the effect of orographic lifting aloft is enhanced by the nighttime convergence west of Hilo resulting in a high rainfall frequency. Throughout the night, with continued nocturnal cooling at the surface, the coldest daily surface temperature on the slopes is observed just before sunrise (~0600 HST) (Fig. 10). The island divergence (Fig. 21d) computed from a line integral technique from stations along the coast over the entire island also shows increasing divergence throughout the night, reaching a maximum around sunrise. This maximum divergence around sunrise supports Garrett's (1980) speculation that the offshore flow is strongest just before sunrise. With increasing katabatic–land-breeze flow throughout the night, the rainfall frequencies on the windward slopes diminish. At 0600 HST, the region of maximum rainfall frequency is located in the coastal area (Fig. 22g).

After sunrise, the islandwide divergence rapidly decreases (Fig. 21c) as the land breeze weakens due to increasing solar heating on the slopes. It turns to convergence between 0800 and 0900 HST as the upslope–sea-breeze flow develops. Over the Hilo region, the convergence due to the interaction between the katabatic flow and the opposing trade winds disappears and becomes divergence (Fig. 21b). The offshore flow along the windward coast is gradually replaced by the splitting onshore flow (Fig. 8). The rainfall frequencies over the windward lowland continue to decrease with a maximum occuring on the coast (Fig. 22h), suggesting that the precipitation along the coastal region is produced by the drifting of the frequently observed early morning offshore rainbands as reported in early studies (Leopold 1949; Fullerton 1972; Takahashi 1977; Garrett 1980). Confirmation was made by radar observations at Hilo airport and Paradise Park during HaRP.

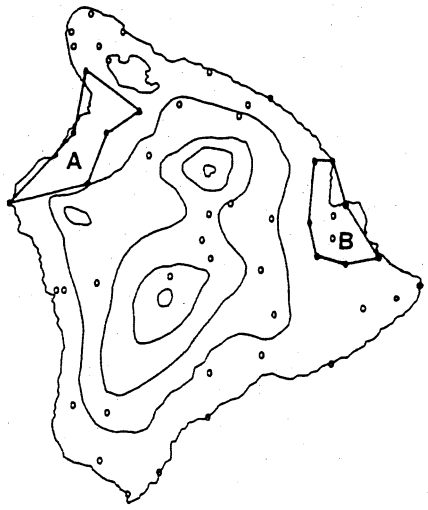

FIG. 20. Areas selected for the divergence calculations using the line integral technique. Regions A and B represent the Waikoloa coastal region and the Hilo area, respectively.

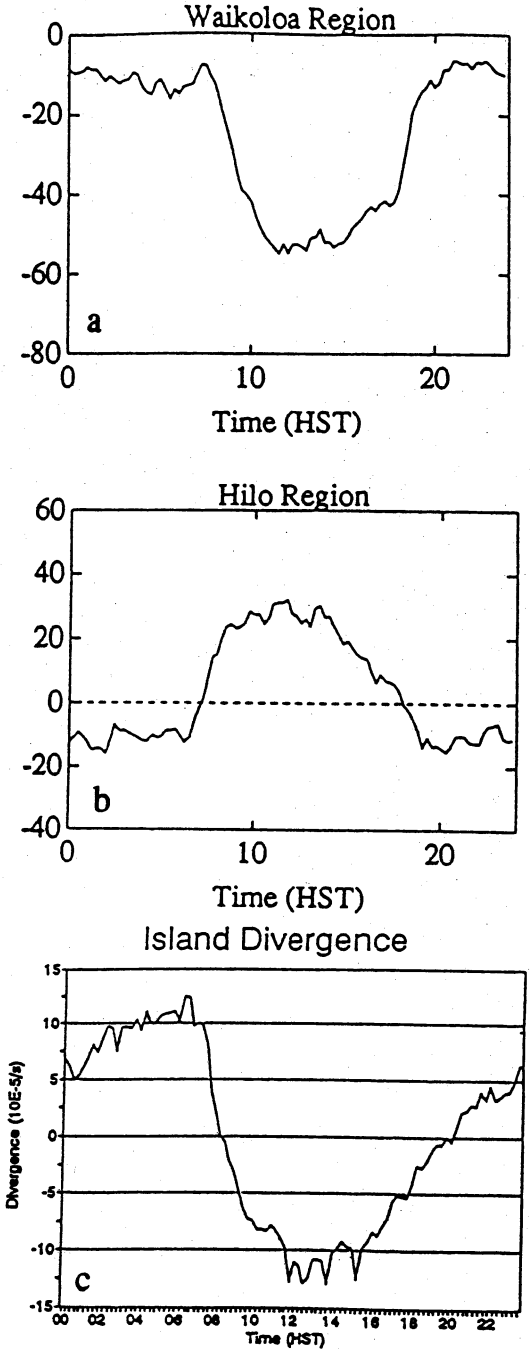

FIG. 21. Time series of area-averaged divergence during the diurnal cycle for (a) Waikoloa region (region A), (b) Hilo region (region B), and (c) the entire island.

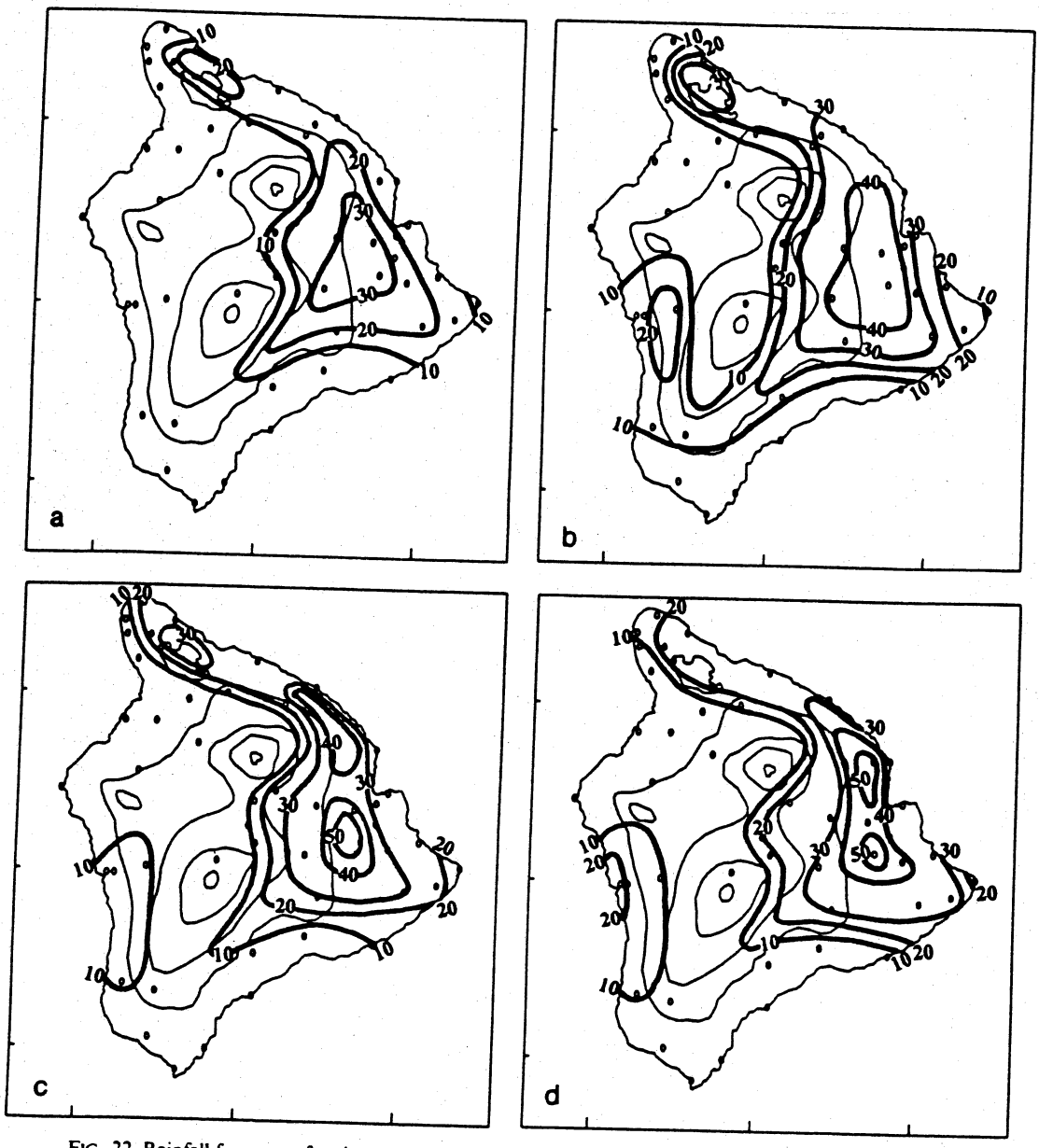

FIG. 22. Rainfall frequency for given time. The contour interval is 10%: (a) 1400 HST, (b) 1900 HST, (c) 2000 HST, (d) 2100 HST, (e) 0000 HST, (f) 0200 HST, (g) 0600 HST, and (h) 0800 HST.

During the morning and evening transitions, the thermal contrasts between the island and the same elevation at adjacent areas are small. The blocking effects and orographic lifting of the trade wind aloft are important during both periods; however, the rainfall distributions over the island are different for both transition periods. The rainfall distributions during the transition periods are also related to the evolution of the airflow over the island. As discussed earlier, during the evening transition the airflow exhibits katabatic flow on the slopes with onshore flow at the coast. Maximum rainfall frequency is found over the windward lowland where the katabatic flow interacts with the trade winds. During the early morning transition, with increasing solar heating on the slopes, the airflow turns to upslope flow on the windward slopes with offshore flow along the coast. The region of maximum rainfall frequencies is located right on the coast due to the inland drifting of the offshore rainbands (Takahashi 1977; Fullerton 1972). It is apparent that the dynamic effects predicted by numerical models (Smolarkiewicz et al. 1988; Rasmussen et al. 1989; Rasmussen and Smolarkiewicz 1993) are not the only factors that determine the spatial distributions of local showers during these transition periods. The reasons why offshore rainbands are more frequent in

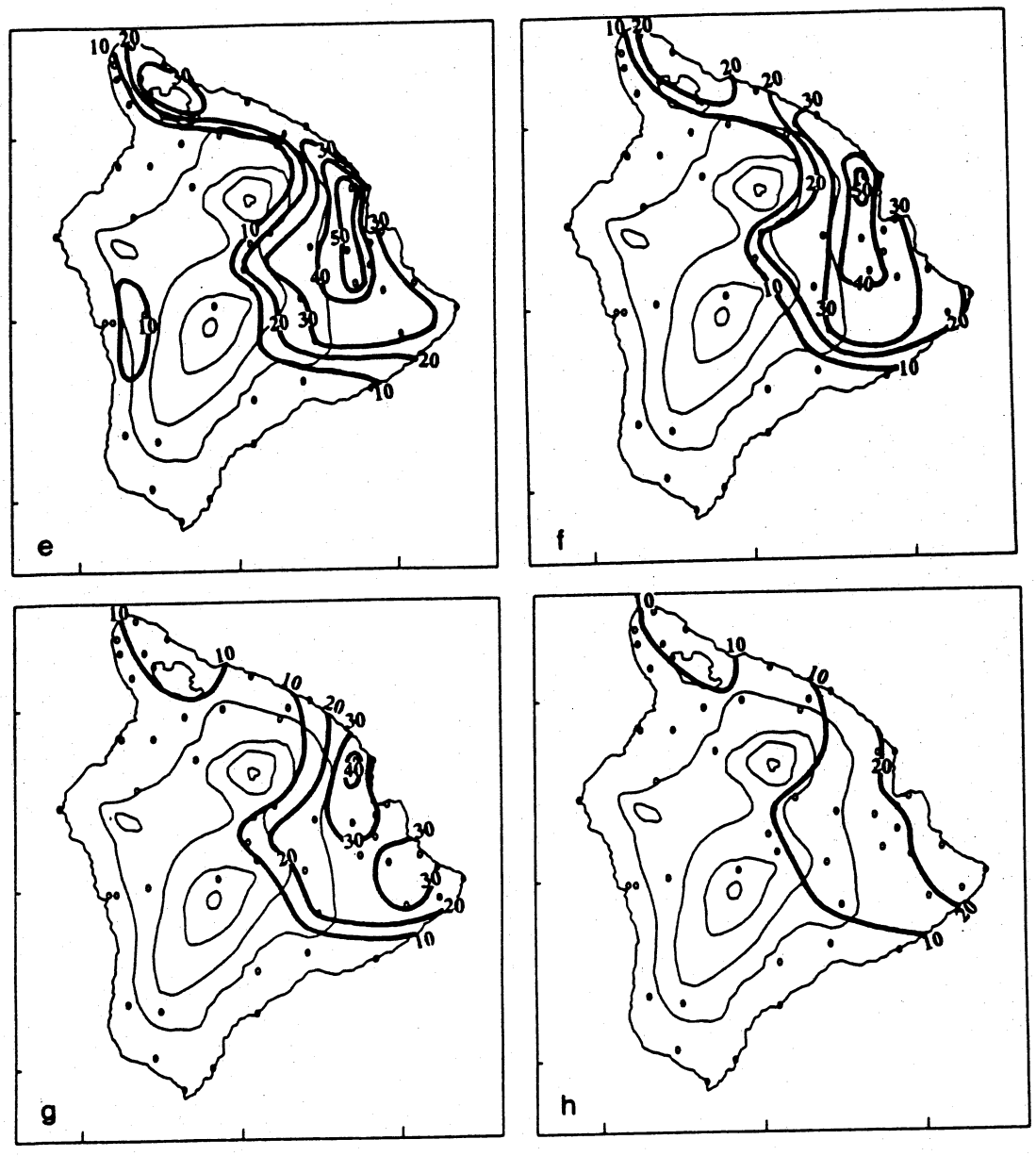

FIG. 22. (*Continued*)

early mornings may be related to the fact that the offshore flow reaches its maximum intensity just before sunrise. Further study on this problem is needed. Without Doppler radar observations, previous studies (Leopold 1949; Garrett 1980; Rasmussen and Smolarkiewicz 1993) suggest that the rainband forms at the location where offshore flow and trade winds meet. During HaRP, in contrast to the speculation suggested by these studies, offshore rainbands frequently formed upstream of the island where the trade winds decelerated. It is very likely that in addition to island blocking the strength of the offshore flow may also affect the upstream flow deceleration. Temporary increase in the depth and strength of downslope flow was also observed at tethersonde sites in response to rain showers on the slopes. Further modeling and observational studies are needed to examine the airflow offshore in relation to the strength of the downslope wind component and the differences in the airflow offshore between the morning and evening transitions.

In general, rainfall occurrences are rare above the trade-wind inversion. Such events occur when the trade-wind inversion is weak (~1 K) (Garrett 1980). The mountain peaks of Mauna Loa and Mauna Kea as well as their upper slopes have a low frequency of precipitation (Fig. 22). When showers occur, the timing is more frequent in the afternoon hours (not

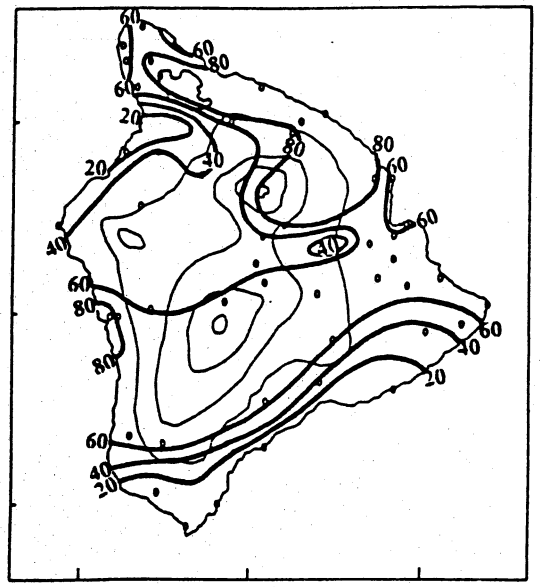

FIG. 23. Percentages of variance in rainfall frequency for the diurnal cycle determined by Fourier analysis.

shown). During this time of the day, the upslope flow carries moist air from lower levels to the upper slopes (Garrett 1980). The southeast flank of Mauna Loa also has a late afternoon and early evening rainfall maximum (Fig. 22) due to orographic lifting provided by the onshore–upslope wind component (Fig. 7a). The region of maximum rainfall frequency is at the elevation between 1 and 2 km (Figs. 22a,b). At night, the rain showers there diminish (Figs. 22c–f) with an offshore–downslope wind component (Fig. 6a).

Along the windward Kohala coast and mountains, the rainfall frequency is relatively high at all hours due to orographic lifting (Fig. 22). During the diurnal cycle, the maximum frequency of rainfall occurs in the late evening with a minimum in the morning hours (Fig. 22). During the morning hours, local showers are frequently observed upstream associated with the arc-shaped offshore rainbands. The southern tip area has a relatively low rainfall frequency (<10%) at all hours (Fig. 22) with no major diurnal signal (Fig. 23). This area is well exposed to trade winds. The rain showers embedded within the trade flow may affect this area at all times of the day.

Rainfall occurrences over the island are also related to synoptic-scale features such as remmants of tropical storms, weak shear lines associated with midlatitude cold fronts, upper-level troughs, and others. Fourier analysis of rainfall frequencies shows that up to 40% of the variance in rainfall frequency is not explained by the diurnal cycle (Fig. 23). The diurnal cycle in rainfall frequency during HaRP is less significant than that obtained by Schroeder et al. (1977), whose study used long-term records and found that the variance contributed by the diurnal cycle is typically between 64% and 90%. The discrepancy may be partly due to the shorter time span of the records in this study. Furthermore, during HaRP, synoptic-scale circulations appear to contribute more to the rainfall than the long-term climatology.

7. Summary and conclusions

The surface airflow over the island of Hawaii has been studied using the high-resolution PAM data from HaRP during 11 July–24 August 1990. Along the windward coast, the winds exhibit a southerly (northerly) wind component north (south) of the valley between Mauna Kea and Mauna Loa with strong easterly winds ($\sim$6–8 m s^{-1}) at both the northern and southern tips of the island as the trade winds are forced to move around the island. The daily mean winds are weak on the windward slopes, where the trade winds are decelerated by the island obstacle and move around the island. On the lee sides of Mauna Kea and Mauna Loa, the trade winds are absent with calm winds. In the Waimea Saddle and Humu'ula Saddle, the flow deceleration because of island blocking is less significant with a large easterly wind component. Except in the high wind regions, most of the island shows an upslope–onshore (downslope–offshore) wind component during the day (night). The nighttime offshore flow reaches the maximum intensity with a maximum islandwide divergence just before sunrise when the surface temperature is coldest. These features are driven by combined effects of thermal contrasts between the elevated terrain and the adjacent areas and the blocking of the trade-wind flow by an island obstacle.

The daytime and nighttime flow regimes are separated by transition periods of roughly 3 h. During the morning (evening) transition, the upslope (downslope) flow starts on the windward slopes and progresses downward. Thus, during the morning (evening) transition, the winds exhibit an upslope (downslope) component on the windward slopes and an offshore (onshore) component at the windward coast. During the early morning hours, offshore rainbands are observed more frequently. These rainbands form upstream where the trade winds decelerate. Once formed, they drift ashore. As a result, during the early morning hours, maximum rainfall frequently is observed along the windward coast.

We also show that the effect of blocking is more significant for the 12 strongest trade-wind days than for the 12 weakest trade-wind days during HaRP. For the strong trade-wind days the surface pressure is higher (0.2–0.5 hPa) on the windward lowland and lower in the lee side as compared to the weak trade-wind days. In addition, the daytime upslope wind (nighttime downslope) component on the windward slope is weaker (stronger) ($\leq$1 m s^{-1}) for the stronger trade-wind days than for weak trade-wind days as a result of blocking. The onset times of the downslope–offshore

and upslope–onshore flow also depend on the strength of the prevailing trade-wind flow especially in the areas where the diurnal wind flow blows in the direction opposing the trade-wind flow. In general, in these areas, it is easier for the diurnal wind to develop under weak trade-wind conditions.

The timing of rainfall occurrences during the diurnal cycle and the horizontal distribution of rainfall patterns are also related to terrain and local winds. During HaRP, most of the rain fell on the windward side of the island with a maximum below the 1000-m elevation west of Hilo in agreement with the climatology presented by Giambelluca et al. (1986). On the lee side, the rainfall accumulation is much less. Except in the windward region, most areas over the island exhibit a maximum in rainfall occurrences during the later afternoon hours in agreement with previous studies (Leopold 1949; Schroeder et al. 1977; Garrett 1980; Schroeder 1981).

On the windward side, the evolution of diurnal rainfall frequency is related to a complex interaction among orographic lifting, thermal forcing, and dynamic blocking. In the afternoon hours, the rainfall frequency has a maximum on the windward slopes because of orographic lifting provided by the anabatic–trade-wind flow as found by Leopold (1949). The windward lowland west of Hilo exhibits divergence during the day due to splitting airflow as a result of island blocking. During the evening transition, the daytime divergence there changes to nighttime convergence due to the interaction between the katabatic winds and trade winds. The rainfall frequencies on the windward lowland increase. As a result, the region of maximum rainfall frequency moves seaward. At night, the area of maximum rainfall frequency is over the windward lowland west of Hilo suggesting that most of the nocturnal precipitation there starts in situ. It appears that the orographic lifting aloft is enhanced by the nighttime convergence as the katabatic winds interact with the trade-wind flow. With continued nocturnal cooling throughout the night, the katabatic winds strengthen with increasing islandwide divergence. The precipitation on the windward slope diminishes.

Acknowledgments. We would like to thank those who contributed to the planning and implementation of HaRP, especially T. A. Schroeder, who sited the PAM network, and the ATD staff, who maintained the network. This work is supported by the National Science Foundation under Grant ATM-8919420. Computer resources are supported in part by the Scientific Computing Division of the National Center for Atmospheric Research (NCAR), which is sponsored by the National Science Foundation. One of us (Y.-L. C.) would like to thank Dr. C.-S. Chen for making arrangements and inviting him to visit the National Central University, Taiwan, during his sabbatical leave. We would like to thank T. A. Schroeder and G. M. Barnes for helpful discussions, and J. Feng and J. Wang for their assistance in computing area-averaged divergence and diurnal rainfall frequencies. Comments from Dr. Edward J. Zipser and anonymous reviewers helped in the presentation of this paper. The manuscript was typed by C.-F. Chan.

REFERENCES

Banta, R. M., 1990: The role of mountain flows in making clouds. *Atmospheric Processes over Complex Terrain*, W. Blumen, Ed., Amer. Meteor. Soc., 229–284.

Bolton, D., 1980: The computation of equivalent potential temperature. *Mon. Wea. Rev.*, **108**, 1046–1053.

Chen, Y-L., R. Burke, and R. M. Rasmussen, 1991: Observations of low-level winds on the windward slope of the Island of Hawaii. *Int. Conf. on Mesoscale Meteorology and TAMEX*. Taipei, National Science Council of Taiwan and American Meteorological Society. 229–233.

Eber, L. E., 1957: Upper air and surface wind observations in Project Shower. *Tellus*, **9**, 558–568.

Fellbaum, S. R., 1984: The effects of the Island of Hawaii on the trade winds and the trade wind inversion. M.S. thesis, University of Hawaii, 86 pp.

Fitzjarrald, D. R., 1984: Katabatic wind in opposing flow. *J. Atmos. Sci.*, **41**, 1143–1158.

Fullerton, C. M., 1972: A rainfall climatology of Hilo, Hawaii. Tech. Rep. 66, Water Resources Research Center, University of Hawaii, 52 pp.

Fett, R. W., and S. D. Burk, 1981: Island barrier effects as observed by satellite and instrumented aircraft, and simulated by a numerical model. *Mon. Wea. Rev.*, **109**, 1527–1541.

Garrett, A. J., 1980: Orographic clouds over the eastern slopes of Mauna Loa volcano, Hawaii, related to insolation and wind. *Mon. Wea. Rev.*, **108**, 931–941.

Giambelluca, T. W., M. A. Nullet, and T. A. Schroeder, 1986: Rainfall atlas of Hawaii, Report R76, Department of Land and Natural Resources, State of Hawaii, 267 pp.

Hunt, C. R., and W. H. Snyder, 1980: Experiments on stably and neutrally stratified flow over a model three-dimensional hill. *J. Fluid Mech.*, **96**, 671–704.

Kusuda, M., and P. Alpert, 1983: Anti-clockwise rotation of the wind hodograph. Part I: Theoretical study. *J. Atmos. Sci.*, **40**, 487–499.

Lavoie, R. L., 1967a: Background data for the warm rain project. *Tellus*, **19**, 348–353.

——, 1967b: Air motions over the windward coast of the island of Hawaii. *Tellus*, **19**, 354–358.

Leopold, L. B., 1949: The interaction of trade wind and sea breeze, Hawaii. *J. Meteor.*, **6**, 312–320.

——, H. Landsberg, C. K. Stidd, T. C., Yeh, C. C. Wallén, J. E. Carson, and J. J. Marciano, 1951: On the rainfall of Hawaii: A group of contributions. *Meteor. Monogr.* No. 3, Amer. Meteor. Soc., 1–55.

Lyons, S. W., 1982: Empirical orthogonal function analysis of Hawaii rainfall. *J. Appl. Meteor.*, **21**, 1713–1729.

Matsumoto, K., 1982: A climatology of the diurnal variation of rainfall over the Island of Hawaii during summer. M.S. thesis, Department of Geography, University of Hawaii, 67 pp.

Meisner, B. N., 1979: Ridge regression-time extrapolation applied to Hawaiian rainfall normals. *J. Appl. Meteor.*, **18**, 904–912.

Mendonca, B. G., 1969: Local wind circulation on the slopes of Mauna Loa. *J. Appl. Meteor.*, **8**, 533–541.

Nash, A. J., 1992: Diurnal surface weather variations on the island of Hawaii. M.S. thesis, University of Hawaii, 127 pp.

Nickerson, E. C., 1979: On the numerical simulation of airflow and clouds over mountainous terrain. *Beitr. Phys. Atmos.*, **52**, 161–175.

——, and M. A. Dias, 1981: On the existence of atmospheric vortices downwind of Hawaii during the HAMEC project. *J. Appl. Meteor.*, **20**, 868–873.

Rasmussen, R. M., and P. K. Smolarkiewicz, 1993: On the dynamics of Hawaiian cloud bands. Part III: Local aspects. *J. Atmos. Sci.*, **50**, 1560–1572.

——, ——, and J. Warner, 1989: On the dynamics of Hawaiian cloud bands: Comparison of model results with observations and island climatology. *J. Atmos. Sci.*, **46**, 1589–1608.

Rotunno, R., 1983: On the linear theory of the land and sea breeze. *J. Atmos. Sci.*, **40**, 1999–2009.

Schroeder, T. A., 1981: Characteristics of local winds in northwest Hawaii. *J. Appl. Meteor.*, **20**, 874–881.

——, B. J. Kilonsky, and B. N. Meisner, 1977: Diurnal variation in rainfall and cloudiness. UHMET 77-03 Report, Department of Meteorology, University of Hawaii, 67 pp.

Smith, R. B., 1979: The influence of mountains on the atmosphere. *Advances in Geophysics*, Vol. 21, Academic Press, 87–230.

——, 1990: Why can't stably stratified air rise over high ground? *Atmospheric Processes over Complex Terrain*, W. Blumen. Ed., Amer. Meteor. Soc., 105–107.

Smolarkiewicz, P. K., R. M. Rasmussen, and T. L. Clark, 1988: On the dynamics of Hawaiian cloud bands: Island forcing. *J. Atmos. Sci.*, **45**, 1872–1905.

Takahashi, T., 1977: Rainfall at Hilo, Hawaii. *J. Meteor. Soc. Japan*, **55**, 121–129.

——, 1986: Wind shear effects on water accumulation and rain duration in Hawaii warm clouds. *J. Meteor. Soc. Japan*, **64**, 575–584.

Taliaferro, W. J. 1959: Rainfall of the Hawaiian Islands. *Hawaii Water Authority*, State of Hawaii, 396 pp.